Preparation of Bifunctional Scaffolds of Gold Nanorods and Gelatin for Photothermal Therapy of Breast Tumor and Adipose Tissue Engineering

Xiuhui WANG

February 2019

Preparation of Bifunctional Scaffolds of Gold Nanorods and Gelatin for Photothermal Therapy of Breast Tumor and Adipose Tissue Engineering

Xiuhui WANG

Doctoral Program in Materials Science and Engineering

Submitted to the Graduate School of
Pure and Applied Sciences
in Partial Fulfillment of the Requirements
for the Degree of Doctor of Philosophy in
Engineering

at the
University of Tsukuba

Content

List of abbreviations

AuNRs	Gold nanorods
RT-PCR	Real-time polymerase chain reaction
BSA	Bovine serum albumin
PTT	Photothermal therapy
FABP4	Fatty acid binding protein 4
SPR	Surface plasmon resonance
DCs	Dendritic cells
hMSCs	Human mesenchymal stem cells
LPS	Lipopolysaccharide
IL-12	Interleukin-12
PPARG	Peroxisome proliferator-activated receptor gamma
IL-6	Interleukin-6
GM-CSF	Granulocyte macrophage colony-stimulating factor
RNA	Ribonucleic acid
CEBPA	CCAAT/enhancer binding protein alpha
TNF-α	Tumor necrosis factor alpha
FBS	Fetal bovine serum
ELISA	Enzyme-linked immunosorbent assay
SEM	Scanning electron microscopy
DNA	Deoxyribonucleic acid
AA	Ascorbic acid
FASN	Fatty acid synthase
PBS	Phosphate buffer saline
FTIR	Fourier transform infrared
GAPDH	Glyceraldehyde 3-phosphate dehydrogenase
MES	2-(N-morpholino) ethanesulfonic acid
EDC	1-ethyl-3-(3-dimethylaminopropyl) carbodiimide
NHS	N-hydroxysuccinimide
RNA	Ribonucleic acid
TEM	Transmission electron microscopy
VIS-NIR	Visible-near infrared
DLS	Dynamic light scattering
CTAB	Hexadecyltrimethylammonium bromide
ICP-OES	Inductively coupled plasma-optical emission spectroscopy
DMEM	Dulbecco's modified eagle medium
IL-1β	Interleukin-1β
SD	Standard deviation

Chapter 1

General introduction

1.1 Breast cancer

Breast cancer is developed from breast tissue, whose symptoms including a lump appeared in the breast site, a change of breast shape, fluid released from a nipple, a red or scaly patch of skin [1]. Nowadays, breast cancer has become one of the major threats to human health with over one million people diagnosed every year [2, 3]. One-third of new cancer patients attribute to breast cancer, and breast cancer has become one of the major leading causes of death especially for women aged 40-50 [4].

Despite many technical breakthroughs have been made in cancer therapy, complete healing is difficult using traditional therapeutic approaches including surgical resection, chemo- or radio-therapy [5, 6]. An ideal cancer therapeutic strategy should not only eradicate the primary tumor but also induce systemic anti-tumor immunity through activating the immune system to control metastatic tumor and prevent tumor recurrence [7, 8]. Moreover, a large breast defect is mostly accompanied after breast tumor resection, which is difficult to self-heal [9]. Therefore, new functional tissues should be reconstructed or regenerated to fill the large surgical defects [1, 10].

1.1.1 Traditional therapies and their limitations for cancer treatment

Over the past decades, several traditional cancer therapies including surgery, chemotherapy, and radiotherapy have been developed and widely applied in clinic [11-13]. Among them, surgical resection is most widely used and preferred therapy because this method can directly and effectively remove the primary tumor and has no biological resistance [14]. However, as shown in Fig. 1.1, surgical resection is difficult to eliminate all the tumor cells due to their blurry boundary between tumor and healthy tissue, which might cause cancer metastases and recurrence. Moreover, surgical resection is mostly accompanied by tumor-initiated breast defects, which are difficult to self-heal [9].

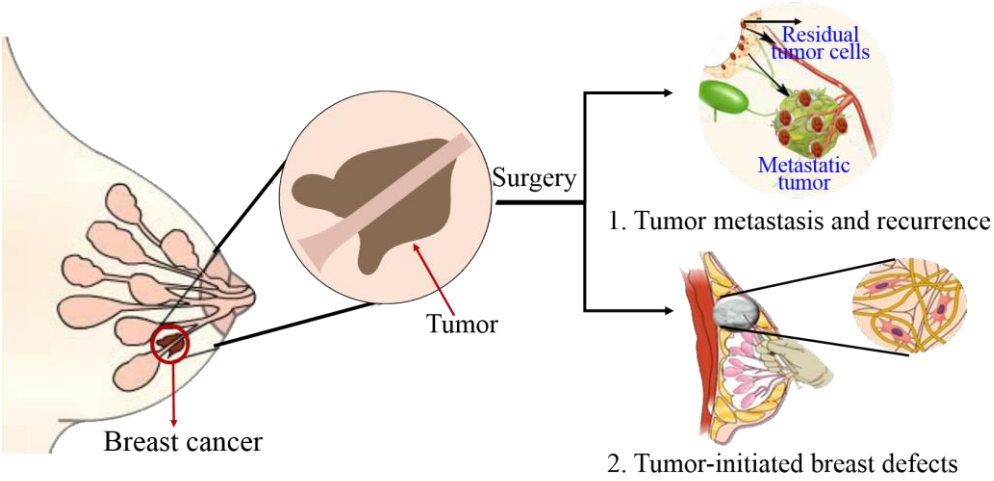

Fig. 1.1 Limitations of surgical resection for breast cancer

Since the middle of 20th century, chemotherapy has been discovered and developed for cancer therapy [15]. Chemotherapy is a type of cancer treatment that uses certain drugs to kill tumor cells or to prevent them from growing and migrating to other parts of the body. Until now, various types of anti-tumor drugs have been explored for chemotherapy [16-18]. For breast cancer therapy, many chemotherapeutic drugs such as abraxane, adriamycin, carboplatin, xeloda, doxil, and halaven have been widely used in the clinic [19-21]. However, all the chemortherapeutic drugs have no specificity to tumor cells, which will induce severe side effects such as hair loss, immunosuppression, and normal tissue damage [22]. Moreover, the tumor cells will become resistant to chemortherapeutic drugs after long-term chemotherapy, further results in the failure of cancer therapy [23].

Radiotherapy uses high-energy particles or waves such as x-ray, γ-ray, electron beams or protons to destroy tumor cells [24]. Unlike chemotherapy, radiotherapy is usually a local treatment. This method is focused on the tumor site to damage tumor cells with little harm to nearby healthy cells [25]. However some side effects can still occur such as skin atrophy and hair loss.

In summary, although these traditional therapies have been widely used in the clinic, a reliable cure is still limited. Therefore, novel approaches with specificity and high efficiency to tumor cells are urgently desired.

1.1.2 New strategies for breast tumor therapy

Due to the limitations of conventional cancer therapy, new therapeutic strategies such as gene therapy, immunotherapy, and hyperthermia therapy has been explored in recent years, which are introduced in detail as follows.

I. Gene therapy

Gene therapy refers to the ability of altered genes or site-specific modification, which is a valid and promising tool to treat different kinds of diseases such as heart disease, diabetes and cancer. Gene therapy works by delivering a healthy copy of a defective gene into patients' cells [26-28]. In order to improve the therapeutic efficiency of delivered genes, vectors have been developed to deliver the gene as shown in Fig. 1.2. The vector is divided into virus and non-viral such as plasmid, nanoparticle, liposome, cationic polymer [29]. Compared with non-viral vectors, the virus has become the most commonly used vectors because of its

high efficiency in invading cells and introducing related genetic materials. Nevertheless, virus vectors always cause strong immune problems [30, 31]. While non-viral vectors will not trigger big immune problem, but it shows low gene transfection efficacy and weak specific target ability, which cannot meet the requirement of gene delivery in the clinic [32, 33].

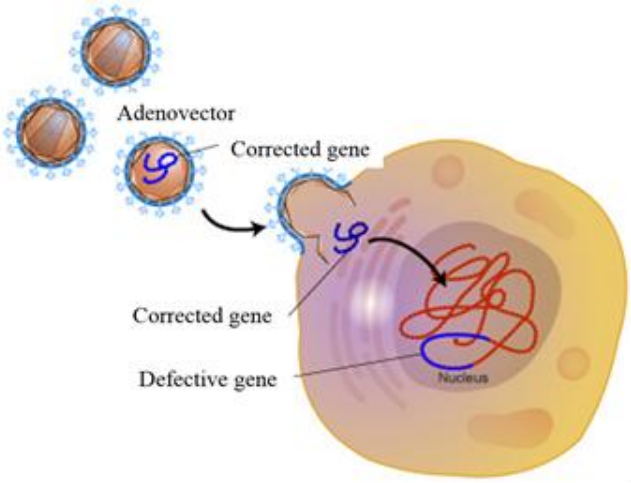

Fig. 1.2 The principle of gene therapy

II. Immunotherapy

Immunotherapy is the use of natural immune system's activation for inhibiting primary and metastatic tumor growth [34]. Since the immunotherapy is firstly discovered by Steven Rosenberg in the late 1980s, immunotherapy has been widely developed and used in the clinic. Based on the immune mechanisms, immunotherapy is divided into several types as shown in Fig. 1.3, which includes monoclonal antibody immunotherapy, checkpoint inhibitor immunotherapy, engineered T cell-mediated immunotherapy and so on [35]. A monoclonal antibody refers to a specific protein and this kind of protein stays in the whole body and then bind to a tumor-associated antigen, further activate the immune system [36]. During immune responses, immune inhibition is always caused by the secretion of CTLA-4, PD-1, and PD-L1, which will inhibit the activation of T cells [37, 38]. In order to increase the number of activated T cells, T cells can be designed to express chimeric antigen receptors (CAR) by genetic engineering and then the engineered CAR-T cells can be injected into patients to activate the immune system and kill tumor cells [39].

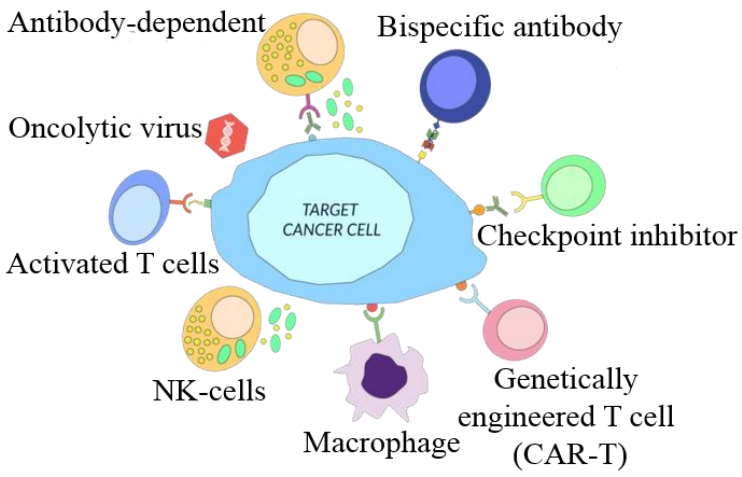

Fig. 1.3 The principle of immunotherapy

III. Hyperthermia therapy

Hyperthermia therapy, known as thermal ablation of the tumor, is based on that high temperature (> 43 ^{o}C) causes tumor cells apoptosis or necrosis by damaging proteins and structure of tumor cells [40]. The successful thermal ablation is preferred that the whole tumor tissue is destroyed while the adjacent normal cells or tissues structure are minimally injured [41]. In order to precisely control the temperature in tumor site, several novel methods including radiofrequency waves, ultrasound, alternative magnetic therapy, and photothermal therapy have been widely explored as shown in Fig. 1.4 [42-45]. The key requirement for thermal technology is that it should be minimally invasive. Appropriate heat depresses the metabolic rate of targeted cells, increases blood flow and also decreases oxygen demand in the tumor. The enhanced permeability of vessel might improve the accumulation of delivered agents in tumor site [46]. Integration of hyperthermia with emerging technologies, such as near infrared (NIR) absorption of nanoparticles, displays more potential of hyperthermia for cancer therapy [47, 48].

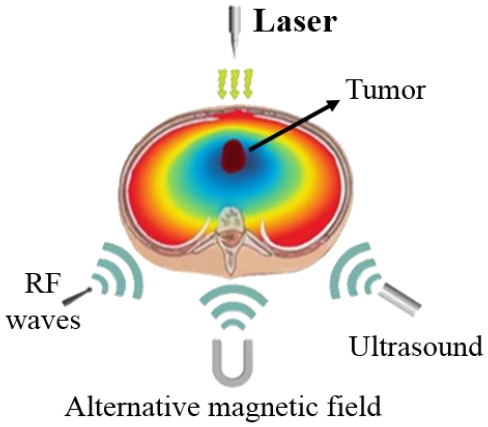

Fig. 1.4 The principle of hyperthermia therapy

1.1.3 Functional biomaterials for breast reconstruction

As above mentioned, all the large breast defects are accompanied by breast tumor resection, which is difficult to self-heal [9]. Therefore, adipose tissue regeneration induced by functional biomaterials is strongly desired to achieve breast reconstruction (Fig. 1.5) [49-51].

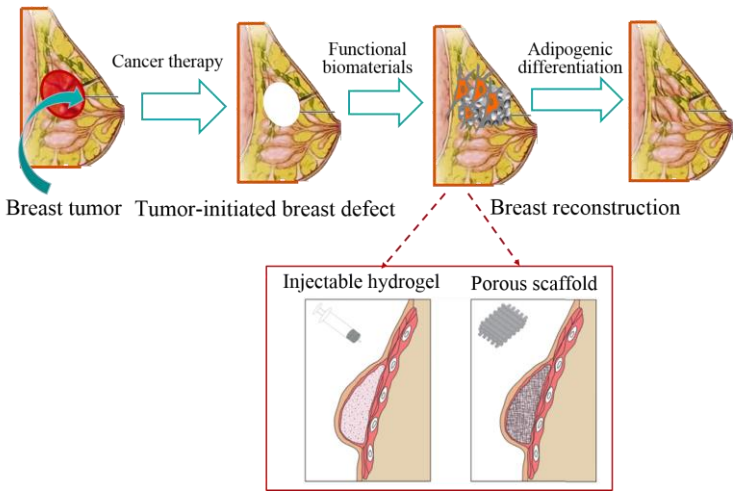

Fig. 1.5 Overview of breast reconstruction: the application of injectable hydrogel and porous scaffold

An ideal strategy for breast reconstruction is the combination of adipose- or bone marrow-derived stem cells with functional biomaterials [52-54]. Moreover, the functional biomaterials should bear soft tissue-like mechanical properties and mimic ECM compounds to regulate the adipogenic differentiation of stem cells [55-59]. Up to date, injectable hydrogels and 3D porous scaffolds have been developed for adipose tissue engineering [60-62]. Injectable hydrogels have been widely used as a matrix platform to encapsulate cells in 3D culture, whose properties effectively mimic ECM microenvironments [63]. More importantly, high water contents in hydrogel provide excellent biocompatibility and soft and rubbery properties of hydrogel closely resemble living tissue [64-66]. 3D porous scaffolds with well-controlled pore structures have also extensively used in adipose tissue regeneration [67]. Cell-cell interactivity in porous scaffolds is critical to stimulate adipose tissue regeneration [68]. The shape of scaffolds is easily remodeled to match with reconstructed tissue [68, 69]. Moreover, the compositions of scaffolds are facilely mediated to promote adipose tissue regeneration [10, 70, 71].

1.2 Photothermal therapy

In recent years, photothermal therapy as a minimally invasive and highly efficient antitumor strategy, has attracted great attention [72]. As shown in Fig. 1.6, photothermal conversion agents produce heat under near infrared laser irradiation, further raise the temperature of tumor and ablate tumor cells [73-75]. In this method, near infrared (NIR) light is preferable because it has high penetration depth (>20 mm) in biological tissue reaching muscle and bone (Fig. 1.6 a) and it also has minimal damage to normal tissue. [76, 77]. In addition, the photothermal agents should have high photothermal conversion efficiency in near infrared region and excellent photothermal ablation efficacy to tumor cells (Fig. 1.6 b). Therefore, the choice and accumulation of photothermal agents in tumor site are critical to effectively ablate the tumor cells.[78, 79].

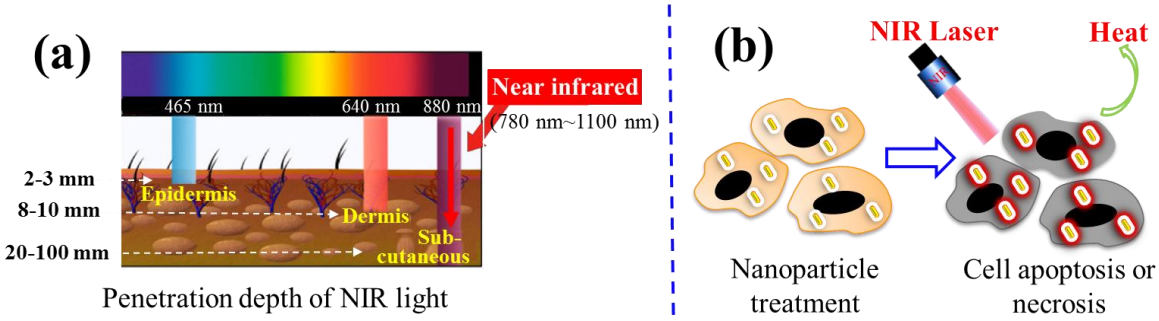

Fig. 1.6 Illustration of photothermal therapy

1.2.1 Nanosystems used for photothermal conversion agents

The ideal photothermal conversion agents should be required to be water soluble, non-cytotoxicity, good photostability, high photothermal conversion efficiency and tumor-enrichment ability [80]. Nowadays, nano-scaled materials (20~300 nm) including organic and inorganic nanomaterial have received much attention due to their enhanced permeability and retention (EPR) effect and tunable surface plasmon resonance (SPR) property [81-83].

As for organic nano-agent, it was divided into several typical classes including NIR dye micelles such as indocyanine green (ICG), porphysomes obtained by self-assembly of porphyrin lipids, protein-based agents such as BSA bound-squaraine (SQ) and HSA bound-IR82, and conjugated polymers such as

polyaniline nanoparticles (PANPs) [84-88] as shown in Fig. 1.7. These organic agents not only have high photothermal conversion efficiency but also have good biocompatibility and appropriate biodegradability [89, 90]. However, there are still some challenges in the future clinical translation such as the poor photothermal stability of ICG and the safety of their degradation product [91].

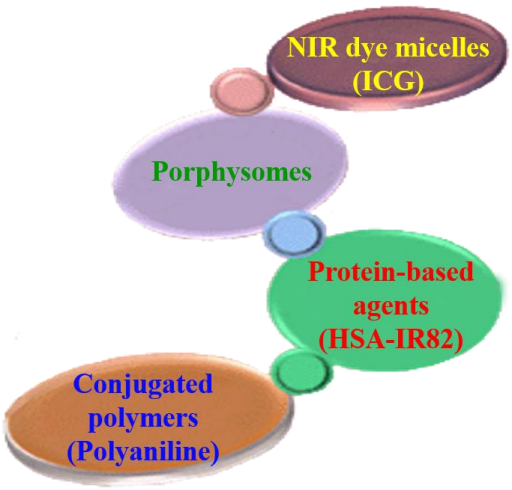

Fig. 1.7 Organic photothermal nano-agents

Compared with organic nano-agents, inorganic nano-agents have received much more attention in recent years. Various inorganic nanoparticles have been widely explored as shown in Fig. 1.8, which including noble metals such as gold nanoparticles, transition metal sulfide or oxide nanoparticles such as CuS and Fe_3O_4, carbon-based nanoparticles such as graphene [92-94]. Among them, gold nanoparticles with a different shape (sphere, rod, and star) and size were widely explored due to their tunable surface plasmon resonance property and facile preparation [95-97]. Despite many these inorganic nano-agents have shown high photothermal therapeutic efficiency in many researches, their non-biodegradability and potential long-term toxicity will restrict their future clinical translation [98].

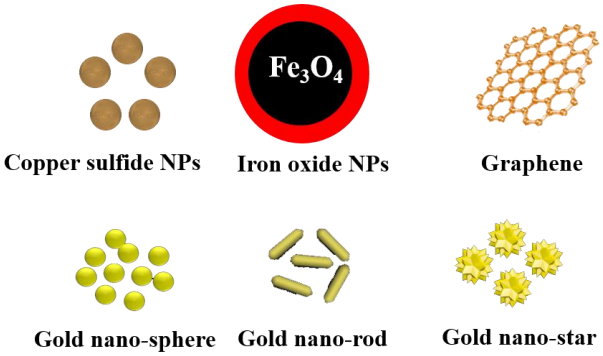

Fig. 1.8 Inorganic photothermal nano-agents

1.2.2 Problems of nanoparticles-mediated photothermal therapy

Although photothermal therapy has been widely developed in recent years due to their high therapeutic efficiency to tumor cells, there are still several problems as follows:

(1) Nanoparticle-mediated photothermal ablation therapy is mainly used in local cancer therapy in currently

used forms. While how the immune responses can be triggered by photothermally ablated tumor cells is still not clear [99, 100].

(2) Although various nanoparticles have shown excellent photothermal conversion efficiency, efficacious and site-specific delivery of free nanoparticles to tumor site is still limited. Upon intravenous injection, most of free nanoparticles undergo uptake by macrophages of the mononuclear phagocyte system and some nanoparticles will distribute to healthy tissue such as liver and spleen, further the accumulation amount of nanoparticles in tumor site is very limited and results in low repeated heating efficiency [45, 101, 102].

1.2.3 Resolution to current problems

In order to address these problems, the reasonable resolution is put forward as follows:

(1). In order to overcome problem 1, the immune responses triggered by photothermal ablated tumor cells should be explored. It has been reported that dead tumor cells and their debris can trigger potent immune responses. Necrotic tumor cells can expose intracellular antigens and release damage associated proteins including calreticulin (CRT), ATP and heat shock protein (HSP) from cytosol and nucleus, which can stimulate systemic immune responses [8, 103, 104]. Apoptotic tumor cells associated with “danger signals” such as heat stress can up-regulate expression of membrane heat shock proteins HSPs (HSP72 and HSP60) and further elicit tumor-specific immunity [105-108]. Then the tumor-related antigens will be uptake by DCs and the released proteins will stimulate the DCs activation, then the mature DCs activate the T cells, subsequently activated T cells will migrate into tumor site and elicit tumor-specific immunity as shown in Fig. 1.9 [37, 109-111]. Therefore, it is desired to investigate if the photothermally ablated tumor cells could induce similar immune responses.

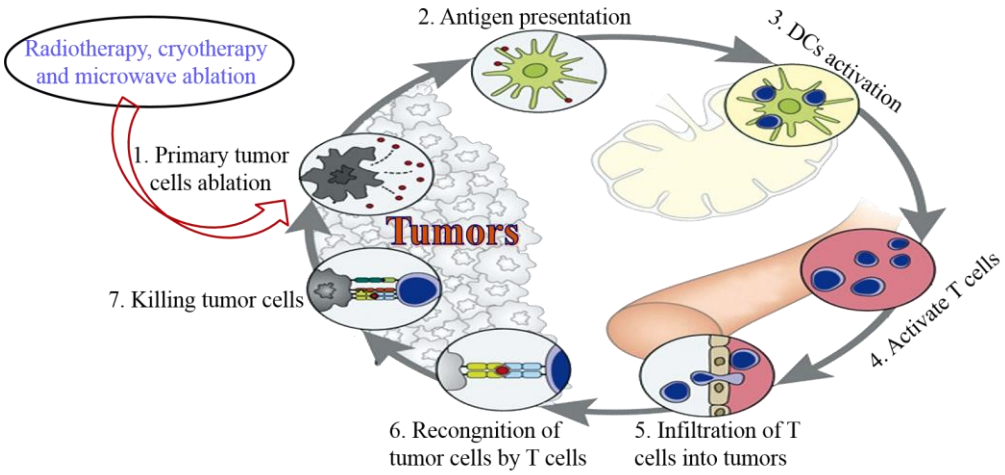

Fig. 1.9 Immune responses triggered by ablated tumor cells

(2). In order to overcome problem 2, some carriers have been explored to load and deliver NPs to the tumor site. Up to now, there are two kinds of carriers: cell-based carriers and scaffold-based carriers. As for the cell-based carriers, the macrophage and stem cells were used to load NPs and migrate to tumor site [112-114]. However this method may cause second malignancy by the implanted cells transformation. As for the scaffold-based carriers, the NPs was immobilized into the scaffold to prepare photothermal scaffold [70]. This method could realize high repeated heating efficiency. And this kind of scaffold could not only ablate tumor cells using their photothermal conversion property but also support normal cells penetration and repair

the tumor-initiated tissue defects after tumor ablation, which has been used for bone and skin cancer therapy [115-117]. So, I will focus on the preparation of photothermal scaffold in my study.

1.3 Bifunctional scaffolds for photothermal therapy and tissue regeneration

As introduced in 1.1.3, large tissue defects are always accompanied with tumor therapy, which is difficult to self-heal. Therefore, it has been developed bifunctional scaffolds for both ablations of tumor and regeneration of new tissue in recent years. Wu. et al. reported that 3D-printed scaffolds of graphene oxide-modified tricalcium phosphate bioceramic showed both excellent photothermal therapy for bone tumor and the regeneration of bone tissue [115]. It has also been reported that electrospun micropatterned PLA/PCL incorporated Cu_2S fiber membranes exhibited skin tumor therapy and wound healing [118]. As a result, bifunctional scaffolds incorporated with photothermal agents has received much attention for photothermal cancer therapy and tissue regeneration.

1.3.1 Immobilization of photothermal agents into scaffolds

Various photothermal agents such as graphene, Cu_2S, polydopamine are immobilized into porous scaffolds using different methods. For example, MoS_2-modified akermanite (AKT) scaffolds were prepared by in situ growing MoS_2 nanosheets on 3D-printed AKT bioceramic scaffolds using hydrothermal reaction [117]. While PLA/PCL incorporated Cu_2S fiber membranes were fabricated by directly mixing PLA/PCL solution with Cu_2S suspension before electrospinning [118]. Therefore, immobilization of photothermal nano-agents into porous scaffolds through various methods will be widely explored in the preparation of bifunctional scaffolds.

1.3.2 Requirement of scaffolds for adipose tissue regeneration

In order to achieve breast reconstruction, the scaffolds should support attachment, penetration, and proliferation and adipogenic differentiation of stem cells [119]. Therefore, scaffolds should meet the following requirements.

I. Biocompatibility

Scaffolds is required to be biocompatible with the cells and adjacent biological tissue [120]. Moreover, scaffolds should be beneficial to the attachment, proliferation and regulating adipogenic differentiation of stem cells [121]. In addition, degradation products of scaffolds should be non-cytoxic and non-inflammatory to cells and surrounding tissues.

II. Proper degradability

Scaffolds should be degradable after implantation and their degradation rate should be matched with the growth rate of new tissues, further the implanted scaffolds should be replaced by the newly formed engineered tissues at last [122, 123].

III. Suitable mechanical property

Scaffolds should bear a certain mechanical strength, which not only support cell growth but also match with the mechanical property of implant-position [124]. As shown in Fig. 1.10, there are various mechanical strength with different organs. The elastic modulus of adipose tissue (0.5~1 kPa) is much lower than that of bone tissue (15000 ~20000 kPa), which indicated the scaffolds used for adipose tissue regeneration should bear soft tissue-like mechanical property [125]. Therefore, gelatin scaffolds have been reported to be

favorable for adipose tissue regeneration due to their low elastic modulus, as compared to stiff scaffolds such as poly(lactic-*co*-glycolic acid) scaffolds [56, 57, 126].

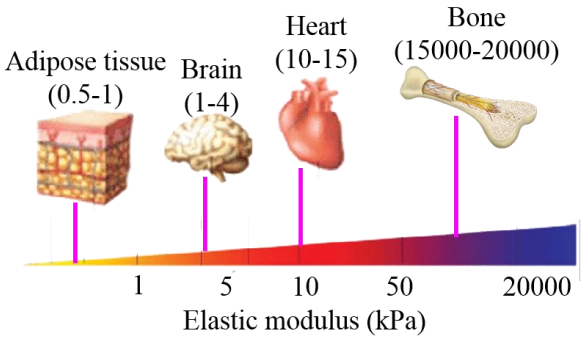

Fig. 1.10 Elastic modulus of different tissue.

IV. Porous structure

3D scaffolds should have an appropriate pore structure with open and interconnected pores to promote cell penetration, distribution and support nutrition and metabolite exchange [127]. Moreover, cell-cell interactivity in porous scaffolds plays critical roles in regulating adipose tissue regeneration [128]. Therefore, the controlled pore structure including proper pore size, well interconnectivity and porosity is urgently required for adipose tissue regeneration.

1.3.3 Fabrication methods of porous structure

As is well known, the suitable pore structure of the scaffolds is good for cell penetration, cell-cell interaction and new tissue formation. Therefore, it has been developed several commonly used methods including electrospinning method, 3D printing method and porogen-based methods for preparing porous scaffold until now [129-131].

I. Electrospinning method

Electrospinning, as a common used electrostatic fiber fabrication technique, has received much attention in recent years [132]. The device used for electrospinning consists of a syringe pump containing polymer solution, a metal collector and a high voltage supplier [133]. Among them, types of polymers and setting of parameters are the key factors which determine the quality and application of electrospun scaffolds. Various polymers such as collagen as typical natural polymer and PLGA polymers as synthetic polymers could be used this method to prepare porous fibers scaffolds for tissue engineering [134, 135]. However, there are some disadvantages such as too small pore size and too small thickness to limit their application [136]. In addition, the organic solvent used in this method has certain toxicity to cells and tissues [137].

II. 3D printing method

3D printing technology has been extensively developed to construct different pore structure of scaffolds in recent years [138]. Many biomaterials including inorganic bioceramic such as hydroxyapatite (HA) and organic polymers such as chitosan and PCL has been used in printing inks to prepare porous scaffolds [139-141]. This method could easily control the pore size, pore shape, and porosity of scaffolds. Moreover, the thickness and shape of the scaffolds could be easily constructed using this method. What's more, the printed pores have well interconnectivity, which is benefit of cell penetration and distribution [142]. However, the expensive equipment is required for 3D printing, which will be limited to the application of this technique.

III. Porogen-based methods

Several common used porogen such as sodium chloride particles, carbon dioxide (CO_2) gas and ice crystals has been developed to construct the porous structure of scaffold recently [143]. The porous scaffolds are prepared by removal of porogen materials from the mixture. Based on different types of porogen, the porogen-based method was divided into particle leaching, gas foaming, and freeze-drying.

Particle leaching method is using calibrated particles as a porogen to obtain pore structure of scaffolds. The calibrated particles consist of NaCl inorganic particle or paraffin organic microspheres, which are facile fabrication and easily removed during preparation process of scaffolds [144]. This method could regulate pore structure of scaffolds by changing the amount, shape and size of the calibrated particles. Nevertheless, there are still some limitations including limited thickness and poor interconnectivity of obtained scaffold. In order to completely remove all the immobilized particles from scaffolds, the thickness of prepared scaffold is usually controlled less than 2 mm. In addition, the immobilized particles is independent and not connected with each other in scaffolds, which results in the poor interconnectivity of scaffold. Moreover, the residue of immobilized particles might result in the toxicity for the cells and tissues.

Gas foaming method is depended on the CO_2 gas with high pressure in polymer disk and quickly releases of CO_2 gas by decreasing pressure to ambient atmospheric pressure within 15 seconds, further form bubbles leading to the formation of highly porous scaffolds [145, 146]. The porosity of porous scaffolds prepared by this method reach to 93%. Nevertheless, there are still some limitations of this method such as closed pore structure and poor interconnectivity.

Freeze-drying is using newly formed ice crystals during freezing process as porogen to obtain the pore structures through sublimation of ice crystals during the freeze-drying process [147]. The freezing rate and temperature could control the pore size and interconnectivity of scaffolds. Although the pore size could be controlled during freezing process, the pores are too small for cell penetration and distribution into porous scaffolds. Moreover, the pore structure is randomly formed in the polymer matrix, which has no certain shape.

In order to solve their limitations, ice particles with proper size as an ideal template to prepare porous scaffolds (Fig. 11) have been explored in recent years [148]. This method is the combination of the particle leaching and freeze-drying methods. In this method, ice particles with proper size are optimized by sieving with different meshes and then mixed with polymer matrix to obtain porous scaffolds through freezing and freeze-drying. In addition, the size of spherical micropores could be well regulated by changing the size of pre-prepared ice particles and the interconnected pores could be formed by the new ice crystals around the ice particulates during freezing process [149]. Moreover, the porosity can be regulated by changing the amount of ice particulates. Therefore, the porous scaffolds with controlled pore size and well interconnectivity could be fabricated by using this method in this study.

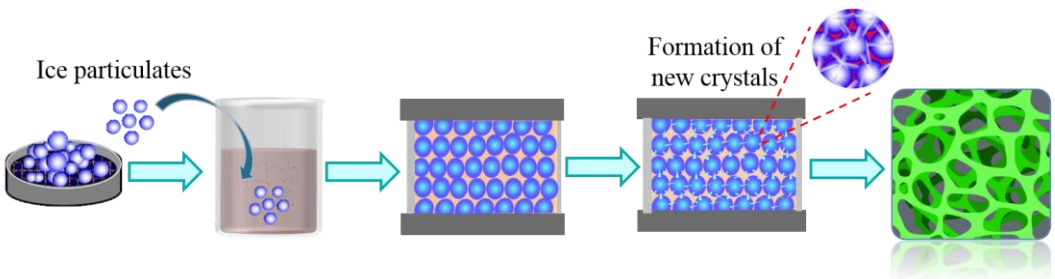

Fig. 1.11 Ice particles as an template to prepare polymer scaffold with controlled pore structure

1.4 Motivation, objective and outline

1.4.1 Motivation and objective

Despite many technical breakthroughs have been made in cancer therapy, complete healing is difficult using traditional therapeutic approaches including surgical resection, chemo- or radio-therapy. An ideal cancer therapeutic strategy should not only eradicate the primary tumor but also induce systemic anti-tumor immunity through activating the immune system to control metastatic tumor and prevent tumor recurrence. Meanwhile, new functional tissues should be reconstructed or regenerated to fill the tumor-initiated breast defects. Therefore, it is strongly desired to design a bifunctional material for effective breast cancer therapy and breast reconstruction.

Photothermal therapy (PPT) as a minimally invasive and highly efficient antitumor strategy has attracted great attention in recent years. However, nanoparticle-mediated photothermal ablation therapy, in currently used forms, has been primarily used in local cancer therapy. It remains unclear how the immune responses can be triggered by photothermal ablated tumor cells, which may be useful for synergistic photothermal-immunotherapy of primary and metastatic cancer. In addition, although various nanoparticles (NPs) have excellent photothermal conversion efficiency, efficacious and site-specific delivery of free NPs to tumor site is still limited. To address these issues, the immobilization of NPs into three-dimensional (3D) scaffolds is necessary. In addition, gelatin-based materials have been used to prepare scaffolds for adipose tissue engineering because of their good biocompatibility and soft tissue-like mechanical property. Moreover, It have been reported that gold nanoparticles might affect the fate of stem cells such as cell phenotype, proliferation and differentiation.

Based on the above background and motivation, the objective of this study is to prepare bifunctional scaffolds that can both ablate tumor cells and promote adipose tissue regeneration. To achieve this objective, this study was divided into three sub-targets as follows:

(1) To evaluate the photothermal ablation effects of BSA-coated AuNRs towards breast tumor cells and investigate the immune responses triggered by photothermally ablated tumor.

(2) To prepare AuNRs-gelatin porous composite scaffolds for photothermal ablation therapy of breast tumor cells and activation of dendritic cells.

(3) To investigate the adipogenic differentiation of hMSCs in the AuNRs-gelatin porous composite scaffolds.

1.4.2 Outline

BSA-coated AuNRs were synthesized and bifunctional scaffolds of AuNRs and gelatin were prepared for breast cancer therapy and adipose tissue regeneration.

In chapter 2, BSA-coated AuNRs were applied to evaluate their photothermal ablation effects after uptake by breast tumor cells. The immune-stimulatory responses of immature DCs triggered by the photothermally ablated tumor cells were investigated by direct co-culture or transwell co-culture of immature DCs and photothermally ablated tumor cells to disclose the involvement of cell–cell interaction and soluble factors in the immune responses of DCs

In chapter 3, AuNRs-gelatin composite scaffolds were used to evaluate their photothermal performance by changing the incorporated Au concentration (0.0, 2.0, 4.0 mM) and varying power intensities of an 805 nm laser. Their photothermal ablation efficiency of breast tumor cells was evaluated by *in vitro* cell culture and *in vivo* animal experiment. Moreover, the immune response of dendritic cells by photothermally ablated

tumor cells in AuNRs-gelatin composite scaffolds was also investigated.

In chapter 4, The influence of AuNRs-gelatin composite porous scaffolds on adhesion, proliferation and adipogenic differentiation including lipid vacuoles formation and adipogenesis-related gene expression of human mesenchymal stem cells (hMSCs) was investigated by culture of hMSCs in the AuNRs-gelatin composite porous scaffolds for 14 days.

In chapter 5, The summary and conclusion supported by this study were described and the future prospect of this study were also proposed.

1.5 References

1. Combellack, E. J.; Jessop, Z. M.; Naderi, N.; Griffin, M.; Dobbs, T.; Ibrahim, A.; Evans, S.; Burnell, S.; Doak, S. H.; Whitaker, I. S., Adipose regeneration and implications for breast reconstruction: update and the future. *Gland surgery* **2016,** 5, (2), 227-41.
2. Li, H.; Wang, K.; Yang, X.; Zhou, Y.; Ping, Q.; Oupicky, D.; Sun, M., Dual-function nanostructured lipid carriers to deliver IR780 for breast cancer treatment: Anti-metastatic and photothermal anti-tumor therapy. *Acta biomaterialia* **2017,** 53, 399-413.
3. Micalizzi, D. S.; Maheswaran, S., On the trail of invasive cells in breast cancer. *Nature* **2018,** 554, (7692), 308-309.
4. Libson, S.; Lippman, M., A review of clinical aspects of breast cancer. *International review of psychiatry (Abingdon, England)* **2014,** 26, (1), 4-15.
5. Li, Y.; He, L.; Dong, H.; Liu, Y.; Wang, K.; Li, A.; Ren, T.; Shi, D.; Li, Y., Fever-Inspired Immunotherapy Based on Photothermal CpG Nanotherapeutics: The Critical Role of Mild Heat in Regulating Tumor Microenvironment. *Advanced science* **2018,** 5, (6), 1700805.
6. Xie, Y.; Ma, X.; Liu, X., Carrier-Free Microspheres of an Anti-Cancer Drug Synthesized via a Sodium Catalyst for Controlled-Release Drug Delivery. *Materials* **2018,** 11, (2), 281.
7. Min, Y.; Roche, K. C.; Tian, S.; Eblan, M. J.; McKinnon, K. P.; Caster, J. M.; Chai, S.; Herring, L. E.; Zhang, L.; Zhang, T.; DeSimone, J. M.; Tepper, J. E.; Vincent, B. G.; Serody, J. S.; Wang, A. Z., Antigen-capturing nanoparticles improve the abscopal effect and cancer immunotherapy. *Nature Nanotechnology* **2017,** 12, 877.
8. Slovak, R.; Ludwig, J. M.; Gettinger, S. N.; Herbst, R. S.; Kim, H. S., Immuno-thermal ablations - boosting the anticancer immune response. *Journal for immunotherapy of cancer* **2017,** 5, (1), 78.
9. Quirke, P.; Durdey, P.; Dixon, M. F.; Williams, N. S., Local recurrence of rectal adenocarcinoma due to inadequate surgical resection. Histopathological study of lateral tumour spread and surgical excision. *Lancet (London, England)* **1986,** 2, (8514), 996-9.
10. Rossi, E.; Guerrero, J.; Aprile, P.; Tocchio, A.; Kappos, E. A.; Gerges, I.; Lenardi, C.; Martin, I.; Scherberich, A., Decoration of RGD-mimetic porous scaffolds with engineered and devitalized extracellular matrix for adipose tissue regeneration. *Acta biomaterialia* **2018,** 73, 154-166.
11. Ruda, R.; Bruno, F.; Soffietti, R., What Have We Learned from Recent Clinical Studies in Low-Grade Gliomas? *Current treatment options in neurology* **2018,** 20, (8), 33.
12. Seton-Rogers, S., A downside of chemotherapy. *Nature Reviews Cancer* **2012,** 13, 5.
13. Sharma, R. A.; Plummer, R.; Stock, J. K.; Greenhalgh, T. A.; Ataman, O.; Kelly, S.; Clay, R.; Adams, R. A.; Baird, R. D.; Billingham, L.; Brown, S. R.; Buckland, S.; Bulbeck, H.; Chalmers, A. J.; Clack, G.; Cranston, A. N.; Damstrup, L.; Ferraldeschi, R.; Forster, M. D.; Golec, J.; Hagan, R. M.; Hall, E.; Hanauske, A.-R.; Harrington, K. J.; Haswell, T.; Hawkins, M. A.; Illidge, T.; Jones, H.; Kennedy, A.

S.; McDonald, F.; Melcher, T.; O'Connor, J. P. B.; Pollard, J. R.; Saunders, M. P.; Sebag-Montefiore, D.; Smitt, M.; Staffurth, J.; Stratford, I. J.; Wedge, S. R.; on behalf of the, N. C. A.-P. J. W. G., Clinical development of new drug–radiotherapy combinations. *Nature Reviews Clinical Oncology* **2016,** 13, 627.

14. Arruebo, M.; Vilaboa, N.; Sáez-Gutierrez, B.; Lambea, J.; Tres, A.; Valladares, M.; González-Fernández, A., Assessment of the evolution of cancer treatment therapies. *Cancers* **2011,** 3, (3), 3279-3330.
15. Huang, B.; Abraham, W. D.; Zheng, Y.; Bustamante López, S. C.; Luo, S. S.; Irvine, D. J., Active targeting of chemotherapy to disseminated tumors using nanoparticle-carrying T cells. *Science translational medicine* **2015,** 7, (291), 291ra94-291ra94.
16. El-Sayed, I. H.; Huang, X.; El-Sayed, M. A., Selective laser photo-thermal therapy of epithelial carcinoma using anti-EGFR antibody conjugated gold nanoparticles. *Cancer letters* **2006,** 239, (1), 129-35.
17. Johnson, I. S.; Armstrong, J. G.; Gorman, M.; Burnett, J. P., Jr., THE VINCA ALKALOIDS: A NEW CLASS OF ONCOLYTIC AGENTS. *Cancer research* **1963,** 23, 1390-427.
18. Heidelberger, C.; Chaudhuri, N. K.; Danneberg, P.; Mooren, D.; Griesbach, L.; Duschinsky, R.; Schnitzer, R. J.; Pleven, E.; Scheiner, J., Fluorinated Pyrimidines, A New Class of Tumour-Inhibitory Compounds. *Nature* **1957,** 179, (4561), 663-666.
19. Chen, Q.; Liang, C.; Wang, C.; Liu, Z., An imagable and photothermal "Abraxane-like" nanodrug for combination cancer therapy to treat subcutaneous and metastatic breast tumors. *Advanced materials* **2015,** 27, (5), 903-10.
20. Jones, S. E.; Durie, B. G.; Salmon, S. E., Combination chemotherapy with adriamycin and cyclophosphamide for advanced breast cancer. *Cancer* **1975,** 36, (1), 90-7.
21. Fan, L.; Liu, W.-C.; Zhang, Y.-J.; Ren, J.; Pan, B.-R.; Liu, D.-H.; Chen, Y.; Yu, Z.-C., Oral Xeloda plus bi-platinu two-way combined chemotherapy in treatment of advanced gastrointestinal malignancies. *World journal of gastroenterology* **2005,** 11, (28), 4300-4304.
22. Demain, A. L.; Vaishnav, P., Natural products for cancer chemotherapy. *Microbial biotechnology* **2011,** 4, (6), 687-699.
23. Huang, C.-Y.; Ju, D.-T.; Chang, C.-F.; Muralidhar Reddy, P.; Velmurugan, B. K., A review on the effects of current chemotherapy drugs and natural agents in treating non-small cell lung cancer. *BioMedicine* **2017,** 7, (4), 23-23.
24. Baskar, R.; Lee, K. A.; Yeo, R.; Yeoh, K. W., Cancer and radiation therapy: current advances and future directions. *International journal of medical sciences* **2012,** 9, (3), 193-9.
25. Yang, Y.-S.; Carney, R. P.; Stellacci, F.; Irvine, D. J., Enhancing Radiotherapy by Lipid Nanocapsule-Mediated Delivery of Amphiphilic Gold Nanoparticles to Intracellular Membranes. *ACS Nano* **2014,** 8, (9), 8992-9002.
26. Hanna, E.; Rémuzat, C.; Auquier, P.; Toumi, M., Gene therapies development: slow progress and promising prospect. *Journal of market access & health policy* **2017,** 5, (1), 1265293-1265293.
27. Manjila, S. B.; Baby, J. N.; Bijin, E. N.; Constantine, I.; Pramod, K.; Valsalakumari, J., Novel gene delivery systems. *International journal of pharmaceutical investigation* **2013,** 3, (1), 1-7.
28. Ginn, S. L.; Amaya, A. K.; Alexander, I. E.; Edelstein, M.; Abedi, M. R., Gene therapy clinical trials worldwide to 2017: An update. *The journal of gene medicine* **2018,** 20, (5), e3015.
29. Thomas, C. E.; Ehrhardt, A.; Kay, M. A., Progress and problems with the use of viral vectors for gene therapy. *Nature reviews. Genetics* **2003,** 4, (5), 346-58.

30. Yang, Y.; Zhao, H.; Jia, Y.; Guo, Q.; Qu, Y.; Su, J.; Lu, X.; Zhao, Y.; Qian, Z., A novel gene delivery composite system based on biodegradable folate-poly (ester amine) polymer and thermosensitive hydrogel for sustained gene release. *Scientific Reports* **2016,** 6, 21402.
31. Jeevanandam, J.; Pal, K.; Danquah, M. K., Virus-like nanoparticles as a novel delivery tool in gene therapy. *Biochimie* **2019,** 157, 38-47.
32. Li, S.; Huang, L., Nonviral gene therapy: promises and challenges. *Gene therapy* **2000,** 7, (1), 31-4.
33. Fewell, J. G.; Matar, M.; Slobodkin, G.; Han, S. O.; Rice, J.; Hovanes, B.; Lewis, D. H.; Anwer, K., Synthesis and application of a non-viral gene delivery system for immunogene therapy of cancer. *Journal of controlled release : official journal of the Controlled Release Society* **2005,** 109, (1-3), 288-98.
34. Rosenberg, S. A.; Yang, J. C.; Restifo, N. P., Cancer immunotherapy: moving beyond current vaccines. *Nature medicine* **2004,** 10, (9), 909-915.
35. Sabado, R. L.; Balan, S.; Bhardwaj, N., Dendritic cell-based immunotherapy. *Cell Research* **2016,** 27, 74.
36. Adams, G. P.; Weiner, L. M., Monoclonal antibody therapy of cancer. *Nature biotechnology* **2005,** 23, (9), 1147-57.
37. Ascierto, P. A.; Addeo, R.; Carten ̀, G.; Daniele, B.; De Laurentis, M.; Ianniello, G. P.; Morabito, A.; Palmieri, G.; Pepe, S.; Perrone, F.; Pignata, S.; Montesarchio, V., The role of immunotherapy in solid tumors: report from the Campania Society of Oncology Immunotherapy (SCITO) meeting, Naples 2014. *Journal of translational medicine* **2014,** 12, 291-291.
38. Rosenzweig, N.; Dvir-Szternfeld, R.; Tsitsou-Kampeli, A.; Keren-Shaul, H.; Ben-Yehuda, H.; Weill-Raynal, P.; Cahalon, L.; Kertser, A.; Baruch, K.; Amit, I.; Weiner, A.; Schwartz, M., PD-1/PD-L1 checkpoint blockade harnesses monocyte-derived macrophages to combat cognitive impairment in a tauopathy mouse model. *Nature Communications* **2019,** 10, (1), 465.
39. Hucks, G.; Rheingold, S. R., The journey to CAR T cell therapy: the pediatric and young adult experience with relapsed or refractory B-ALL. *Blood Cancer Journal* **2019,** 9, (2), 10.
40. Strohbehn, J. W.; Douple, E. B., Hyperthermia and cancer therapy: a review of biomedical engineering contributions and challenges. *IEEE transactions on bio-medical engineering* **1984,** 31, (12), 779-87.
41. Luk, K. H.; Hulse, R. M.; Phillips, T. L., Hyperthermia in cancer therapy. *The Western journal of medicine* **1980,** 132, (3), 179-185.
42. Kennedy, J. E., High-intensity focused ultrasound in the treatment of solid tumours. *Nature reviews. Cancer* **2005,** 5, (4), 321-7.
43. Ahmed, H. U.; Zacharakis, E.; Dudderidge, T.; Armitage, J. N.; Scott, R.; Calleary, J.; Illing, R.; Kirkham, A.; Freeman, A.; Ogden, C.; Allen, C.; Emberton, M., High-intensity-focused ultrasound in the treatment of primary prostate cancer: the first UK series. *British journal of cancer* **2009,** 101, (1), 19-26.
44. Das, P.; Colombo, M.; Prosperi, D., Recent advances in magnetic fluid hyperthermia for cancer therapy. *Colloids and surfaces. B, Biointerfaces* **2018,** 174, 42-55.
45. Hsiao, C. W.; Chuang, E. Y.; Chen, H. L.; Wan, D.; Korupalli, C.; Liao, Z. X.; Chiu, Y. L.; Chia, W. T.; Lin, K. J.; Sung, H. W., Photothermal tumor ablation in mice with repeated therapy sessions using NIR-absorbing micellar hydrogels formed in situ. *Biomaterials* **2015,** 56, 26-35.
46. Griffin, R. J.; Dings, R. P.; Jamshidi-Parsian, A.; Song, C. W., Mild temperature hyperthermia and radiation therapy: role of tumour vascular thermotolerance and relevant physiological factors.

International journal of hyperthermia : the official journal of European Society for Hyperthermic Oncology, North American Hyperthermia Group **2010,** 26, (3), 256-63.

47. Kumar, S.; Srivastava, A., Numerical investigation of thermal response of laser irradiated tissue phantoms embedded with optical inhomogeneities. *International Journal of Heat and Mass Transfer* **2014,** 77, 262-277.
48. Oldenburg, S. J.; Averitt, R. D.; Westcott, S. L.; Halas, N. J., Nanoengineering of optical resonances. *Chemical Physics Letters* **1998,** 288, (2), 243-247.
49. Van Nieuwenhove, I.; Tytgat, L.; Ryx, M.; Blondeel, P.; Stillaert, F.; Thienpont, H.; Ottevaere, H.; Dubruel, P.; Van Vlierberghe, S., Soft tissue fillers for adipose tissue regeneration: From hydrogel development toward clinical applications. *Acta biomaterialia* **2017,** 63, 37-49.
50. Unnithan, A. R.; Sasikala, A. R. K.; Thomas, S. S.; Nejad, A. G.; Cha, Y. S.; Park, C. H.; Kim, C. S., Strategic Design and Fabrication of Biomimetic 3D Scaffolds: Unique Architectures of Extracellular Matrices for Enhanced Adipogenesis and Soft Tissue Reconstruction. *Scientific Reports* **2018,** 8, (1), 5696.
51. Ogino, S.; Morimoto, N., Development of a novel bioabsorbable implant that is substituted by adipose tissue in vivo. **2018,** 12, (3), 633-641.
52. Gimble, J. M.; Katz, A. J.; Bunnell, B. A., Adipose-derived stem cells for regenerative medicine. *Circulation research* **2007,** 100, (9), 1249-60.
53. Gomillion, C. T.; Burg, K. J., Stem cells and adipose tissue engineering. *Biomaterials* **2006,** 27, (36), 6052-63.
54. Zuk, P. A.; Zhu, M.; Ashjian, P.; De Ugarte, D. A.; Huang, J. I.; Mizuno, H.; Alfonso, Z. C.; Fraser, J. K.; Benhaim, P.; Hedrick, M. H., Human adipose tissue is a source of multipotent stem cells. *Molecular biology of the cell* **2002,** 13, (12), 4279-95.
55. Stosich, M. S.; Bastian, B.; Marion, N. W.; Clark, P. A.; Reilly, G.; Mao, J. J., Vascularized adipose tissue grafts from human mesenchymal stem cells with bioactive cues and microchannel conduits. *Tissue engineering* **2007,** 13, (12), 2881-2890.
56. Hong, L.; Peptan, I.; Clark, P.; Mao, J. J., Ex Vivo Adipose Tissue Engineering by Human Marrow Stromal Cell Seeded Gelatin Sponge. *Annals of Biomedical Engineering* **2005,** 33, (4), 511-517.
57. Kimura, Y.; Ozeki, M.; Inamoto, T.; Tabata, Y., Adipose tissue engineering based on human preadipocytes combined with gelatin microspheres containing basic fibroblast growth factor. *Biomaterials* **2003,** 24, (14), 2513-21.
58. Kimura, Y.; Inamoto, T.; Tabata, Y., Adipose tissue formation in collagen scaffolds with different biodegradabilities. *Journal of biomaterials science. Polymer edition* **2010,** 21, (4), 463-76.
59. Kimura, Y.; Tsuji, W.; Yamashiro, H.; Toi, M.; Inamoto, T.; Tabata, Y., In situ adipogenesis in fat tissue augmented by collagen scaffold with gelatin microspheres containing basic fibroblast growth factor. *Journal of tissue engineering and regenerative medicine* **2010,** 4, (1), 55-61.
60. Kona, S.; Wadajkar, A. S.; Nguyen, K. T., 6 - Tissue engineering applications of injectable biomaterials. In *Injectable Biomaterials*, Vernon, B., Ed. Woodhead Publishing: 2011; pp 142-182.
61. Fu, Y.; Kao, W. J., In situ forming poly(ethylene glycol)-based hydrogels via thiol-maleimide Michael-type addition. *Journal of biomedical materials research. Part A* **2011,** 98, (2), 201-211.
62. Cheung, H. K.; Han, T. T. Y.; Marecak, D. M.; Watkins, J. F.; Amsden, B. G.; Flynn, L. E., Composite hydrogel scaffolds incorporating decellularized adipose tissue for soft tissue engineering with adipose-derived stem cells. *Biomaterials* **2014,** 35, (6), 1914-1923.
63. Sivashanmugam, A.; Arun Kumar, R.; Vishnu Priya, M.; Nair, S. V.; Jayakumar, R., An overview of

injectable polymeric hydrogels for tissue engineering. *European Polymer Journal* **2015,** 72, 543-565.

64. Peppas, N. A.; Hoffman, A. S., Chapter I.2.5 - Hydrogels. In *Biomaterials Science (Third Edition)*, Ratner, B. D.; Hoffman, A. S.; Schoen, F. J.; Lemons, J. E., Eds. Academic Press: 2013; pp 166-179.
65. Seliktar, D., Designing cell-compatible hydrogels for biomedical applications. *Science (New York, N.Y.)* **2012,** 336, (6085), 1124-8.
66. Van Vlierberghe, S.; Dubruel, P.; Schacht, E., Biopolymer-based hydrogels as scaffolds for tissue engineering applications: a review. *Biomacromolecules* **2011,** 12, (5), 1387-408.
67. Flynn, L.; Woodhouse, K. A., Adipose tissue engineering with cells in engineered matrices. *Organogenesis* **2008,** 4, (4), 228-35.
68. Pati, F.; Ha, D.-H.; Jang, J.; Han, H. H.; Rhie, J.-W.; Cho, D.-W., Biomimetic 3D tissue printing for soft tissue regeneration. *Biomaterials* **2015,** 62, 164-175.
69. Gruene, M.; Pflaum, M.; Deiwick, A.; Koch, L.; Schlie, S.; Unger, C.; Wilhelmi, M.; Haverich, A.; Chichkov, B. N., Adipogenic differentiation of laser-printed 3D tissue grafts consisting of human adipose-derived stem cells. *Biofabrication* **2011,** 3, (1), 015005.
70. Ma, H.; Feng, C.; Chang, J.; Wu, C., 3D-printed bioceramic scaffolds: From bone tissue engineering to tumor therapy. *Acta biomaterialia* **2018,** 79, 37-59.
71. Kolle, S. F.; Fischer-Nielsen, A.; Mathiasen, A. B.; Elberg, J. J.; Oliveri, R. S.; Glovinski, P. V.; Kastrup, J.; Kirchhoff, M.; Rasmussen, B. S.; Talman, M. L.; Thomsen, C.; Dickmeiss, E.; Drzewiecki, K. T., Enrichment of autologous fat grafts with ex-vivo expanded adipose tissue-derived stem cells for graft survival: a randomised placebo-controlled trial. *Lancet (London, England)* **2013,** 382, (9898), 1113-20.
72. Cheng, L.; Wang, C.; Feng, L.; Yang, K.; Liu, Z., Functional nanomaterials for phototherapies of cancer. *Chemical reviews* **2014,** 114, (21), 10869-939.
73. Zou, L.; Wang, H.; He, B.; Zeng, L.; Tan, T.; Cao, H.; He, X.; Zhang, Z.; Guo, S.; Li, Y., Current Approaches of Photothermal Therapy in Treating Cancer Metastasis with Nanotherapeutics. *Theranostics* **2016,** 6, (6), 762-772.
74. Sun, M.; Peng, D.; Hao, H.; Hu, J.; Wang, D.; Wang, K.; Liu, J.; Guo, X.; Wei, Y.; Gao, W., Thermally Triggered in Situ Assembly of Gold Nanoparticles for Cancer Multimodal Imaging and Photothermal Therapy. *ACS applied materials & interfaces* **2017,** 9, (12), 10453-10460.
75. Abadeer, N. S.; Murphy, C. J., Recent Progress in Cancer Thermal Therapy Using Gold Nanoparticles. *The Journal of Physical Chemistry C* **2016,** 120, (9), 4691-4716.
76. Huang, Y.; Chen, C.; Li, H.; Xiao, A.; Guo, T.; Guan, B.-O., Insight into the local near-infrared photothermal dynamics of graphene oxide functionalized polymers through optical microfibers. *Physical Chemistry Chemical Physics* **2018,** 20, (7), 5256-5263.
77. Shirata, C.; Kaneko, J.; Inagaki, Y.; Kokudo, T.; Sato, M.; Kiritani, S.; Akamatsu, N.; Arita, J.; Sakamoto, Y.; Hasegawa, K.; Kokudo, N., Near-infrared photothermal/photodynamic therapy with indocyanine green induces apoptosis of hepatocellular carcinoma cells through oxidative stress. *Scientific Reports* **2017,** 7, (1), 13958.
78. Ren, Y.; Chen, Q.; Qi, H.; Ruan, L., Experimental Comparison of Photothermal Conversion Efficiency of Gold Nanotriangle and Nanorod in Laser Induced Thermal Therapy. *Nanomaterials (Basel, Switzerland)* **2017,** 7, (12), 416.
79. Guo, L.; Liu, W.; Niu, G.; Zhang, P.; Zheng, X.; Jia, Q.; Zhang, H.; Ge, J.; Wang, P., Polymer nanoparticles with high photothermal conversion efficiency as robust photoacoustic and thermal

theranostics. *Journal of Materials Chemistry B* **2017,** 5, (15), 2832-2839.

80. Hu, J.-J.; Cheng, Y.-J.; Zhang, X.-Z., Recent advances in nanomaterials for enhanced photothermal therapy of tumors. *Nanoscale* **2018,** 10, (48), 22657-22672.
81. Jaque, D.; Martínez Maestro, L.; del Rosal, B.; Haro-Gonzalez, P.; Benayas, A.; Plaza, J. L.; Martín Rodríguez, E.; García Solé, J., Nanoparticles for photothermal therapies. *Nanoscale* **2014,** 6, (16), 9494-9530.
82. Gobin, A. M.; Watkins, E. M.; Quevedo, E.; Colvin, V. L.; West, J. L., Near-infrared-resonant gold/gold sulfide nanoparticles as a photothermal cancer therapeutic agent. *Small (Weinheim an der Bergstrasse, Germany)* **2010,** 6, (6), 745-52.
83. Chen, J.; Ning, C.; Zhou, Z.; Yu, P.; Zhu, Y.; Tan, G.; Mao, C., Nanomaterials as photothermal therapeutic agents. *Progress in Materials Science* **2019,** 99, 1-26.
84. Wang, X.; Li, H.; Liu, X.; Tian, Y.; Guo, H.; Jiang, T.; Luo, Z.; Jin, K.; Kuai, X.; Liu, Y.; Pang, Z.; Yang, W.; Shen, S., Enhanced photothermal therapy of biomimetic polypyrrole nanoparticles through improving blood flow perfusion. *Biomaterials* **2017,** 143, 130-141.
85. Robinson, J. T.; Tabakman, S. M.; Liang, Y.; Wang, H.; Casalongue, H. S.; Vinh, D.; Dai, H., Ultrasmall reduced graphene oxide with high near-infrared absorbance for photothermal therapy. *Journal of the American Chemical Society* **2011,** 133, (17), 6825-31.
86. Poinard, B.; Neo, S. Z. Y.; Yeo, E. L. L.; Heng, H. P. S.; Neoh, K. G.; Kah, J. C. Y., Polydopamine Nanoparticles Enhance Drug Release for Combined Photodynamic and Photothermal Therapy. *ACS applied materials & interfaces* **2018,** 10, (25), 21125-21136.
87. Chen, Z.; Wang, Q.; Wang, H.; Zhang, L.; Song, G.; Song, L.; Hu, J.; Wang, H.; Liu, J.; Zhu, M.; Zhao, D., Ultrathin PEGylated W18O49 nanowires as a new 980 nm-laser-driven photothermal agent for efficient ablation of cancer cells in vivo. *Advanced materials* **2013,** 25, (14), 2095-100.
88. Wang, S.; Li, K.; Chen, Y.; Chen, H.; Ma, M.; Feng, J.; Zhao, Q.; Shi, J., Biocompatible PEGylated MoS2 nanosheets: controllable bottom-up synthesis and highly efficient photothermal regression of tumor. *Biomaterials* **2015,** 39, 206-17.
89. Jung, H. S.; Verwilst, P.; Sharma, A.; Shin, J.; Sessler, J. L.; Kim, J. S., Organic molecule-based photothermal agents: an expanding photothermal therapy universe. *Chemical Society Reviews* **2018,** 47, (7), 2280-2297.
90. Zhou, B.; Li, Y.; Niu, G.; Lan, M.; Jia, Q.; Liang, Q., Near-Infrared Organic Dye-Based Nanoagent for the Photothermal Therapy of Cancer. *ACS applied materials & interfaces* **2016,** 8, (44), 29899-29905.
91. Zheng, M.; Zhao, P.; Luo, Z.; Gong, P.; Zheng, C.; Zhang, P.; Yue, C.; Gao, D.; Ma, Y.; Cai, L., Robust ICG Theranostic Nanoparticles for Folate Targeted Cancer Imaging and Highly Effective Photothermal Therapy. *ACS applied materials & interfaces* **2014,** 6, (9), 6709-6716.
92. Bao, Z.; Liu, X.; Liu, Y.; Liu, H.; Zhao, K., Near-infrared light-responsive inorganic nanomaterials for photothermal therapy. *Asian Journal of Pharmaceutical Sciences* **2016,** 11, (3), 349-364.
93. Estelrich, J.; Busquets, M. A., Iron Oxide Nanoparticles in Photothermal Therapy. **2018,** 23, (7).
94. Ben Salem, S.; Achour, Z. B.; Thamri, K.; Touayar, O., Study and characterization of porous copper oxide produced by electrochemical anodization for radiometric heat absorber. *Nanoscale research letters* **2014,** 9, (1), 577-577.
95. Gharatape, A.; Davaran, S.; Salehi, R.; Hamishehkar, H., Engineered gold nanoparticles for photothermal cancer therapy and bacteria killing. *RSC Advances* **2016,** 6, (112), 111482-111516.
96. Wu, Y.; Ali, M. R. K.; Dong, B.; Han, T.; Chen, K.; Chen, J.; Tang, Y.; Fang, N.; Wang, F.; El-Sayed,

M. A., Gold Nanorod Photothermal Therapy Alters Cell Junctions and Actin Network in Inhibiting Cancer Cell Collective Migration. *ACS Nano* **2018,** 12, (9), 9279-9290.

97. Park, J.-E.; Atobe, M.; Fuchigami, T., Synthesis of multiple shapes of gold nanoparticles with controlled sizes in aqueous solution using ultrasound. *Ultrasonics Sonochemistry* **2006,** 13, (3), 237-241.
98. Cherukula, K.; Manickavasagam Lekshmi, K.; Uthaman, S.; Cho, K.; Cho, C. S.; Park, I. K., Multifunctional Inorganic Nanoparticles: Recent Progress in Thermal Therapy and Imaging. *Nanomaterials (Basel)* **2016,** 6, (4).
99. Chen, Q.; Xu, L.; Liang, C.; Wang, C.; Peng, R.; Liu, Z., Photothermal therapy with immune-adjuvant nanoparticles together with checkpoint blockade for effective cancer immunotherapy. *Nature Communications* **2016,** 7, 13193.
100. Yang, G.; Xu, L.; Chao, Y.; Xu, J.; Sun, X.; Wu, Y.; Peng, R.; Liu, Z., Hollow MnO2 as a tumor-microenvironment-responsive biodegradable nano-platform for combination therapy favoring antitumor immune responses. *Nature Communications* **2017,** 8, (1), 902.
101. Blanco, E.; Shen, H.; Ferrari, M., Principles of nanoparticle design for overcoming biological barriers to drug delivery. *Nature biotechnology* **2015,** 33, (9), 941-51.
102. Snipstad, S.; Hak, S.; Baghirov, H.; Sulheim, E.; Morch, Y.; Lelu, S.; von Haartman, E.; Back, M.; Nilsson, K. P. R.; Klymchenko, A. S.; de Lange Davies, C.; Aslund, A. K. O., Labeling nanoparticles: Dye leakage and altered cellular uptake. *Cytometry. Part A : the journal of the International Society for Analytical Cytology* **2017,** 91, (8), 760-766.
103. Larmonier, N.; Merino, D.; Nicolas, A.; Cathelin, D.; Besson, A.; Bateman, A.; Solary, E.; Martin, F.; Katsanis, E.; Bonnotte, B., Apoptotic, necrotic, or fused tumor cells: an equivalent source of antigen for dendritic cell loading. *Apoptosis : an international journal on programmed cell death* **2006,** 11, (9), 1513-24.
104. Ogawa, M.; Tomita, Y.; Nakamura, Y.; Lee, M. J.; Lee, S.; Tomita, S.; Nagaya, T.; Sato, K.; Yamauchi, T.; Iwai, H.; Kumar, A.; Haystead, T.; Shroff, H.; Choyke, P. L.; Trepel, J. B.; Kobayashi, H., Immunogenic cancer cell death selectively induced by near infrared photoimmunotherapy initiates host tumor immunity. *Oncotarget* **2017,** 8, (6), 10425-10436.
105. Feng, H.; Zeng, Y.; Whitesell, L.; Katsanis, E., Stressed apoptotic tumor cells express heat shock proteins and elicit tumor-specific immunity. *Blood* **2001,** 97, (11), 3505-12.
106. Feng, H.; Zeng, Y.; Graner, M. W.; Katsanis, E., Stressed apoptotic tumor cells stimulate dendritic cells and induce specific cytotoxic T cells. *Blood* **2002,** 100, (12), 4108-15.
107. Feng, H.; Zeng, Y.; Graner, M. W.; Likhacheva, A.; Katsanis, E., Exogenous stress proteins enhance the immunogenicity of apoptotic tumor cells and stimulate antitumor immunity. *Blood* **2003,** 101, (1), 245-52.
108. Garg, A. D.; Agostinis, P., Cell death and immunity in cancer: From danger signals to mimicry of pathogen defense responses. *Immunological reviews* **2017,** 280, (1), 126-148.
109. <CW_76-Grandround.pdf>.
110. Banchereau, J.; Steinman, R. M., Dendritic cells and the control of immunity. *Nature* **1998,** 392, (6673), 245-52.
111. Shimamura, H.; Sunamura, M.; Tsuchihara, K.; Egawa, S.; Takeda, K.; Matsuno, S., Irradiated pancreatic cancer cells undergo both apoptosis and necrosis, and could be phagocytized by dendritic cells. *European surgical research. Europaische chirurgische Forschung. Recherches chirurgicales europeennes* **2005,** 37, (4), 228-34.

112. Li, Z.; Huang, H.; Tang, S.; Li, Y.; Yu, X. F.; Wang, H.; Li, P.; Sun, Z.; Zhang, H.; Liu, C.; Chu, P. K., Small gold nanorods laden macrophages for enhanced tumor coverage in photothermal therapy. *Biomaterials* **2016,** 74, 144-54.
113. Choi, J.; Kim, H. Y.; Ju, E. J.; Jung, J.; Park, J.; Chung, H. K.; Lee, J. S.; Lee, J. S.; Park, H. J.; Song, S. Y.; Jeong, S. Y.; Choi, E. K., Use of macrophages to deliver therapeutic and imaging contrast agents to tumors. *Biomaterials* **2012,** 33, (16), 4195-203.
114. Kang, S.; Bhang, S. H.; Hwang, S.; Yoon, J. K.; Song, J.; Jang, H. K.; Kim, S.; Kim, B. S., Mesenchymal Stem Cells Aggregate and Deliver Gold Nanoparticles to Tumors for Photothermal Therapy. *ACS Nano* **2015,** 9, (10), 9678-90.
115. Ma, H.; Jiang, C.; Zhai, D.; Luo, Y.; Chen, Y.; Lv, F.; Yi, Z.; Deng, Y.; Wang, J.; Chang, J., A bifunctional biomaterial with photothermal effect for tumor therapy and bone regeneration. *Advanced Functional Materials* **2016,** 26, (8), 1197-1208.
116. Ma, H.; Luo, J.; Sun, Z.; Xia, L.; Shi, M.; Liu, M.; Chang, J.; Wu, C., 3D printing of biomaterials with mussel-inspired nanostructures for tumor therapy and tissue regeneration. *Biomaterials* **2016,** 111, 138-148.
117. Wang, X.; Li, T.; Ma, H.; Zhai, D.; Jiang, C.; Chang, J.; Wang, J.; Wu, C., A 3D-printed scaffold with MoS2 nanosheets for tumor therapy and tissue regeneration. *Npg Asia Materials* **2017,** 9, e376.
118. Wang, X.; Lv, F.; Li, T.; Han, Y.; Yi, Z.; Liu, M.; Chang, J., Electrospun Micropatterned Nanocomposites Incorporated with Cu2S Nanoflowers for Skin Tumor Therapy and Wound Healing. **2017,** 11, (11), 11337-11349.
119. Yu, C.; Bianco, J.; Brown, C.; Fuetterer, L.; Watkins, J. F.; Samani, A.; Flynn, L. E., Porous decellularized adipose tissue foams for soft tissue regeneration. *Biomaterials* **2013,** 34, (13), 3290-302.
120. Naahidi, S.; Jafari, M.; Logan, M.; Wang, Y.; Yuan, Y.; Bae, H.; Dixon, B.; Chen, P., Biocompatibility of hydrogel-based scaffolds for tissue engineering applications. *Biotechnology Advances* **2017,** 35, (5), 530-544.
121. Galli, C.; Parisi, L.; Piergianni, M.; Smerieri, A.; Passeri, G.; Guizzardi, S.; Costa, F.; Lumetti, S.; Manfredi, E.; Macaluso, G. M., Improved scaffold biocompatibility through anti-Fibronectin aptamer functionalization. *Acta biomaterialia* **2016,** 42, 147-156.
122. Sung, H. J.; Meredith, C.; Johnson, C.; Galis, Z. S., The effect of scaffold degradation rate on three-dimensional cell growth and angiogenesis. *Biomaterials* **2004,** 25, (26), 5735-42.
123. Zhang, H.; Zhou, L.; Zhang, W., Control of scaffold degradation in tissue engineering: a review. *Tissue engineering. Part B, Reviews* **2014,** 20, (5), 492-502.
124. Velasco, M. A.; Lancheros, Y.; Garzón-Alvarado, D. A., Geometric and mechanical properties evaluation of scaffolds for bone tissue applications designing by a reaction-diffusion models and manufactured with a material jetting system. *Journal of Computational Design and Engineering* **2016,** 3, (4), 385-397.
125. Akhtar, R.; Sherratt, M. J.; Cruickshank, J. K.; Derby, B., Characterizing the elastic properties of tissues. *Materials today (Kidlington, England)* **2011,** 14, (3), 96-105.
126. Flynn, L.; Woodhouse, K. A., Adipose tissue engineering with cells in engineered matrices. *Organogenesis* **2008,** 4, (4), 228-235.
127. Hutmacher, D. W., Scaffolds in tissue engineering bone and cartilage. *Biomaterials* **2000,** 21, (24), 2529-43.
128. Dutta, R. C.; Dutta, A. K., Cell-interactive 3D-scaffold; advances and applications. *Biotechnology*

Advances **2009,** 27, (4), 334-339.

129. Zhang, Y.; Zhai, D.; Xu, M.; Yao, Q.; Chang, J.; Wu, C., 3D-printed bioceramic scaffolds with a Fe3O4/graphene oxide nanocomposite interface for hyperthermia therapy of bone tumor cells. *Journal of Materials Chemistry B* **2016,** 4, (17), 2874-2886.
130. Mele, E., Electrospinning of natural polymers for advanced wound care: towards responsive and adaptive dressings. *Journal of Materials Chemistry B* **2016,** 4, (28), 4801-4812.
131. Yoon, J. J.; Park, T. G., Degradation behaviors of biodegradable macroporous scaffolds prepared by gas foaming of effervescent salts. *Journal of biomedical materials research* **2001,** 55, (3), 401-8.
132. Chen, W.; Chen, S.; Morsi, Y.; El-Hamshary, H.; El-Newhy, M.; Fan, C.; Mo, X., Superabsorbent 3D Scaffold Based on Electrospun Nanofibers for Cartilage Tissue Engineering. *ACS applied materials & interfaces* **2016,** 8, (37), 24415-24425.
133. Bhardwaj, N.; Kundu, S. C., Electrospinning: A fascinating fiber fabrication technique. *Biotechnology Advances* **2010,** 28, (3), 325-347.
134. Braghirolli, D. I.; Steffens, D.; Pranke, P., Electrospinning for regenerative medicine: a review of the main topics. *Drug Discovery Today* **2014,** 19, (6), 743-753.
135. Chew, S. Y.; Wen, Y.; Dzenis, Y.; Leong, K. W., The role of electrospinning in the emerging field of nanomedicine. *Current pharmaceutical design* **2006,** 12, (36), 4751-4770.
136. Khorshidi, S.; Solouk, A.; Mirzadeh, H.; Mazinani, S.; Lagaron, J. M.; Sharifi, S.; Ramakrishna, S., A review of key challenges of electrospun scaffolds for tissue-engineering applications. *Journal of tissue engineering and regenerative medicine* **2016,** 10, (9), 715-38.
137. Croisier, F.; Jérôme, C., Chitosan-based biomaterials for tissue engineering. *European Polymer Journal* **2013,** 49, (4), 780-792.
138. Shakor, P.; Nejadi, S.; Paul, G.; Malek, S., Review of Emerging Additive Manufacturing Technologies in 3D Printing of Cementitious Materials in the Construction Industry. *Frontiers in Built Environment* **2019,** 4, (85).
139. Xu, M.; Zhai, D.; Xia, L.; Li, H.; Chen, S.; Fang, B.; Chang, J.; Wu, C., Hierarchical bioceramic scaffolds with 3D-plotted macropores and mussel-inspired surface nanolayers for stimulating osteogenesis. *Nanoscale* **2016,** 8, (28), 13790-13803.
140. Zhang, Y.; Zhai, D.; Xu, M.; Yao, Q.; Zhu, H.; Chang, J.; Wu, C., 3D-printed bioceramic scaffolds with antibacterial and osteogenic activity. *Biofabrication* **2017,** 9, (2), 025037.
141. Dong, L.; Wang, S.-J.; Zhao, X.-R.; Zhu, Y.-F.; Yu, J.-K., 3D- Printed Poly(ε-caprolactone) Scaffold Integrated with Cell-laden Chitosan Hydrogels for Bone Tissue Engineering. *Scientific Reports* **2017,** 7, (1), 13412.
142. An, J.; Teoh, J. E. M.; Suntornnond, R.; Chua, C. K., Design and 3D Printing of Scaffolds and Tissues. *Engineering* **2015,** 1, (2), 261-268.
143. Chan, B. P.; Leong, K. W., Scaffolding in tissue engineering: general approaches and tissue-specific considerations. *European spine journal : official publication of the European Spine Society, the European Spinal Deformity Society, and the European Section of the Cervical Spine Research Society* **2008,** 17 Suppl 4, (Suppl 4), 467-479.
144. Kim, U. J.; Park, J.; Kim, H. J.; Wada, M.; Kaplan, D. L., Three-dimensional aqueous-derived biomaterial scaffolds from silk fibroin. *Biomaterials* **2005,** 26, (15), 2775-85.
145. Costantini, M.; Barbetta, A., 6 - Gas foaming technologies for 3D scaffold engineering. In *Functional 3D Tissue Engineering Scaffolds*, Deng, Y.; Kuiper, J., Eds. Woodhead Publishing: 2018; pp 127-149.

146. Dehghani, F.; Annabi, N., Engineering porous scaffolds using gas-based techniques. *Current opinion in biotechnology* **2011,** 22, (5), 661-6.
147. Autissier, A.; Visage, C. L.; Pouzet, C.; Chaubet, F.; Letourneur, D., Fabrication of porous polysaccharide-based scaffolds using a combined freeze-drying/cross-linking process. *Acta biomaterialia* **2010,** 6, (9), 3640-3648.
148. Chen, G.; Kawazoe, N., Porous Scaffolds for Regeneration of Cartilage, Bone and Osteochondral Tissue. *Advances in experimental medicine and biology* **2018,** 1058, 171-191.
149. Lu, H.; Oh, H. H.; Kawazoe, N.; Yamagishi, K.; Chen, G., PLLA-collagen and PLLA-gelatin hybrid scaffolds with funnel-like porous structure for skin tissue engineering. *Science and technology of advanced materials* **2012,** 13, (6), 064210-064210.

Chapter 2

Preparation of BSA-coated AuNRs and activation of dendritic cells by photothermally ablated tumor cells

2.1 Summary

Nanoparticle-mediated photothermal therapy has been widely studied for cancer treatment. It is important to disclose how photothermally ablated tumor cells trigger immune responses. In this study, bovine serum albumin (BSA)-coated gold nanorods (BSA-coated AuNRs) were prepared and used for photothermal ablation of breast tumor cells. The BSA-coated AuNRs showed high photothermal conversion efficiency and good photothermal ablation effect towards tumor cells. The ablated tumor cells were co-cultured with immature dendritic cells (DCs) through a direct cell contacting model and diffusion model to confirm the stimulatory effects of cell–cell interaction and soluble factors released from ablated tumor cells. The results indicated that photothermally ablated tumor cells induced immune-stimulatory responses of DCs through both cell–cell interaction and soluble factors. The results should be useful for synergistic photothermal-immunotherapy of primary and metastatic cancer.

2.2 Introduction

Cancer is a severe threat to human life and causes more than seven million deaths each year [1]. Despite some technical breakthroughs that have been explored in cancer therapy, complete healing is difficult using traditional therapeutic approaches including surgical resection, chemo- or radio-therapy [2, 3]. In recent years, photothermal ablation therapy, which employs photothermal conversion agents produce heat under near infrared laser irradiation, further raise the temperature of tumor and ablate tumor cells, provides a highly efficient antitumor strategy for cancer therapy [4, 5]. Various nanomaterials such as polypyrrole, polydopamine, indocyanine green, carbon nanotubes, graphene oxide, molybdenum sulfide, tungsten oxide, CuS nanoparticles and gold-based nanoparticles can be used for photothermal ablation therapy [6-16]. Among them, gold nanoparticles with a different shape (sphere, rod, and star) and size were widely explored due to their tunable surface plasmon resonance property and facile preparation. However, nanoparticle-mediated photothermal ablation therapy, in currently used forms, has been primarily used in local cancer therapy [17-19].

An ideal photothermal ablation therapy should not only eradicate the primary tumor but also induce systemic anti-tumor immunity through activating the immune system to control metastatic tumor and to prevent tumor recurrence [20, 21]. It has been reported that dead tumor cells and their debris can trigger potent immune responses [22-24]. Necrotic tumor cells can release intracellular antigens and damage associated proteins including calreticulin (CRT), ATP and heat shock protein (HSP) from cytosol and nucleus, which can stimulate systemic immune responses [22, 25, 26]. Apoptotic tumor cells associated with "danger signals" such as heat stress can up-regulate expression of membrane HSPs (HSP72 and HSP60) and further elicit tumor-specific immunity [27-29].

During immune responses, dendritic cells (DCs) have the most effective antigen-presentation for initiation of T cell-dependent immune responses as compared to other antigen-presenting cells such as macrophages or B cells [30-32]. Dendritic cell-based immunotherapy caused by necrotic tumor cells and apoptotic tumor cells with "danger signals" is a promising strategy to inhibit metastatic tumor recurrence [33, 34]. However, it is not clear how the immune responses of DCs can be triggered by photothermally ablated tumor cells.

In this study, BSA-coated AuNRs were prepared and used for photothermal ablation of breast tumor cells. The immune-stimulatory responses of immature DCs triggered by the photothermally ablated tumor cells were investigated by direct co-culture or transwell co-culture of immature DCs and photothermally ablated tumor cells to disclose the involvement of cell–cell interaction and soluble factors in the immune responses of DCs.

2.3 Materials and methods

2.3.1 Fabrication and characterization of BSA-coated AuNRs

Gold nanorods were synthesized by a seed-mediated growth method [35-37]. Firstly, gold seed solution were obtained via the reaction of hydrogen tetrachloroaurate (Ⅲ) tetrahydrate ($HAuCl_4 \cdot 4H_2O$, Wako) and sodium borohydride ($NaBH_4$, Sigma) in hexadecyltrimethylammonium bromide (CTAB, 0.1 mol/L, 7.5 mL) aqueous solution. The Au seeds were used within 2 h after preparation. Subsequently, a growth solution was prepared by adding $HAuCl_4$ (0.01 mol/L, 15.0 mL), HCl (1 mol/L, 6.0 mL), $AgNO_3$ (0.01 mol/L, 3.3 mL) and ascorbic acid (0.1 mol/L, 2.4 mL) into CTAB (0.1 mol/L, 300.0 mL) aqueous solution. Finally, the pre-prepared gold seeds grew up along the silver crystal in the growth solution under gentle stirring for 12 h to allow the formation of AuNRs. The AuNRs were collected by centrifugation under 8000 rpm for 10 min. In order to remove the CTAB, the collected AuNRs were washed with ultrapure water. Moreover, bovine serum albumin (BSA) were coated on the surface of AuNRs by mixing AuNRs solution with 10 mg/mL BSA aqueous solution and the mixture solution was kept stirring for 1 day. Subsequently, the BSA-coated AuNRs were obtained by centrifugation under 8000 rpm for 10 min and suspended in ultrapure water for the following experiments.

The morphology of AuNRs and BSA-coated AuNRs was characterized with a transmission electron microscope (TEM, JEM-2100F, JEOL Ltd., Tsukuba, Japan). The BSA coating layer on the surface of AuNRs was observed with copper grids containing super ultrahigh resolution carbon support film (Okenshoji Co., Ltd., Tokyo, Japan) by JEM-2100F TEM system at 200 kV accelerating voltage. The hydrodynamic size of BSA-coated AuNRs was measured using particle size analyzer (ELSZ-2000, Otsuka Electronics Co., Ltd., Osaka, Japan) under dynamic light scattering software. Moreover, the zeta potential of BSA-coated AuNRs was also measured using the same machine under zeta potential software [38]. The mean and standard deviation were calculated through three parallel samples. Fourier transform infrared (FTIR) spectrum was measured with an 8400S FTIR spectrometer (Shimadzu Corp., Kyoto, Japan). Visible-near infrared (VIS-NIR)

spectrum was measured using UV-VIS spectrophotometer (V-660, Jasco Corp., Tokyo, Japan). The concentration of Au was detected by inductively coupled plasma atomic emission spectrometry (ICP-AES, SPS3520UV-DD, SII Nano Technology Inc., Chiba, Japan).

2.3.2 Photothermal performance of BSA-Coated AuNRs

To evaluate photothermal performance of BSA-coated AuNRs, 80 μL aqueous suspension of BSA-coated AuNRs in medium with different gold concentration (0.0, 0.2, 0.4, 0.6, 0.8, 1.0 mM) in each well were used to irradiation under a near infrared (NIR) laser with the wavelength of 805 nm at different power intensities of 1.4, 1.6 and 1.8 W cm^{-2} for 10 min. Irradiation at the condition of power intensity of 1.6 W cm^{-2} with irradiation time of 10 min was repeated five times to check the stability of the photothermal conversion of BSA-coated AuNRs. In addition, the real-time temperature was detected by inserting the thermocouple probe into BSA-coated AuNRs solution with different gold concentration and recorded with the digital thermometer (AS ONE Corp., Tokyo, Japan) during laser irradiation.

2.3.3 Viability analysis of cells cultured with BSA-Coated AuNRs

Viability of cells cultured with BSA-coated AuNRs was evaluated by WST-1 assay. Mouse breast tumor cells that stably express luciferase (4T1-Luc) were obtained from JCR cell bank (Tsukuba, Japan). The 4T1-Luc cells were subcultured in RPMI1640 medium (Gibco, Grand Island, New York, USA) containing 10% FBS in a humidified incubator at 37 ℃. When the cells proliferated to 80% in the flask, the medium was removed and washed with PBS. Then 0.25% trypsin solution was added into flask and incubated for 5 min to detach the cells from the surface of flask. The harvested 4T1-Luc cells were re-suspended in RPMI1640 medium and used for following experiments. 100 μL cell suspension solution with the concentration of 2.0×10^5 cells/mL was dropped into each well of a 96-well plate and cultured for 12 h to allow cell adhesion. Afterwards, the medium was changed to 100 μL fresh medium containing BSA-coated AuNRs at different Au concentrations (0.0, 0.2, 0.4, 0.6, 0.8 and 1.0 mM) and cultured for 24 h. Subsequently, the cell viability was evaluated by WST-1 assay. Briefly, after being removed the medium, 100 μL 10% WST-1 dilute solution was added into each well and incubated for 3 h at 37 ℃. Then, the absorbance of WST-1 solution was detected via a microplate reader at the wavelength of 440 nm. The mean and standard deviation were calculated through three parallel samples of each group.

2.3.4 Cellular uptake assay of BSA-Coated AuNRs

Uptake amount of AuNRs by breast tumor cells *in vitro* was measured via ICP-AES. At first, breast tumor cells (4T1-Luc cells, 2×10^5 cells/well) were seeded and cultured in culture plate for 12 h to make cell adhesion. Subsequently, the 0.0, 0.2, 0.4 and 0.6 mM BSA-coated AuNRs in medium were used to treat with 4T1-Luc cells for 6 h. Then the free BSA-coated AuNRs were removed via washing with phosphate buffer solution. After that, the adhered cells were detached from each well and then the detached cells were centrifuged and re-suspended in phosphate buffer solution. The number of harvested cells was calculated using the hemocytometer. Finally, the nitrohydrochloric acid was used to lyse the collected cells. Then the gold amount in each group was detected with ICP-OES. The mean and standard deviation were calculated through three parallel samples of each group.

2.3.5 Photothermal ablation of breast tumor cells by BSA-Coated AuNRs

The 4T1-Luc cells (2×10^4 cells/well) were seeded in culture plate and cultured for 12 h to make cell attachment. Subsequently, the 0.0, 0.2, 0.4 and 0.6 mM BSA-coated AuNRs in medium were used to treat with 4T1-Luc cells for 6 h. Then the free BSA-coated AuNRs were removed via washing with phosphate buffer solution. Each well containing 4T1-Luc cells after uptake of BSA-coated AuNRs were used to irradiation under a near infrared (NIR) laser with the wavelength of 805 nm at the power intensities of 1.6 W cm^{-2} for 10 min. After that, the breast tumor cells were cultured in RPMI1640 medium supplemented with 10% FBS for another 4 h. The live and dead cells before and after laser irradiation were stained by Calcein-AM/PI double staining kit (Dojindo, Kumamoto, Japan). The stained cells in 96-well plate were observed by an inverted fluorescence microscope (Olympus, Tokyo, Japan). In addition, cell viability before and after laser irradiation was quantified by a WST-1 assay. The mean and standard deviation were calculated through three parallel samples of each group.

2.3.6 Interaction between DCs and ablated breast tumor cells

The 4T1-Luc cells (2×10^4 cells/well) were seeded into 96-well plates and cultured for 12 h. Subsequently, the 0.4 mM BSA-coated AuNRs in fresh medium were used to treat with 4T1-Luc cells for 6 h. After that, the free BSA-coated AuNRs were removed via washing with phosphate buffer solution. Each well containing 4T1-Luc cells after uptake of BSA-coated AuNRs were used to irradiation under a near infrared (NIR) laser with the wavelength of 805 nm at the power intensities of 1.6 W cm^{-2} for 10 min.

Mouse bone marrow-derived immature DCs (ATCC, Manassas, Virginia, USA) were used to investigate immune responses induced by photothermally ablated tumor cells. Dendritic cells were cultured in MEM-α medium containing 20% fetal bovine serum and 5 ng/mL GM-CSF, whose growth property was a mixture of adherent and floating cells. For subculture of DCs, the adherent cells were detached by a 0.25% trypsin solution, and the floating cells were directly transferred into tubes. After the detached cells and floating cells were mixed in tubes, then all the cells were collected by centrifugation under 1000 rpm for 10 minutes. The cells were re-suspended in fresh medium and used for subculture. Culture medium was changed once per week.

To investigate interaction between DCs and photothermally ablated 4T1-Luc cells, three experiments were conducted. The first experiment was designed to investigate the effect of soluble factors released from the ablated 4T1-Luc cells. Dendritic cells (1×10^4 cells/well) were seeded in a 96-well transwell insert which consisting of the porous membrane (the diameter of pore: 1.0 μm). The transwell insert was put in the upper of a 96-well receiver plate cultured the ablated 4T1-Luc cells, which enabled diffusion of soluble factors while blocking direct cell-to-cell contact (diffusion model). The second experiment was designed to investigate the effect of cell–cell interaction. The soluble factors released from the ablated 4T1-Luc cells were completely removed by washing with phosphate buffer solution in each well. After washing, DCs (1×10^4 cells/well) suspension were dropped in the 96-well culture plate containing the ablated 4T1-Luc cells (cell contacting model). The third experiment was designed to investigate the effects of both soluble factors and cell–cell interaction. Dendritic cells (1×10^4 cells/well) suspension were directly dropped in the 96-well culture plate after photothermal ablation of 4T1-Luc cells (combination effects of diffusion model and cell contacting model). As positive and negative controls, DCs (1×10^4 cells/well) suspension were dropped in blank 96-well culture plate and incubated with or without 1 μg/mL lipopolysaccharide (LPS) stimulation, respectively. For all the experiments, DCs were incubated in MEM-α medium with 5 ng/mL GM-CSF for 24 h. Finally, DCs supernatants were harvested to measure the secretion amount of cytokines including

interleukin 6, 12 and 1β (IL-6, 12 and 1β), tumor necrosis factor alpha (TNF-α) by the Elisa kit based on the protocol referred by company instruction (PEPROTECH, Rocky Hill, New Jersey, USA). The mean and standard deviation were calculated through three parallel samples of each group.

2.3.7 Statistical analysis

The quantitative experiment in this study was repeated using three parallel samples and the results were expressed with average ± standard deviation (SD). The statistical analysis including significant difference was carried out by one-way ANOVA analysis software. The p value of 0.05 was considered statistically significant difference. The data were classified according to their p values and denoted by (*) for p less than 0.05, (**) for p less than 0.01 and (***) for p less than 0.001.

2.4 Results

2.4.1 Physical and chemical properties of BSA-Coated AuNRs

The morphology of AuNRs and BSA-coated AuNRs was observed by TEM. Transmission electron microscopy images (Fig. 2.1a) showed that the gold nanoparticles had a rod-like structure. Gold nanorods and BSA-coated AuNRs had the same morphology and dimension. Their dimension measured from TEM images was 62.3 ± 4.5 nm × 11.6 ± 3.8 nm. The TEM image of BSA-coated AuNRs demonstrated the BSA coating layer on the surface of AuNRs. Moreover, the hydrodynamic size of AuNRs and BSA-coated AuNRs distributed in water was measured by dynamic light scattering (DLS) as shown in Fig. 2.1b. The average hydrodynamic size of AuNRs and BSA-coated AuNRs was 55.3 ± 5.8 and 68.1 ± 8.2 nm, respectively. The average hydrodynamic size of BSA-coated AuNRs was a little larger than that of AuNRs, which should be due to the swelling of BSA coating on the surface of AuNRs. Zeta potential of AuNRs and BSA-coated AuNRs (Fig. 2.1c) was detected to check the change of surface-charge after BSA coating. The results demonstrated that the zeta potential of AuNRs and BSA-coated AuNRs was 41.43 ± 3.80 and −28.82 ± 1.63 mV, respectively, which indicated the surface charge of AuNRs was changed from positive to negative after BSA coating.

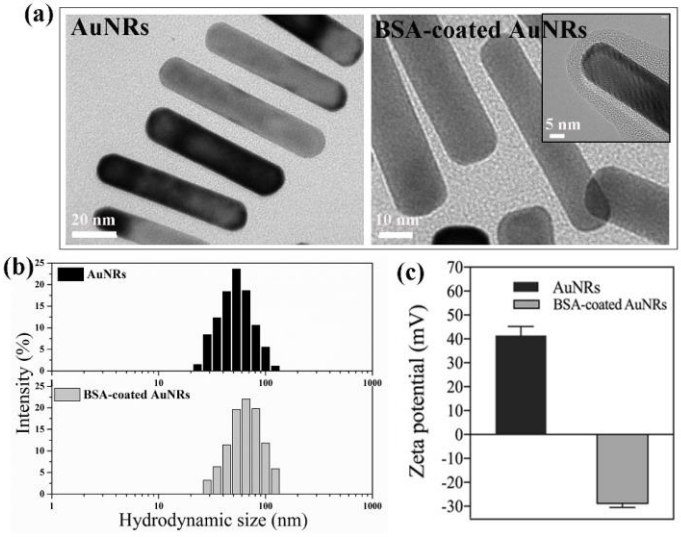

Fig. 2.1 High-resolution transmission electron microscopy image (a), distribution of hydrodynamic sizes (b) and zeta potentials (c) of gold nanorods (AuNRs) and BSA-coated AuNRs.

Fourier transform infrared spectrum was used to further confirm the successful coating of BSA on the surface of AuNRs. As shown in Fig. 2.2a, the BSA-coated AuNRs showed two apparent peaks at the wavenumber of 1640 and 1524 cm^{-1}, which is ascribed to the NH_2-I and II band NH_2-II of bovine serum albumin (BSA). While for the AuNRs without coating, no peaks were detected at the same wavenumber, which indicated the bovine serum albumin was successfully coated on the surface of AuNRs. Bovine serum albumin molecules should be bound to the surface of AuNRs through electrostatic interaction of positively charged AuNRs and negatively charged BSA and Au-S bond between AuNRs and thiol groups in BSA. Colloid solutions of BSA-coated AuNRs in ultrapure water and medium were stable without aggregation for a long time, indicating stable BSA coating on the surface of AuNRs. Protein-coating has been reported to increase colloid stability of gold nanorods [39].

A visible-near infrared absorption spectrum (Fig. 2b) was used to characterize the optical property of AuNRs. Both AuNRs and BSA-coated AuNRs demonstrated two apparent absorbance peaks at 535 nm and 848 nm, which corresponded to their transverse and longitudinal plasmon modes, respectively.

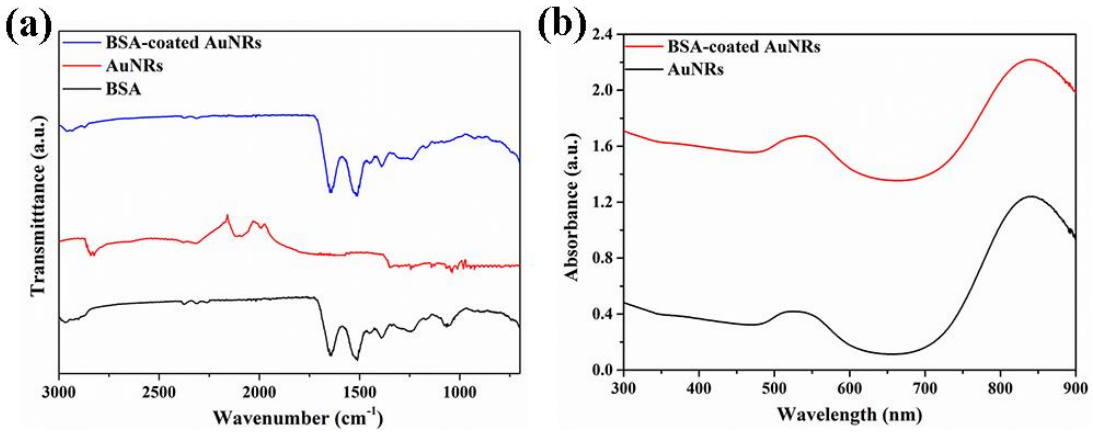

Fig. 2.2 Fourier transform infrared spectra of bovine serum albumin (BSA), AuNRs and BSA-coated AuNRs (a) and VIS-NIR spectra of AuNRs and BSA-coated AuNRs (b).

2.4.2 Photothermal performance of BSA-Coated AuNRs

Photothermal performance of BSA-coated AuNRs was evaluated by irradiation with an 805 nm laser. Different laser irradiation power densities (1.4, 1.6 and 1.8 W cm^{-2}) were used. Heating curves (Fig. 2.3a–c) showed that the temperature of BSA-coated AuNRs aqueous solution in medium increased rapidly compared with control group (0.0 mM, only medium without AuNRs). Temperature increase rate became faster when Au concentration was higher and the laser intensity became stronger. Temperature change data (Fig. 2.3d) after laser irradiation with an intensity of 1.4, 1.6 and 1.8 W cm^{-2} for 10 min indicated that the temperature change of BSA-coated AuNRs aqueous solution increased from 5.9 ± 0.7 to 30.1 ± 4.8 ℃, from 8.5 ± 1.1 to 34.4 ± 3.8 ℃ and from 12.3 ± 1.6 ℃ to 44.5 ± 6.1 ℃, respectively, when the concentration of AuNRs aqueous solution varied from 0.0 mM to 1.0 mM. All these results suggested that the BSA-coated AuNRs had an excellent photothermal conversion efficiency and their photothermal conversion efficiency could be modulated by changing AuNRs concentration in the aqueous solution and laser power intensity. Laser power density of 1.6 W cm^{-2} was used in following experiments because temperature increase of BSA-coated AuNRs solution was high while temperature change of control (medium without AuNRs) was not so high.

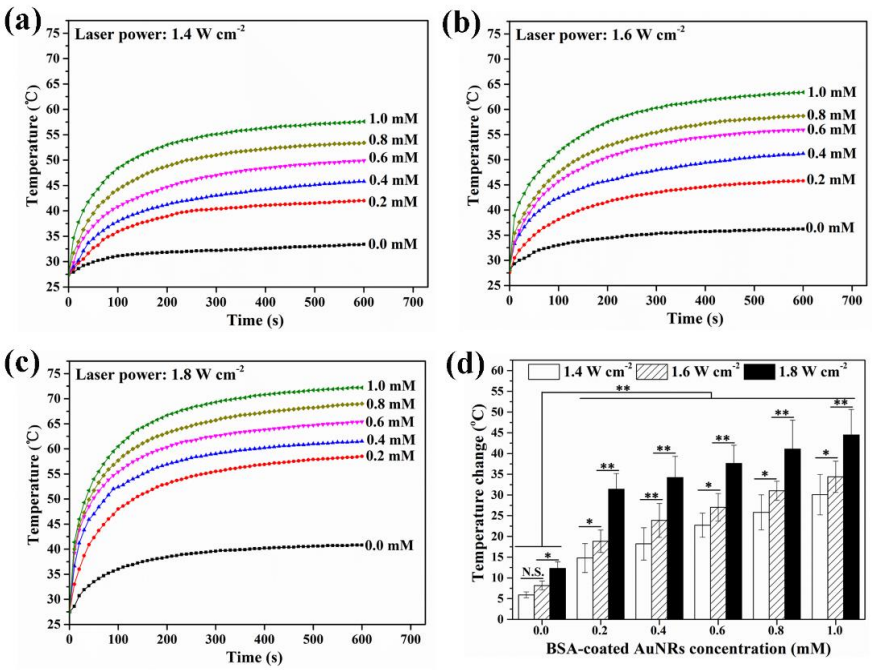

Fig. 2.3 Heating curves of BSA-coated AuNRs aqueous solution at different Au concentration of 0.0, 0.2, 0.4, 0.6, 0.8 and 1.0 mM under continuous NIR irradiation with different laser power intensity of 1.4, 1.6 and 1.8 W cm^{-2} (a–c). Temperature change of BSA-coated AuNRs aqueous solution at different Au concentration of 0.0, 0.2, 0.4 and 0.6, 0.8 and 1.0 mM after NIR irradiation with different laser power intensity of 1.4, 1.6 and 1.8 W cm^{-2} for 10 min (d). Data are presented as mean ± standard deviation, n = 3. No significant difference: N.S.; Significant difference: * $p < 0.01$, ** $p < 0.01$.

Bovine serum albumin-coated AuNRs aqueous solution in medium at different Au concentration of 0.0, 0.2, 0.4, 0.6, 0.8 and 1.0 mM was repeatedly irradiated for 5 cycles under continuous NIR irradiation at the laser power intensity of 1.6 W cm^{-2} for 10 min (Fig. 2.4). The heating curves (Fig. 2.4a) were almost the same for each cycle. Visible-near infrared absorption spectrum (Fig. 2.4b) and zeta potential (Fig. 2.4c) of BSA-coated AuNRs did not change before or after laser irradiation. The results suggested photothermal stability of the BSA-coated AuNRs during laser irradiation.

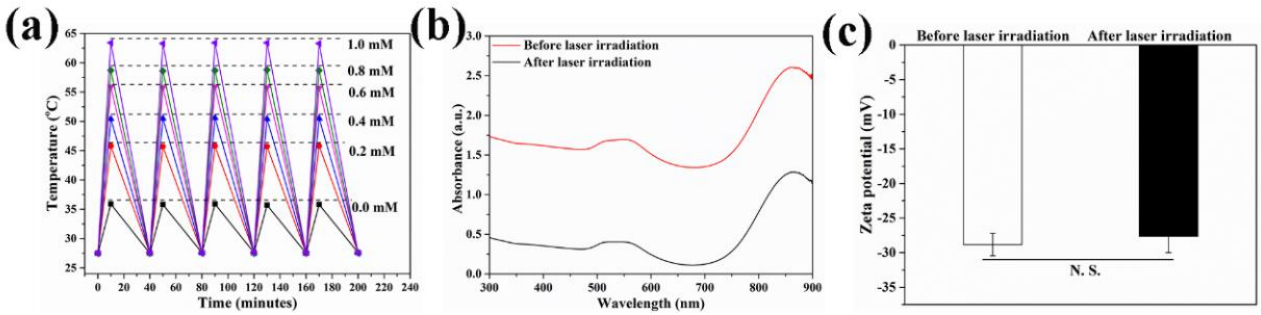

Fig. 2.4 Temperature change curves of BSA-coated AuNRs aqueous solution in medium at different Au concentration of 0.0, 0.2, 0.4, 0.6, 0.8 and 1.0 mM over five laser on-off cycles (a). VIS-NIR spectrum (b) and Zeta potential (c) of BSA-coated AuNRs before laser irradiation and after five laser on-off cycles. The laser power intensity of 1.6 W cm^{-2} was used. Data are presented as mean ± standard deviation, n = 3. No significant difference: N.S.

2.4.3 Influence of BSA-Coated AuNRs on cell viability

Cell viability decreased when Au concentration increased (Fig. 2.5). The 4T1-Luc cells cultured in medium containing BSA-AuNRs at an Au concentration of 0.6 mM still showed a high viability (85.0% compared to that of control group). However, when concentration of BSA-AuNRs increased to 0.8 and 1.0 mM, cell viability decreased to 74.4 ± 10.8% and 57.1 ± 7.4%, respectively. For biomedical application, BSA-coated AuNRs as a photothermal conversion agent should have low toxicity to cells before laser irradiation. Cell ablation effect should be switched on only when laser irradiation is applied. Therefore, BSA-coated AuNRs at an Au concentration less than 0.6 mM were used to investigate photothermal ablation efficiency of tumor cells in the following experiment.

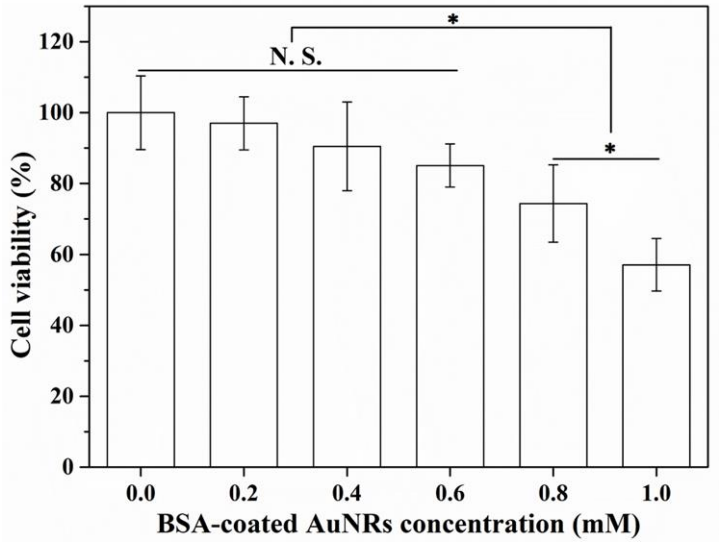

Fig. 2.5 Cell viability of 4T1-Luc cells incubated in medium containing BSA-coated AuNRs at different Au concentrations (0.0 mM, 0.2 mM, 0.4 mM, 0.6 mM, 0.8 mM and 1.0 mM) for 1 day. Data are expressed with average ± standard deviation, n = 3. No significant difference: N.S.; significant difference: * $p < 0.05$.

2.4.4 Cellular uptake of BSA-Coated AuNRs

Cellular uptake amount of BSA-coated AuNRs was measured by ICP-OES (Fig2.6). The BSA-coated AuNRs were uptaken during cell culture. After 4T1-Luc cells were cultured in medium containing BSA-coated AuNRs at different gold concentration of 0.2, 0.4 and 0.6 mM for 6 h, the percentage of Au uptake was 5.1 ± 0.1%, 4.7 ± 0.3% and 4.2 ± 0.3%, respectively, which was not significantly different (Fig 2.6 a). Cellular uptake amount of BSA-coated AuNRs was 7.5 ± 0.1 pg/cell, 11.8 ± 0.9 pg/cell and 21.9 ± 2.1 pg/cell, respectively (Fig2.6 b). Cellular uptake amount of BSA-coated AuNRs significantly increased when Au concentration in the medium increased.

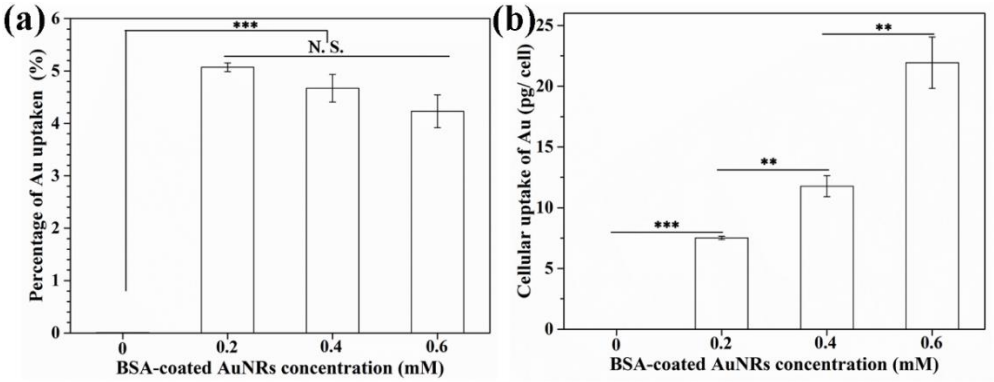

Fig. 2.6 Percentage of Au uptaken by 4T1-Luc cells (a) and cellular uptake amount of Au per cell (b) after being cultured in medium containing BSA-coated AuNRs at different Au concentration of 0.0, 0.2, 0.4 and 0.6 mM for 6 h. Data are presented as mean ± standard deviation, n = 3. No significant difference: N.S.; Significant difference: ** $p < 0.01$; *** $p < 0.001$.

2.4.5 Photothermal ablation effect of BSA-Coated AuNRs

Photothermal ablation effect of BSA-coated AuNRs was evaluated by using calcein-AM/PI double staining kit and WST-1 assay. Live/dead staining images (Fig. 2.7 a–h) showed that after incubation with BSA-coated AuNRs at an gold concentration of 0.0, 0.2, 0.4 and 0.6 mmol/L for 6 h, most of the cells were live before laser irradiation. However, after laser irradiation for 10 min, a small portion of 4T1-Luc cells were dead in the group cultured with an Au concentration of 0.2 mM and almost all the tumor cells were dead in the groups cultured with an Au concentration of 0.4 and 0.6 mM. The cells of control group remained alive even after laser irradiation. In addition, quantification of cell viability (Fig. 2.7 i) showed that cell viability in the groups cultured with BSA-coated AuNRs at an gold concentration of 0.0, 0.2, 0.4 and 0.6 mM decreased to 92.1 ± 9.3%, 80.4 ± 13.0%, 1.1 ± 3.3% and 1.0 ± 4.3%, respectively, after laser irradiation for 10 min. The results indicated that photothermal ablation effect of BSA-coated AuNRs increased with the increase of Au concentration. Incubation with BSA-coated AuNRs at an gold concentration of 0.4 and 0.6 mM could ablate all the tumor cells by laser irradiation.

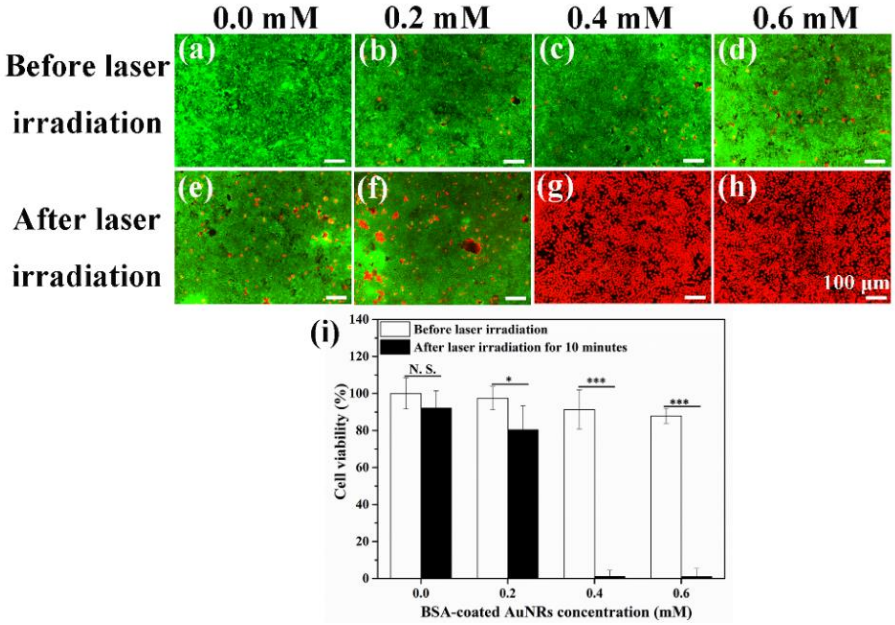

Fig. 2.7 Live/dead staining (a–h) and viability (i) of 4T1-Luc cells before and after NIR laser irradiation for 10 min after the cells were cultured in medium containing BSA-coated AuNRs at different Au concentrations of 0.0, 0.2, 0.4 and 0.6 mM for 6 h. Green color indicates live cells while red color indicates dead cells. Data are presented as mean ± standard deviation, n = 3. No significant difference: N.S.; significant difference: * $p < 0.05$; *** $p < 0.001$.

2.4.6 Immune responses of DCs triggered by photothermally ablated breast tumor cells

Effects of soluble factors released from the ablated 4T1-Luc cells, direct cell–cell interaction and their combination on DCs were analyzed by using three different cell-culture models to distinguish these effects. Secretion of multiple cytokines including IL-6, IL-12, IL-1β and TNF-α from DCs was measured by ELISA Kit after transwell co-culture (diffusion model) or direct co-culture of immature DCs with the ablated breast tumor cells (cell contacting model) for 24 h. As shown in Fig. 2.8a-c, both cell–cell interaction and soluble factors released from ablated 4T1-Luc cells promoted the secretion level of IL-6, IL-12 and IL-1β as compared to those of negative control group. As for the secretion of TNF-α (Fig. 2.8d), only cell–cell interaction showed a promotive effect, while soluble factors released from the ablated 4T1-Luc cells could not promote TNF-α secretion as compared with the negative control group.

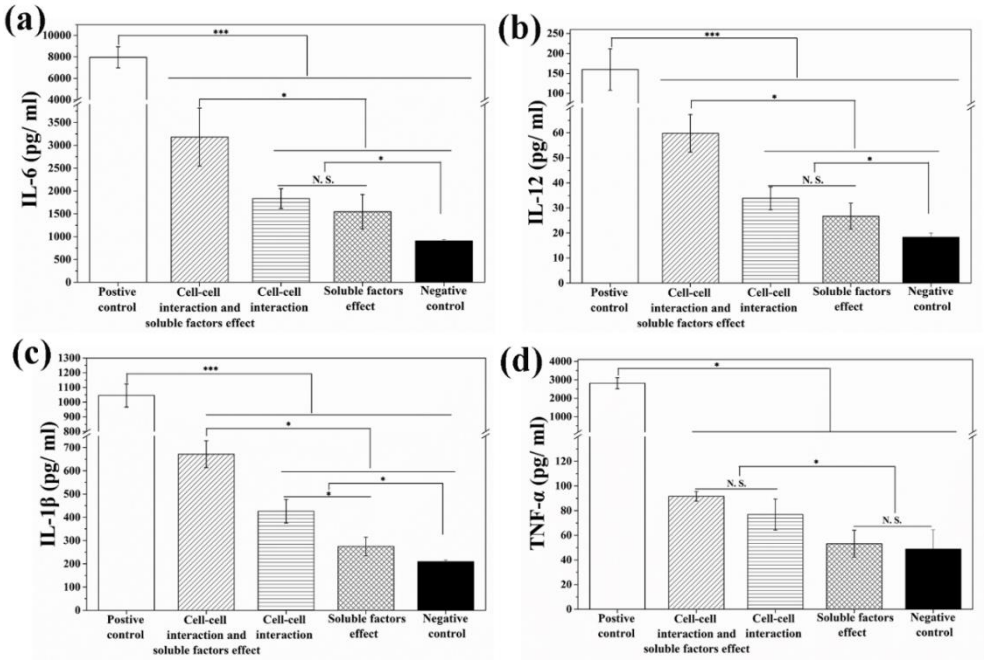

Fig. 2.8 Secretion level of cytokines IL-6 (a), IL-12 (b), IL-1β (c) and TNF-α (d) by dendritic cells (DCs) after co-culture of immature DCs with photothermally ablated tumor cells under different co-culture models. Data are presented as mean ± standard deviation, n = 3. No significant difference: N.S.; significant difference: * $p < 0.05$; *** $p < 0.001$.

2.5 Discussion

Photothermal therapy using NIR light-responsive nanoparticles to ablate primary tumor has been widely studied [16, 40, 41]. However, it remains unclear if the ablated tumor cells can stimulate immune responses. In

this study, BSA-coated AuNRs were prepared and used to ablate tumor cells for investigation of the interaction between ablated tumor cells and immune cells. Photothermal ablation efficiency towards breast tumor cells after cellular uptake of BSA-coated AuNRs and immune-stimulatory response of DCs triggered by ablated breast tumor cells were investigated.

Gold nanorods were synthesized by a seed-mediated growth method. They were further coated with BSA for good colloid stability and biocompatibility. The BSA-coated AuNRs had a rod-like morphology and showed a strong SPR adsorption peak at 848 nm corresponding to their longitudinal plasmon modes, which indicated AuNRs could be used as a photothermal conversion agent. The heating curve and temperature change induced by NIR laser irradiation could be modulated by changing the concentration of AuNRs and laser power intensity, which indicated that BSA-coated AuNRs had an excellent photothermal performance. Moreover, heating curves from five cycles of laser on/off suggested BSA-coated AuNRs had excellent photothermal stability.

The BSA-coated AuNRs possessed low cytotoxicity in a broad Au concentration range of 0.0~0.6 mM. In this study, an Au concentration of 0.4 mM was used for photothermal ablation experiments. If gold nanoparticles are hybridized with other matrices, the amount of gold nanoparticles can be further increased [42]. Hybridization of various nanoparticles with polymer matrices has been used to increase biocompatibility of nanoparticles for controlling cell functions [19, 38]. In this study, after the breast tumor cells were cultured with BSA-coated AuNRs, BSA-coated AuNRs could be uptaken by tumor cells and the cellular uptake amount increased significantly with the increase of AuNRs concentration in culture medium, which should be beneficial for photothermal ablation. The breast tumor cells could be efficiently ablated by the uptaken BSA-coated AuNRs after NIR laser irradiation when the Au concentration in cell culture medium was 0.4 and 0.6 mM. At a low gold concentration of 0.2 mM, the BSA-coated AuNRs could partially ablate the breast tumor cells. When Au concentration was higher, more AuNRs were uptaken by cells and more rapid heating and higher temperatures could be reached to ablate tumor cells.

To investigate whether the photothermally ablated tumor cells could induce immune response, immature DCs as a key antigen-presenting cells [43] were directly co-cultured with photothermally ablated tumor cells for 24 h. Moreover, to determine whether soluble factors released from photothermally ablated tumor cells were involved in DCs maturation, immature DCs and photothermally ablated tumor cells were co-cultured in a diffusion model, which enabled diffusion of soluble factor in the culture medium while blocking direct cell-to-cell contact. When DCs are matured, they can increased the secretion amount of cytokines to induce the activation of immune cells such as T lymphocyte, which plays crucial roles in inducing the immune responses [44]. IL-6, IL-12 and IL-1β are typical markers of humoral immunity [33] and TNF-α is a typical marker of cellular immunity [33, 45]. Secretion of IL-6, IL-12 and IL-1β was promoted by both cell–cell interaction (cell contact) and soluble factors, while secretion of TNF-α was only promoted by cell-cell interaction. The results suggested that photothermally ablated tumor cells by BSA-coated AuNRs were able to induce immune responses of DCs, which should be useful for cancer immunotherapy.

2.6 Conclusions

Gold nanorods were prepared by a seed-mediated growth method and coated with BSA for photothermal ablation of breast tumor cells. The BSA-coated AuNRs showed good monodispersity, low cytotoxicity as well as high cellular uptake by tumor cells in the studied concentration. The BSA-coated AuNRs showed excellent photothermal performance based on the strong SPR absorption in NIR region and showed high photothermal ablating efficiency towards breast tumor cells. Moreover, the photothermally

ablated tumor cells triggered immune-stimulatory responses of immature DCs through both cell–cell interaction and soluble factors released from the ablated tumor cells.

2.7 References

1. Ferlay, J.; Shin, H. R.; Bray, F.; Forman, D.; Mathers, C.; Parkin, D. M., Estimates of worldwide burden of cancer in 2008: GLOBOCAN 2008. *International journal of cancer* **2010,** 127, (12), 2893-917.
2. Li, Y.; He, L.; Dong, H.; Liu, Y.; Wang, K.; Li, A.; Ren, T.; Shi, D.; Li, Y., Fever-Inspired Immunotherapy Based on Photothermal CpG Nanotherapeutics: The Critical Role of Mild Heat in Regulating Tumor Microenvironment. *Advanced science* **2018,** 5, (6), 1700805.
3. Xie, Y.; Ma, X.; Liu, X., Carrier-Free Microspheres of an Anti-Cancer Drug Synthesized via a Sodium Catalyst for Controlled-Release Drug Delivery. *Materials* **2018,** 11, (2), 281.
4. Cheng, L.; Wang, C.; Feng, L.; Yang, K.; Liu, Z., Functional Nanomaterials for Phototherapies of Cancer. *Chemical reviews* **2014,** 114, (21), 10869-10939.
5. El-Sayed, I. H.; Huang, X.; El-Sayed, M. A., Selective laser photo-thermal therapy of epithelial carcinoma using anti-EGFR antibody conjugated gold nanoparticles. *Cancer letters* **2006,** 239, (1), 129-35.
6. Wang, X.; Li, H.; Liu, X.; Tian, Y.; Guo, H.; Jiang, T.; Luo, Z.; Jin, K.; Kuai, X.; Liu, Y.; Pang, Z.; Yang, W.; Shen, S., Enhanced photothermal therapy of biomimetic polypyrrole nanoparticles through improving blood flow perfusion. *Biomaterials* **2017,** 143, 130-141.
7. Poinard, B.; Neo, S. Z. Y.; Yeo, E. L. L.; Heng, H. P. S.; Neoh, K. G.; Kah, J. C. Y., Polydopamine Nanoparticles Enhance Drug Release for Combined Photodynamic and Photothermal Therapy. *ACS applied materials & interfaces* **2018,** 10, (25), 21125-21136.
8. Yan, F.; Wu, H.; Liu, H.; Deng, Z.; Liu, H.; Duan, W.; Liu, X.; Zheng, H., Molecular imaging-guided photothermal/photodynamic therapy against tumor by iRGD-modified indocyanine green nanoparticles. *Journal of controlled release : official journal of the Controlled Release Society* **2016,** 224, 217-228.
9. Robinson, J. T.; Tabakman, S. M.; Liang, Y.; Wang, H.; Casalongue, H. S.; Vinh, D.; Dai, H., Ultrasmall reduced graphene oxide with high near-infrared absorbance for photothermal therapy. *Journal of the American Chemical Society* **2011,** 133, (17), 6825-31.
10. Wang, S.; Li, K.; Chen, Y.; Chen, H.; Ma, M.; Feng, J.; Zhao, Q.; Shi, J., Biocompatible PEGylated MoS2 nanosheets: controllable bottom-up synthesis and highly efficient photothermal regression of tumor. *Biomaterials* **2015,** 39, 206-17.
11. Chen, Z.; Wang, Q.; Wang, H.; Zhang, L.; Song, G.; Song, L.; Hu, J.; Wang, H.; Liu, J.; Zhu, M.; Zhao, D., Ultrathin PEGylated W18O49 nanowires as a new 980 nm-laser-driven photothermal agent for efficient ablation of cancer cells in vivo. *Advanced materials* **2013,** 25, (14), 2095-100.
12. Li, Y.; Lu, W.; Huang, Q.; Huang, M.; Li, C.; Chen, W., Copper sulfide nanoparticles for photothermal ablation of tumor cells. *Nanomedicine* **2010,** 5, (8), 1161-71.
13. Huang, X.; Jain, P. K.; El-Sayed, I. H.; El-Sayed, M. A., Plasmonic photothermal therapy (PPTT) using gold nanoparticles. *Lasers in medical science* **2008,** 23, (3), 217-28.
14. Chen, Y. W.; Su, Y. L.; Hu, S. H.; Chen, S. Y., Functionalized graphene nanocomposites for enhancing photothermal therapy in tumor treatment. *Advanced drug delivery reviews* **2016,** 105, 190-204.

15. Dai, W.; Dong, H., A Semimetal-Like Molybdenum Carbide Quantum Dots Photoacoustic Imaging and Photothermal Agent with High Photothermal Conversion Efficiency. *Materials* **2018,** 11, (9), 1776.
16. An, L.; Wang, Y.; Tian, Q.; Yang, S., Small Gold Nanorods: Recent Advances in Synthesis, Biological Imaging, and Cancer Therapy. *Materials* **2017,** 10, (12), 1372.
17. Hsiao, C. W.; Chuang, E. Y.; Chen, H. L.; Wan, D.; Korupalli, C.; Liao, Z. X.; Chiu, Y. L.; Chia, W. T.; Lin, K. J.; Sung, H. W., Photothermal tumor ablation in mice with repeated therapy sessions using NIR-absorbing micellar hydrogels formed in situ. *Biomaterials* **2015,** 56, 26-35.
18. Jaque, D.; Martinez Maestro, L.; del Rosal, B.; Haro-Gonzalez, P.; Benayas, A.; Plaza, J. L.; Martin Rodriguez, E.; Garcia Sole, J., Nanoparticles for photothermal therapies. *Nanoscale* **2014,** 6, (16), 9494-530.
19. Zhang, J.; Li, J.; Chen, S.; Kawazoe, N.; Chen, G., Preparation of gelatin/Fe3O4 composite scaffolds for enhanced and repeatable cancer cell ablation. *Journal of Materials Chemistry B* **2016,** 4, (34), 5664-5672.
20. Chen, W. R.; Singhal, A. K.; Liu, H.; Nordquist, R. E., Antitumor immunity induced by laser immunotherapy and its adoptive transfer. *Cancer research* **2001,** 61, (2), 459-61.
21. Min, Y.; Roche, K. C.; Tian, S.; Eblan, M. J.; McKinnon, K. P.; Caster, J. M.; Chai, S.; Herring, L. E.; Zhang, L.; Zhang, T.; DeSimone, J. M.; Tepper, J. E.; Vincent, B. G.; Serody, J. S.; Wang, A. Z., Antigen-capturing nanoparticles improve the abscopal effect and cancer immunotherapy. *Nature Nanotechnology* **2017,** 12, 877.
22. Slovak, R.; Ludwig, J. M.; Gettinger, S. N.; Herbst, R. S.; Kim, H. S., Immuno-thermal ablations - boosting the anticancer immune response. *Journal for immunotherapy of cancer* **2017,** 5, (1), 78.
23. Chu, K. F.; Dupuy, D. E., Thermal ablation of tumours: biological mechanisms and advances in therapy. *Nature reviews. Cancer* **2014,** 14, (3), 199-208.
24. Chen, D. S.; Mellman, I., Oncology meets immunology: the cancer-immunity cycle. *Immunity* **2013,** 39, (1), 1-10.
25. Ogawa, M.; Tomita, Y.; Nakamura, Y.; Lee, M. J.; Lee, S.; Tomita, S.; Nagaya, T.; Sato, K.; Yamauchi, T.; Iwai, H.; Kumar, A.; Haystead, T.; Shroff, H.; Choyke, P. L.; Trepel, J. B.; Kobayashi, H., Immunogenic cancer cell death selectively induced by near infrared photoimmunotherapy initiates host tumor immunity. *Oncotarget* **2017,** 8, (6), 10425-10436.
26. Larmonier, N.; Merino, D.; Nicolas, A.; Cathelin, D.; Besson, A.; Bateman, A.; Solary, E.; Martin, F.; Katsanis, E.; Bonnotte, B., Apoptotic, necrotic, or fused tumor cells: an equivalent source of antigen for dendritic cell loading. *Apoptosis : an international journal on programmed cell death* **2006,** 11, (9), 1513-24.
27. Feng, H.; Zeng, Y.; Whitesell, L.; Katsanis, E., Stressed apoptotic tumor cells express heat shock proteins and elicit tumor-specific immunity. *Blood* **2001,** 97, (11), 3505-12.
28. Feng, H.; Zeng, Y.; Graner, M. W.; Likhacheva, A.; Katsanis, E., Exogenous stress proteins enhance the immunogenicity of apoptotic tumor cells and stimulate antitumor immunity. *Blood* **2003,** 101, (1), 245-52.
29. Garg, A. D.; Agostinis, P., Cell death and immunity in cancer: From danger signals to mimicry of pathogen defense responses. *Immunological reviews* **2017,** 280, (1), 126-148.
30. Banchereau, J.; Steinman, R. M., Dendritic cells and the control of immunity. *Nature* **1998,** 392, (6673), 245-52.
31. Steinman, R. M., The dendritic cell system and its role in immunogenicity. *Annual review of*

immunology **1991,** 9, 271-96.

32. Schuler, G.; Steinman, R. M., Dendritic cells as adjuvants for immune-mediated resistance to tumors. *The Journal of experimental medicine* **1997,** 186, (8), 1183-1187.
33. Wang, C.; Xu, L.; Liang, C.; Xiang, J.; Peng, R.; Liu, Z., Immunological responses triggered by photothermal therapy with carbon nanotubes in combination with anti-CTLA-4 therapy to inhibit cancer metastasis. *Advanced materials* **2014,** 26, (48), 8154-62.
34. Shimamura, H.; Sunamura, M.; Tsuchihara, K.; Egawa, S.; Takeda, K.; Matsuno, S., Irradiated pancreatic cancer cells undergo both apoptosis and necrosis, and could be phagocytized by dendritic cells. *European surgical research. Europaische chirurgische Forschung. Recherches chirurgicales europeennes* **2005,** 37, (4), 228-34.
35. Xiang, Y.; Wu, X.; Liu, D.; Feng, L.; Zhang, K.; Chu, W.; Zhou, W.; Xie, S., Tuning the Morphology of Gold Nanocrystals by Switching the Growth of {110} Facets from Restriction to Preference. *The Journal of Physical Chemistry C* **2008,** 112, (9), 3203-3208.
36. Li, J.; Li, J. E. J.; Zhang, J.; Wang, X.; Kawazoe, N.; Chen, G., Gold nanoparticle size and shape influence on osteogenesis of mesenchymal stem cells. *Nanoscale* **2016,** 8, (15), 7992-8007.
37. Wang, X.; Zhang, J.; Li, J.; Chen, Y.; Chen, Y.; Kawazoe, N.; Chen, G., Bifunctional scaffolds for the photothermal therapy of breast tumor cells and adipose tissue regeneration. *Journal of Materials Chemistry B* **2018,** 10.1039/c8tb02325e.
38. Chen, Y.; Li, J.; Kawazoe, N.; Chen, G., Preparation of dexamethasone-loaded calcium phosphate nanoparticles for the osteogenic differentiation of human mesenchymal stem cells. *Journal of Materials Chemistry B* **2017,** 5, (33), 6801-6810.
39. Tebbe, M.; Kuttner, C.; Männel, M.; Fery, A.; Chanana, M., Colloidally Stable and Surfactant-Free Protein-Coated Gold Nanorods in Biological Media. *ACS applied materials & interfaces* **2015,** 7, (10), 5984-5991.
40. Li, J.; Cai, R.; Kawazoe, N.; Chen, G., Facile preparation of albumin-stabilized gold nanostars for the targeted photothermal ablation of cancer cells. *Journal of Materials Chemistry B* **2015,** 3, (28), 5806-5814.
41. Liu, J.; He, H.; Xiao, D.; Yin, S.; Ji, W.; Jiang, S.; Luo, D.; Wang, B.; Liu, Y., Recent Advances of Plasmonic Nanoparticles and their Applications. *Materials* **2018,** 11, (10), 1833.
42. Zhang, J.; Li, J.; Kawazoe, N.; Chen, G., Composite scaffolds of gelatin and gold nanoparticles with tunable size and shape for photothermal cancer therapy. *Journal of Materials Chemistry B* **2017,** 5, (2), 245-253.
43. Zheng, J.; Liu, Q.; Yang, J.; Ren, Q.; Cao, W.; Yang, J.; Yu, Z.; Yu, F.; Wu, Y.; Shi, H.; Liu, W., Co-culture of apoptotic breast cancer cells with immature dendritic cells: a novel approach for DC-based vaccination in breast cancer. *Brazilian journal of medical and biological research = Revista brasileira de pesquisas medicas e biologicas* **2012,** 45, (6), 510-5.
44. Mellman, I.; Steinman, R. M., Dendritic cells: specialized and regulated antigen processing machines. *Cell* **2001,** 106, (3), 255-8.
45. Chen, Q.; Xu, L.; Liang, C.; Wang, C.; Peng, R.; Liu, Z., Photothermal therapy with immune-adjuvant nanoparticles together with checkpoint blockade for effective cancer immunotherapy. *Nature Communications* **2016,** 7, 13193.

Chapter 3

Preparation of AuNRs-gelatin composite scaffolds for photothermal therapy and activation of dendritic cells

3.1 Summary

Breast cancer is a major public health issue, whose morbidity and mortality are increasing across the world. It is still a challenge to completely ablate breast tumor cells by nanoparticles-mediated photothermal therapy. Photothermal scaffolds by incorporating photothermal nano-agents into porous scaffold are a desirable option to achieve the effect. In this study, composite porous scaffolds of gold nanorods (AuNRs) and gelatin with well controlled pore structures were prepared by introducing AuNRs into the porous matrices of gelatin and mixing with ice particles as a template. The AuNRs-gelatin composite scaffolds demonstrated high photothermal conversion effect, whose photothermal temperature could be modulated by the amount of incorporated AuNRs, NIR laser power intensity and irradiation time. The AuNRs-gelatin composite scaffolds exhibited excellent photothermal ablation capacity of breast tumor cells in *vitro* and in *vivo*. Furthermore, photothermally ablated tumor cells also induced activation of DCs by co-culture with immature DCs and ablated tumor cells in AuNRs-gelatin scaffolds.

3.2 Introduction

Breast cancer becomes one of the major threats to human life due to its increasing morbidity and mortality [1, 2]. Until now, surgery, chemo- or radio-therapy and their combination have been widely applied to treat breast tumor in clinic [3-6]. However, surgical resection cannot completely remove all the tumor cells [7]. Chemotherapy and radiotherapy can give rise to adverse effects such as drug-resistance and radio-resistance [8-10].

In recent years, photothermal therapy (PTT), as a minimally invasive and highly efficient antitumor strategy, has attracted great attention [11, 12]. Various photothermal conversion agents such as carbon-based nanomaterials, copper sulfide nanoparticles and gold-based nanomaterials have been extensively explored [13-16]. Among them, gold nanoparticles, especially gold nanorods (AuNRs), have raised much attention due to their tunable surface plasmon resonance property and facile preparation and good cytocompatibility [17-19]. However, efficacious and site-specific delivery of free nanoparticles to tumor site still has some problems [20-22]. Upon intravenous

injections of nanoparticles, the nanoparticles (NPs) undergo uptake by macrophages of mononuclear phagocyte system, which results in high accumulation of NPs in healthy organs such as liver and spleen [23-25]. To address these issues, immobilization of PTT NPs into three-dimensional (3D) scaffolds has been recently explored to realize repeat heating and local tumor therapy [26-29].

Based on the above consideration, functional composite scaffold of AuNRs and gelatin were fabricated by incorporating AuNRs in gelatin matrices through a freeze-drying method in this study. Pre-prepared ice particulates with optimized size were used as a template and mixed with AuNRs/gelatin mixture solution to control the pore structures of the composite scaffolds. Photothermal performance of the composite scaffolds under near infrared (NIR) laser at various power intensities was investigated. Their photothermal killing efficiency of breast tumor cells was evaluated by *in vitro* cell culture and *in vivo* animal experiment. Moreover, the effects of photothermally ablated tumor cells in AuNRs-gelatin composite scaffolds on the activation of dendritic cells were also investigated by co-culture with immature DCs and ablated tumor cells in AuNRs-gelatin scaffolds.

3.3 Materials and methods

3.3.1 Synthesis and characterization of gelatin-stabilized AuNRs

AuNRs were synthesized by a seed-mediated growth method [30, 31]. First gold seed solution were obtained via the reaction of hydrogen tetrachloroaurate(Ⅲ) tetrahydrate ($HAuCl_4 \cdot 4H_2O$, Wako) and sodium borohydride ($NaBH_4$, Sigma) in hexadecyltrimethylammonium bromide (CTAB, 0.1 mol/L, 7.5 mL) aqueous solution. The prepared Au seeds were used within 2 hours. Subsequently, a growth solution was obtained by mixing CTAB (0.1 mol/L, 100.0 mL) solution with $HAuCl_4$ (0.01 mol/L, 5.0 mL), HCl (1 mol/L, 2.0 mL), $AgNO_3$ (0.01 mol/L, 1.1 mL) and ascorbic acid (0.1 mol/L, 0.8 mL) solutions in sequence. Finally, the pre-prepared gold seeds grew up along the silver crystal in the growth solution under gentle stirring for 12 h to allow the formation of AuNRs. The AuNRs were collected by centrifugation under 8000 rpm for 10 min. In order to remove the CTAB, the collected AuNRs were washed with ultrapure water.

In order to avoid agglomeration of AuNRs and to make the homogeneously distributed AuNRs suspension in ultrapure water, the AuNRs were coated with gelatin by dispersing them into 0.5% (w/v) gelatin solution under stirring for 24 hours. The gelatin-coated AuNRs were obtained by centrifugation. The gelatin-coated AuNRs were resuspended in ultrapure water for the following experiments.

The morphology of gelatin-coated AuNRs was characterized with a transmission electron microscope (TEM, JEOL 2011F, Japan). The size of AuNRs was measured from TEM images with a ImageJ software (ImageJ2, NIH). Visible-near infrared (VIS−NIR) spectrum of aqueous solution of AuNRs was measured with a UV-660 UV-VIS spectrophotometer (Jasco Corp., Japan)

3.3.2 Preparation and characterization of AuNRs–gelatin composite scaffolds

AuNRs-gelatin composite porous scaffolds were prepared by freeze-drying the mixture solution of gelatin-coated AuNRs, gelatin and pre-prepared ice particulates as previously reported [32, 33]. Briefly, the ultrapure water were sprayed into liquid nitrogen to prepare the ice particles. Then the proper size (between 425 μm and 500 μm) of pre-prepared ice particles was optimized by sieving the ice particles with two meshes. Subsequently, A 70% acetic acid solution of 8 (w/v) % gelatin was mixed with 4.0 or 8.0 mM

AuNRs solution at a ratio of 1:1 (v/v) under sonication to prepare AuNRs/gelatin mixture solutions. The final concentration of gelatin in the mixture solutions was 4 (w/v) % while AuNRs concentration was 2.0 and 4.0 mM because our previous study showed that these two concentrations had good heating effect. The ice particulates, gelatin aqueous solution and AuNRs/gelatin mixture solution were kept in the chamber setting the temperature of -4 ℃ for 6 hours to balance. Subsequently, 7.0 g ice particles were homogenously mixed with 3 mL AuNRs-gelatin mixture solution. The mixture of ice particulates and AuNRs-gelatin solution was poured into a silicone mold. Finally, the whole constructs were transferred into -20 ℃ freezer for 12 hours and then moved to a -80 ℃ freezer for 4 hours. After that, the constructs were transferred into the freeze-dryer (FDU-2200, Japan) for freeze-drying to obtain the porous scaffolds. Then the AuNRs-gelatin porous composite scaffolds were chemically cross-linked using 1-ethyl-3-(3-dimethylaminopropyl) carbodiimide and N-hydroxysuccimide (EDC/NHS) to obtain the AuNRs-gelatin composite porous scaffolds. The morphology of AuNRs-gelatin composite scaffolds was characterized with a field emission scanning electron microscope (FESEM: SU8220, Hitachi, Japan). The AuNRs-gelatin composite scaffold prepared with an AuNRs concentration of 2.0 and 4.0 mM was defined as 2.0 mM AuNRs-gelatin scaffold and 4.0 mM AuNRs-gelatin scaffold, respectively. Gelatin scaffold without incorporation of AuNRs was also prepared as a control with the above-mentioned procedures without addition of AuNRs.

Pore size of gelatin scaffold and AuNRs-gelatin composite scaffolds was analyzed by measuring the diameters of pores in SEM images by Image-J software. The photothermal performance of gelatin scaffold, 2.0 mM AuNRs-gelatin scaffold and 4.0 mM AuNRs-gelatin scaffold was investigated by irradiation with an 805 nm laser (Thorlabs Inc., USA). Briefly, the AuNRs-gelatin composite scaffolds (5.0 ×3.0 ×1.0 mm) were immersed with culture medium. Then the hydrated samples were placed in culture plate and irradiated with near infrared laser at the wavelength of 805 nm. The temperature change of the AuNRs-gelatin composite scaffolds under NIR laser irradiation with different power intensity (1.3, 1.4, 1.5 or 1.6 W/cm^2) was recorded by a digital thermometer (As one Corp., Osaka, Japan) in real time.

3.3.3 Photothermal ablation of *in vitro* cultured breast tumor cells in AuNRs–gelatin scaffolds

The AuNRs-gelatin composite porous scaffolds (5.0 ×3.0 ×1.0 mm) were immersed in 70% ethanol solution for 4 h and washed with PBS for 6 times to sterilization. Human breast tumor cells that stably express luciferase (MDA-MB231-Luc) were obtained from Japanese collection of research bioresources cell bank (Osaka, Japan). MDA-MB231-Luc cells were cultured in L-15 medium supplemented with 15 % FBS. When the cells proliferated to 80% in the flask, the medium was removed and washed with PBS. Then 0.25% trypsin solution was added into flask and incubated for 5 min to detach the cells from the surface of flask. The harvested 4T1-Luc cells were re-suspended in L-15 medium and used for following experiments. Subsequently, 15 μL of the cell suspension solution was dropped into both two side of the scaffold cubes. The cell/scaffold constructs were transferred to a 24-well culture plate with 1 mL L-15 medium in each well.

After culture of breast tumor cells in AuNRs-gelatin composite porous scaffolds for 24 h, the cells/scaffold were removed from medium and exposed under NIR laser (805 nm) irradiation at different power intensity (1.3 or 1.6 W/cm^2). After that, the breast tumor cells in the composite scaffolds were incubated for 5 hours for live/dead cell staining. Then the live and dead cells in the composite scaffolds before and after laser irradiation were stained by calcein-AM/PI double staining kit (Dojindo, Japan) and then imaged under an inverted fluorescence microscope (Olympus, Japan). In addition, cell viability in the scaffolds before and after irradiation with a power intensity of 1.3 or 1.6 W/cm^2 for 3, 5, 6 and 8 minutes was quantified by WST-1 assay. 400 μL WST-1 reagent diluted by medium (1: 10) was added into each well

containing the cell/scaffold constructs and incubated for 3 hours. And then, the absorbance of WST-1 solution was detected via a microplate reader at the wavelength of 440 nm. The mean and standard deviation were calculated through three parallel samples of each group.

3.3.4 Activation of dendritic cells by co-culture with immature DCs and ablated tumor cells in AuNRs-gelatin composite scaffolds

The 4T1-Luc cells (2×10^5 cells/scaffold) were seeded on the 2.0 mM AuNRs-gelatin composite scaffold (5.0 ×3.0 ×1.0 mm) and cultured for 48 h. After that, the 4T1-Luc/AuNRs-gelatin scaffold was taken out from medium and the residual medium inside of scaffolds was absorbed using sterile tissue. Subsequently, the 4T1-Luc/AuNRs-gelatin scaffold construct was transferred into 96-well culture plate and irradiated with an 805 nm laser at a power intensity of 1.6 W cm^{-2} to photothermally ablate tumor cells.

Mouse bone marrow-derived immature dendritic cells (DCs, ATCC, Manassas, Virginia, USA) were used to investigate immune responses induced by photothermally ablated tumor cells in AuNRs-gelatin composite scaffold. Briefly, DCs (1×10^5 cells/scaffold) were seeded on the ablated 4T1-Luc/AuNRs-gelatin scaffold construct after photothermal ablation of tumor cells and cultured in MEM-α medium with 5 ng/mL GM-CSF for 36 h. As for control group, DCs (1×10^5 cells/scaffold) were seeded on the live 4T1-Luc/AuNRs-gelatin scaffold construct without laser irradiation and cultured for 36 h. As positive and negative controls, DCs (1×10^5 cells/scaffold) were directly seeded in 2.0 mM AuNRs-gelatin composite scaffold and cultured with or without 1 μg/mL lipopolysaccharide (LPS) stimulation for 36 h. Finally, supernatants were harvested to measure the secretion amount of interleukin 6 (IL-6), interleukin 12 (IL-10), interleukin 1β (IL-1β) and tumor necrosis factor alpha (TNF-α) by an enzyme-linked immunosorbent assay (ELISA) kit according to the manufacturer's instructions (PEPROTECH, Rocky Hill, New Jersey, USA). Mean and standard deviation were calculated by performing three parallel samples for each group.

3.3.5 Photothermal ablation of *in vivo* implanted breast tumor cells by AuNRs–gelatin scaffolds

The MDA-MB231-Luc cells were seeded in the cubes (5.0 ×3.0 ×1.0 mm) of gelatin porous scaffold and 2.0 mM AuNRs-gelatin scaffold and cultured in vitro for 3 days. The tumor cells/scaffold constructs were subcutaneously implanted into the back of 6-week-old female athymic nude mice. The nude mice were divided into four groups: tumor cells/gelatin scaffold, tumor cells/AuNRs-gelatin scaffold, tumor cells/gelatin scaffold + NIR laser irradiation, tumor cells/ AuNRs-gelatin scaffold + NIR laser irradiation. After implantation for 6 days, the implantation sites of the mice were irradiated with an NIR laser (805 nm) at a power density of 1.3 W/cm^2 for 10 minutes and 1.6 W/cm^2 for 8 minutes. After 1 day, the whole-body bioluminescence image was taken with an in vivo vision system (IVIS Lumina II, Japan) to evaluate the in vivo photothermal ablation effect of 2.0 mM AuNRs-gelatin scaffold. The procedures of animal experiments were supported by the Animal Experiments Committee and then the experiments were carried out according to the committee's guideline.

3.3.6 Statistical analysis

The quantitative experiment in this study was repeated using three parallel samples and the results were

expressed with average ± standard deviation (SD). The statistical analysis including significant difference was carried out by one-way ANOVA analysis software. The p value of 0.05 was considered statistically significant difference. The data were classified according to their p values and denoted by (*) for p less than 0.05, (**) for p less than 0.01 and (***) for p less than 0.001.

3.4 Results

3.4.1 Physical and chemical properties of gelatin-stabilized AuNRs

The gross appearance of colloid solution of AuNRs (Fig. 3.1a) showed that the gelatin-coated gold nanoparticles were homogeneously dispersed in pure water without aggregation. TEM images (Fig. 3.1b and c) indicated that gold nanoparticles were uniformly distributed without aggregation and had a rod-like shape with a dimension of 66.1 ± 2.3 nm × 13.6 ± 2.5 nm. The visible-near infrared (VIS-NIR) absorption spectrum (Fig. 3.1d) showed that AuNRs had a strong absorption peak in near infrared region, which is beneficial for photothermal therapy.

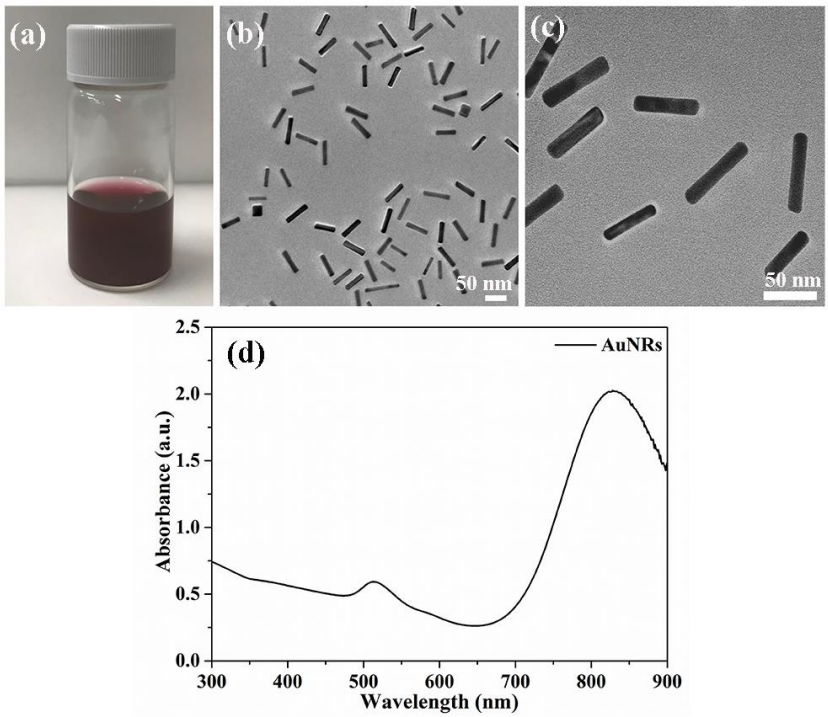

Fig. 3.1 Gross appearance of colloid solution of gelatin-coated AuNRs in pure water (a), TEM images of AuNRs at low (b) and high (c) magnifications and VIS-NIR spectrum of AuNRs colloid solution (d).

3.4.2 Characterization of AuNRs–gelatin composite scaffolds

SEM observation showed that the AuNRs-gelatin composite scaffolds had spherical large micropores with good interconnectivity, which were the same as those of the gelatin porous scaffold (Fig. 3.2a, b and c). Observation at a high magnification showed that AuNRs were individually distributed on the micropore wall of the composite scaffolds (Fig. 3.2e and f). No AuNRs were observed in the gelatin scaffold (Fig. 3.2d).

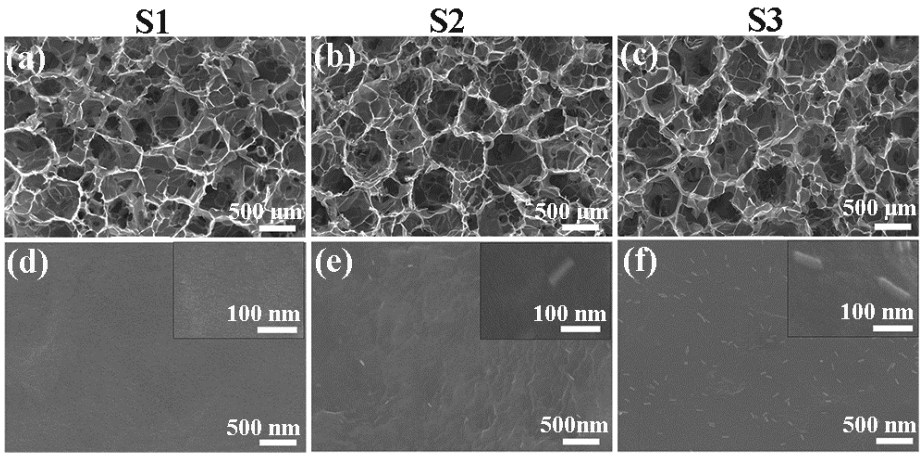

Fig. 3.2 SEM images of gelatin scaffold (a, d), 2.0 mM AuNRs-gelatin scaffold (b, e) and 4.0 mM AuNRs-gelatin scaffold (c, f) at a low magnification (a-c) and a high magnification (d-f). S1, S2 and S3 indicate gelatin scaffold, 2.0 mM AuNRs-gelatin scaffold and 4.0 mM AuNRs-gelatin scaffold, respectively. The insets show the magnified images of the corresponded scaffold.

3.4.3 Photothermal performance of AuNRs–gelatin composite scaffolds

Temperature of AuNRs-gelatin scaffolds increased when the scaffolds were irradiated with a NIR laser of 805 nm (Fig. 3.3). The photothermal temperature of AuNRs-gelatin scaffolds could be effectively modulated by changing the laser power intensity and altering the AuNRs amount. The AuNRs-gelatin scaffolds showed different photothermal efficiency under a variable laser power intensity (Fig. 3.3a and 3.b). Higher laser power intensity resulted in higher temperature. The temperature change data (Table 3.1) indicated that temperature change of gelatin scaffold, 2.0 mM AuNRs/gelatin scaffold and 4.0 mM. AuNRs/gelatin scaffold was 4.4 ± 0.9 ~8.9 ± 0.7 °C, 23.2 ± 0.8~32.9 ± 0.9 °C and 28.1 ± 0.9 ~41.0 ± 1.0 °C, respectively, when the laser power intensity varied from 1.3 W/cm^2 to 1.6 W/cm^2. When different scaffolds were compared, temperature change of gelatin scaffold under NIR laser irradiation was very slow while that of AuNRs-gelatin scaffolds increased rapidly (Fig. 3.3c and 3.3d). The temperature of 4.0 mM AuNRs-gelatin scaffolds was higher than that of 2.0 mM AuNRs-gelatin scaffolds under the same powder density, which indicated that increase of the incorporated AuNRs amount enhanced photothermal conversion efficiency of the composite scaffolds.

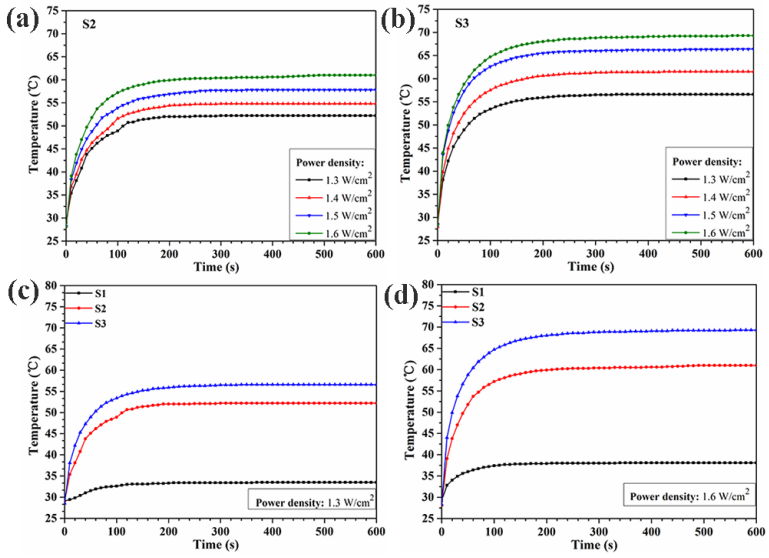

Fig. 3.3 Heating curves of AuNRs-gelatin composite scaffolds under continuous irradiation with 805 nm laser. Temperature-irradiation time curves of 2.0 mM AuNRs-gelatin scaffold (a) and 4.0 mM AuNRs-gelatin scaffold (b) under NIR laser irradiation at a power density of 1.3, 1.4, 1.5 and 1.6 W/cm^2. Temperature-irradiation time curves of gelatin scaffold, 2.0 mM AuNRs-gelatin scaffold and 4.0 mM AuNRs-gelatin scaffold under NIR laser irradiation at a power intensity of 1.3 W/cm^2 (c) and 1.6 W/cm^2 (d). S1, S2 and S3 indicate gelatin scaffold, 2.0 mM AuNRs-gelatin scaffold and 4.0 mM AuNRs-gelatin scaffold, respectively.

Table 3.1 Temperature change (^{o}C) of gelatin scaffold (S1), 2.0 mM AuNRs-gelatin scaffold (S2) and 4.0 mM AuNRs-gelatin scaffold (S3) after irradiation at different laser power densities for 10 minutes

Sample / Power density	S1	S2	S3
1.3 W/cm^2	4.4 ± 0.9	23.2 ± 0.8	28.1 ± 0.9
1.4 W/cm^2	6.9 ± 0.6	26.6 ± 1.1	33.5 ± 1.3
1.5 W/cm^2	7.9 ± 0.5	29.6 ± 0.7	38.0 ± 1.4
1.6 W/cm^2	8.9 ± 0.7	32.9 ± 0.9	41.0 ± 1.0

3.4.4 Photothermal ablation effect of AuNRs–gelatin composite scaffolds towards breast tumor cells *in vitro*

The photothermal ablation of breast tumor cells cultured in AuNRs-gelatin scaffolds was explored by NIR laser irradiation with the power density of 1.3 and 1.6 W/cm^2. Live/dead staining showed that almost all the tumor cells were live within the porous scaffolds before NIR laser irradiation (Fig. 3.4 a-c). After laser irradiation at the laser power intensity of 1.3 W/cm^2 for 8 minutes and 1.6 W/cm^2 for 6 minutes, almost all the breast tumor cells were dead in the AuNRs-gelatin composite scaffolds, while the breast tumor cells still kept alive in the gelatin scaffolds (Fig. 3.4 d-i). Quantification of cell viability showed that cellular viability of MDA-MB231-Luc cells cultured in gelatin scaffold had no significant change before and after NIR laser irradiation, while cellular viability in AuNRs-gelatin composite scaffolds significantly decreased after NIR laser irradiation (Fig. 3.4 j and k). Cell viability in AuNRs-gelatin composite scaffolds significantly decreased after NIR laser irradiation. Increase of irradiation time significantly decreased cell viability. Cell viability of MDA-MB231-Luc cells cultured in 2.0 mM AuNRs-gelatin scaffold and 4.0 mM AuNRs-gelatin scaffold decreased to 0% after NIR laser irradiation at the power density of 1.3 W/cm^2 for 8 minutes or 1.6 W/cm^2 for 6 minutes. Increase of NIR laser density resulted in further decrease of cell viability. Under the same NIR laser irradiation condition, cells cultured in 4.0 mM AuNRs-gelatin scaffold showed quicker decrease of viability than did those cultured in 2.0 mM AuNRs-gelatin scaffold, suggesting that increase of AuNRs raised the photothermal killing effect of tumor cells.

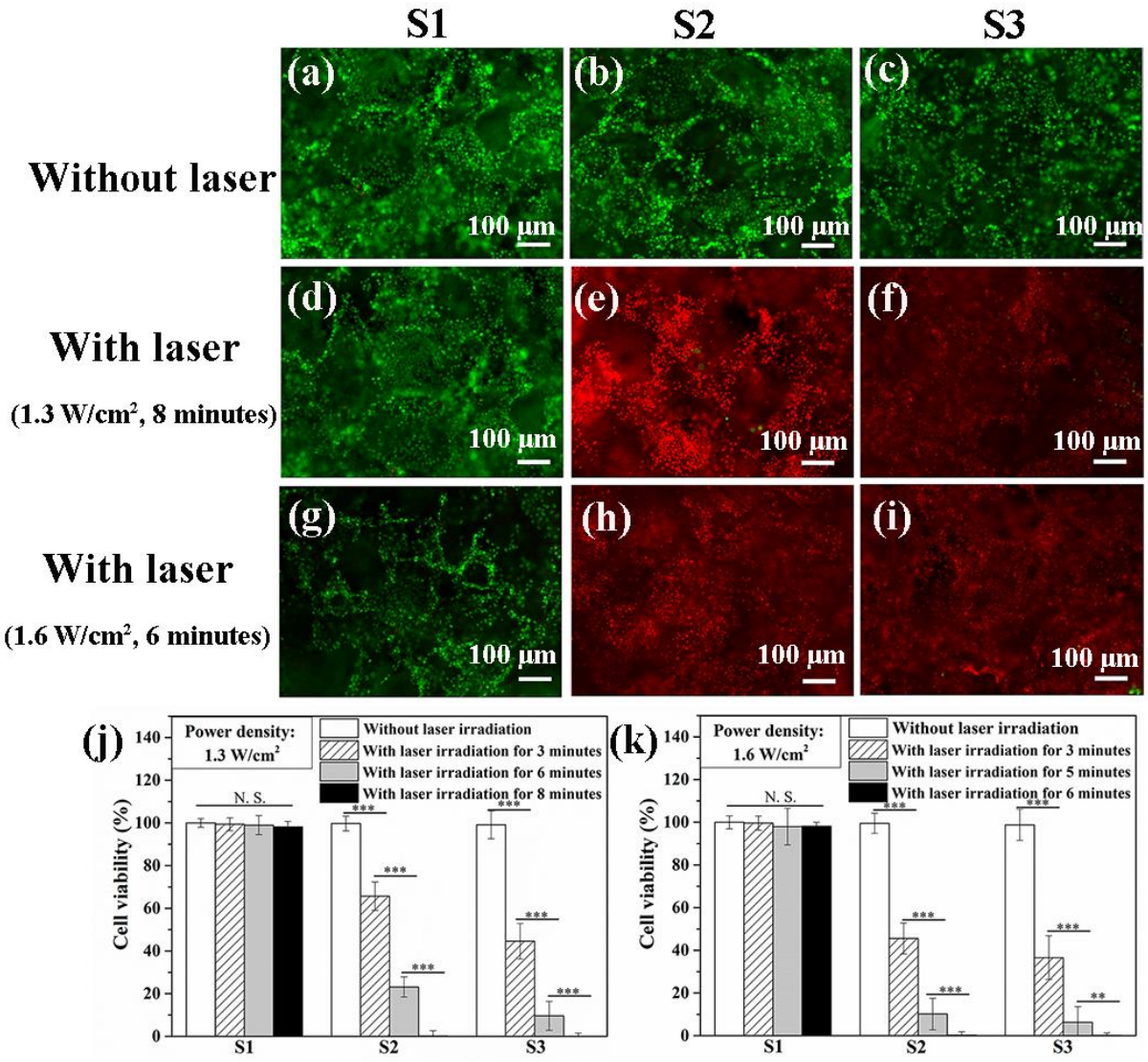

Fig. 3.4 Live/dead staining of breast tumor cells (MDA-MB231-Luc cells) cultured in gelatin scaffold (a, d, g), 2.0 mM AuNRs-gelatin scaffold (b, e, h) and 4.0 mM AuNRs-gelatin scaffold (c, f, i) without (a-c) and with NIR laser irradiation (d-i) at a laser power intensity of 1.3 W/cm^2 for 8 minutes (d-f) and a laser power intensity of 1.6 W/cm^2 for 6 minutes (g-i). Green color displays live cells stained by calcein-AM while red color displays dead cells stained by PI. Viability of MDA-MB231-Luc cells cultured in gelatin scaffold and AuNRs-gelatin composite scaffolds after irradiation for different time with a laser power intensity of 1.3 W/cm^2 (j) and 1.6 W/cm^2 (k). S1, S2 and S3 indicate gelatin scaffold, 2.0 mM AuNRs-gelatin scaffold and 4.0 mM AuNRs-gelatin scaffold, respectively. The data are displayed as average ± standard deviation, n = 3. No significant difference: N.S.; significant difference: * $p < 0.05$; ** $p < 0.01$; *** $p < 0.001$.

3.4.5 Activation of dendritic cells by photothermally ablated cells in AuNRs–gelatin composite scaffolds

SEM images (Fig. 3.5) demonstrated that before laser irradiation, the breast tumor cells were attached well on the wall of micropores in 2.0 mM AuNRs-gelatin composite scaffolds. And the tumor cells distributed throughout the scaffolds. Moreover, the ablated tumor cells still remained in the AuNRs-gelatin composite scaffolds after laser irradiation, which will induce the activation of DCs when co-culture of

immature DCs and photothermally ablated tumor cells in the AuNRs-gelatin composite scaffolds.

To investigate the activation of DCs by photothermally ablated tumor cells in AuNRs-gelatin composite scaffolds, secretion of multiple cytokines including IL-6, IL-10, IL-1β and TNF-α from DCs was measured by ELISA Kit after co-culture of immature DCs and ablated tumor cells in AuNRs-gelatin composite scaffolds for 36 h. As shown in Fig. 3.6, the ablated tumor cells including cell debris and soluble factors promoted the secretion level of IL-6, IL-10, IL-1β and TNF-α as compared to those of live tumor cells. Moreover, the live tumor cells promoted the secretion level of IL-6 and IL-1β in comparation with those of negative control group.

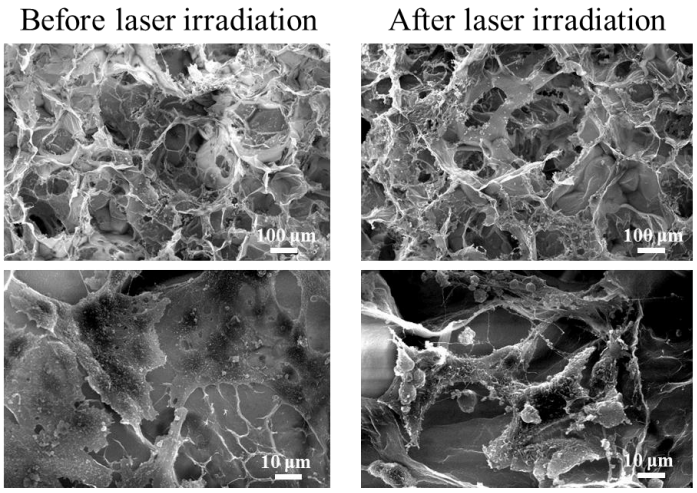

Fig. 3.5 Breast tumor cells morphology in 2.0 mM AuNRs-gelatin composite scaffold before and after laser irradiation at a laser density of 1.6 W/cm^2.

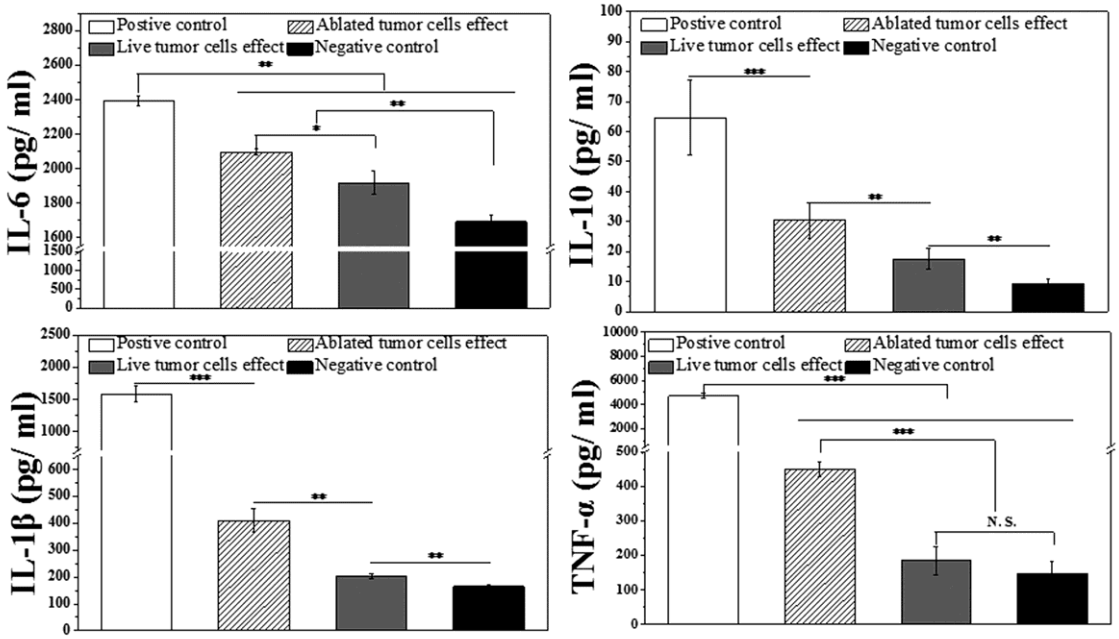

Fig. 3.6 Secretion level of cytokines IL-6 (a), IL-10 (b), IL-1β (c) and TNF-α (d) by dendritic cells (DCs) after co-culture of immature DCs and photothermally ablated tumor cells in 2.0 mM AuNRs-gelatin composite scaffold. Data are presented as mean ± standard deviation, n = 3. No significant difference: N.S.; significant difference: * $p < 0.05$; ** $p < 0.01$; *** $p < 0.001$.

3.4.6 Photothermal ablation of breast tumor cells by AuNRs–gelatin composite scaffolds *in vivo*

The *in vivo* photothermal ablation effect of breast tumor cells by AuNRs-gelatin scaffold was evaluated by the whole-body bioluminescence imaging after laser irradiation. MDA-MB-231-Luc cells were cultured in gelatin scaffold and 2.0 mM AuNRs-gelatin scaffold *in vitro*. Then the MDA-MB-231-Luc cells/ AuNRs-gelatin scaffold construct was subcutaneously implanted on the back of nude mice. After 6 days implantation, the implantation sites of the mice were irradiated with an NIR laser. Bioluminescent images showed that the bioluminescent signal of living MDA-MB231-Luc cells in 2.0 mM AuNRs-gelatin scaffold evidently decreased after NIR laser irradiation, while that in gelatin scaffolds kept almost unchanged (Fig. 3.7). Irradiation at the laser power density of 1.6 W cm^{-2} for 8 minutes showed almost the same effect as that of irradiation at a laser power density of 1.3 W cm^{-2} for 10 minutes. The results indicated that most of the breast cancer cells were killed by 2.0 mM AuNRs-gelatin scaffold under NIR laser irradiation. Gross appearance of the mice showed that the skin tissue near the implanted 2.0 mM AuNRs-gelatin scaffold was obviously damaged after NIR laser irradiation at the high power intensity (1.6 W cm^{-2}) for 8 minutes (Fig. 3.8). Skin damage was suppressed when the irradiation was conducted at the laser power density of 1.3 W cm^{-2} for 10 minutes.

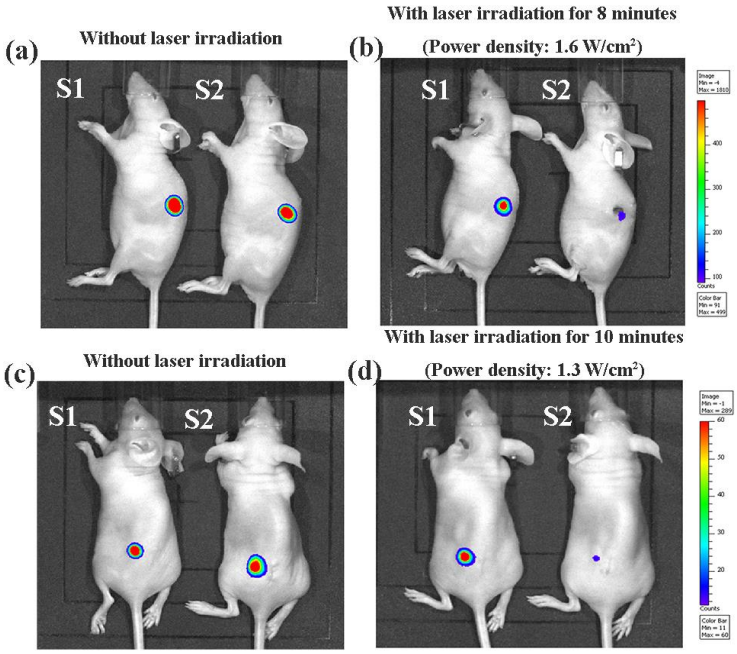

Fig. 3.7 Whole-body bioluminescence imaging of mice subcutaneously implanted with MDA-MB231-Luc cells/gelatin scaffold and MDA-MB231-Luc cells/2.0 mM AuNRs-gelatin scaffold constructs before irradiation (a, c) and after NIR laser irradiation at a laser density of 1.6 W/cm^2 for 8 minutes (b) and a laser density of 1.3 W/cm^2 for 10 minutes (d). S1 and S2 indicate gelatin scaffold and 2.0 mM AuNRs-gelatin scaffold, respectively.

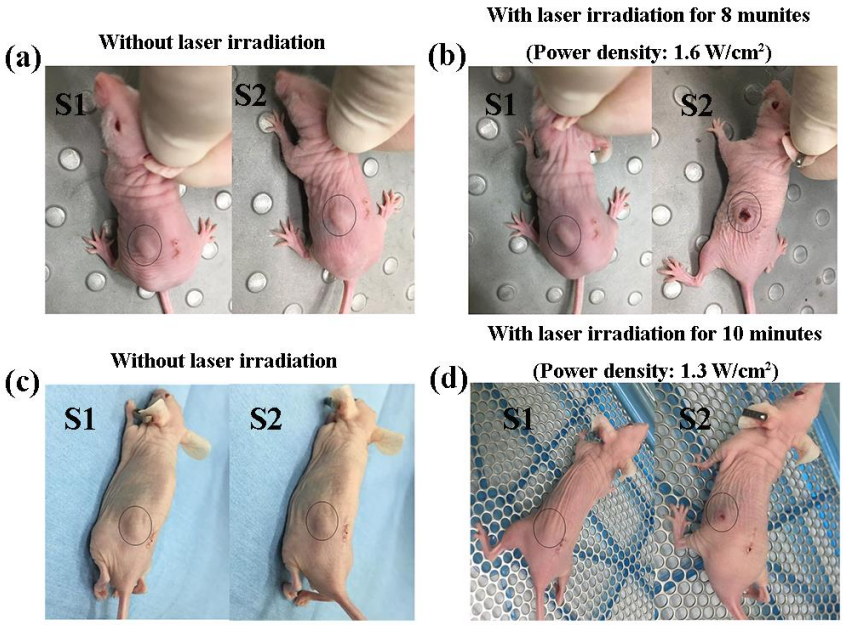

Fig. 3.8 Photographs of mice subcutaneously implanted with MDA-MB231-Luc cells/gelatin scaffold and MDA-MB231-Luc cells/2.0 mM AuNRs-gelatin scaffold constructs before irradiation (a, c) and after NIR laser irradiation at a laser density of 1.6 W/cm^2 for 8 minutes (b) and a laser density of 1.3 W/cm^2 for 10 minutes (d).

3.5 Discussions

Complete ablation of residual breast tumor cells to prevent tumor recurrence still remains a critical challenge in breast cancer therapy [34-36]. To address these issues, AuNRs-gelatin composite porous scaffolds were designed and prepared by incorporating photothermal conversion nanoparticles, AuNRs, in gelatin porous scaffold. AuNRs aqueous solutions at a different concentration of AuNRs (2.0, 4.0 mM) were used to introduce different amount of AuNRs in the composite scaffolds. Optimized ice particles were applied as a template material to regulate the pore structure of composite scaffold. The composite scaffolds had the same size of spherical large micropores and small micropores as those of gelatin scaffold (Fig. 3.2a-c).

The synthesized AuNRs had a strong near-infrared light absorption peaks at a wavelength of 813 nm (Fig. 3.1d), which is skin-penetrative, non-invasive and harmless [37, 38]. AuNRs-gelatin composite scaffolds showed excellent photothermal performance under the NIR (805 nm) irradiation (Fig. 3.3 and Table 3.1). The photothermal conversion of composite scaffolds should be due to the photothermal conversion property of AuNRs. It has been reported that AuNRs can efficiently convert near infrared light into heat [39]. The photothermal-induced temperature changes of the AuNRs-gelatin composite scaffolds could be modulated by changing the laser power intensity, irradiation time and incorporated AuNRs amount.

The excellent photothermal performance of AuNRs-gelatin composite scaffolds was applied for photothermal ablation of breast tumor cells. The *in vitro* cell culture and *in vivo* animal experiment showed that the composite scaffolds could effectively kill breast tumor cells (Fig. 3.4 and 3.7). Composite scaffolds prepared with different concentration of AuNRs (2.0 mM and 4.0 mM) were used for the ablation of tumor cells to examine the effect of AuNRs amount. The *in vitro* cell culture experiments indicated that the two composite scaffolds could effectively kill tumor cells and the killing effect increased with the increase of incorporated AuNRs amount, NIR laser intensity and irradiation time (Fig. 3.4). The dependence of tumor

cell ablation capacity on AuNRs amount, NIR laser intensity and irradiation time should be due to the heating characteristics of AuNRs incorporated in the composite scaffolds. Because both 2.0 mM and 4.0 mM AuNRs-gelatin scaffolds could kill all the breast tumor cells after NIR laser irradiation at the power density of 1.3 W cm^{-2} for 8 minutes and the power density of 1.6 W cm^{-2} for 6 minutes, 2.0 mM AuNRs-gelatin scaffold was used for *in vivo* animal experiments. Moreover, the ablated tumor cells still remained in the AuNRs-gelatin composite scaffolds after laser irradiation as shown in Fig. 3.5. These ablated tumor cells also promoted the secretion level of multiple cytokines (Fig. 3.6) including IL-6, IL-10, IL-1β and TNF-α from DCs after co-culture of immature DCs and ablated tumor cells in AuNRs-gelatin scaffold, which might triggers the immune system to prevent tumor metastasis and recurrence.

For *in vivo* animal experiment, MDA-MB231-Luc cells were seeded in the scaffolds and then subcutaneously implanted in nude mice. The seeded cells could be thought as migrated cells from surrounding tissues and this model was used to confirm the killing effect of composite scaffolds on the migrated cells. NIR laser irradiations at the power density of 1.3 W/cm^2 for 10 minutes and a power intensity of 1.6 W/cm^2 for 8 minutes were used to guarantee the killing effect. The whole-body bioluminescent images showed that the luminescence intensity, which indicated living cells, decreased dramatically after NIR laser irradiation of the 2.0 mM AuNRs-gelatin scaffold (Fig. 3.7). The results indicated that most of breast cancer cells were killed by photothermal ablation of 2.0 mM AuNRs-gelatin composite scaffolds. Both irradiation conditions at the power density of 1.3 W/cm^2 for 10 minutes and a power intensity of 1.6 W/cm^2 for 8 minutes showed dramatic ablation effects. However, the skin tissue near the 2.0 mM AuNRs-gelatin scaffolds was obviously damaged after laser irradiation at a high power density (1.6 W cm^{-2} for 8 minutes) (Fig. 3.8). Therefore, achieving effective tumor ablation under relative low photothermal temperature is critical toward successful clinical application of PTT [40].

3.6 Conclusions

AuNRs-gelatin porous scaffolds were prepared by introducing AuNRs in the porous structure of gelatin matrices via a freeze-drying method. Pre-prepared ice particulates with optimized size were used as a template to construct the pore structure of scaffolds. The AuNRs-gelatin composite scaffolds showed high photothermal conversion efficiency. The AuNRs-gelatin composite scaffolds also showed excellent photothermal ablation capacity of breast tumor cells *in vitro* and *in vivo*. Furthermore, photothermally ablated tumor cells also induced activation of DCs by co-culture of immature DCs and ablated tumor cells in AuNRs-gelatin composite scaffolds, which might triggers the immune system to prevent tumor metastasis and recurrence.

3.7 References

1. Li, H.; Wang, K.; Yang, X.; Zhou, Y.; Ping, Q.; Oupicky, D.; Sun, M., Dual-function nanostructured lipid carriers to deliver IR780 for breast cancer treatment: Anti-metastatic and photothermal anti-tumor therapy. *Acta biomaterialia* **2017,** 53, 399-413.
2. Micalizzi, D. S.; Maheswaran, S., On the trail of invasive cells in breast cancer. *Nature* **2018,** 554, (7692), 308-309.
3. Ruda, R.; Bruno, F.; Soffietti, R., What Have We Learned from Recent Clinical Studies in Low-Grade Gliomas? *Current treatment options in neurology* **2018,** 20, (8), 33.
4. Yang, Y.-S.; Carney, R. P.; Stellacci, F.; Irvine, D. J., Enhancing Radiotherapy by Lipid

Nanocapsule-Mediated Delivery of Amphiphilic Gold Nanoparticles to Intracellular Membranes. *ACS Nano* **2014,** 8, (9), 8992-9002.

5. Baskar, R.; Lee, K. A.; Yeo, R.; Yeoh, K. W., Cancer and radiation therapy: current advances and future directions. *International journal of medical sciences* **2012,** 9, (3), 193-9.
6. Jones, S. E.; Durie, B. G.; Salmon, S. E., Combination chemotherapy with adriamycin and cyclophosphamide for advanced breast cancer. *Cancer* **1975,** 36, (1), 90-7.
7. Quirke, P.; Durdey, P.; Dixon, M. F.; Williams, N. S., Local recurrence of rectal adenocarcinoma due to inadequate surgical resection. Histopathological study of lateral tumour spread and surgical excision. *Lancet (London, England)* **1986,** 2, (8514), 996-9.
8. Stark, G. R., Cancer chemotherapy: Progress in understanding multidrug resistance. *Nature* **1986,** 324, 407.
9. Busenhart, D. M.; Erb, J.; Rigakos, G.; Eliades, T.; Papageorgiou, S. N., Adverse effects of chemotherapy on the teeth and surrounding tissues of children with cancer: A systematic review with meta-analysis. *Oral oncology* **2018,** 83, 64-72.
10. Robinson, R.; Marconi, L.; MacPepple, E.; Hakenberg, O. W.; Watkin, N.; Yuan, Y.; Lam, T.; MacLennan, S.; Adewuyi, T. E.; Coscione, A.; Minhas, S. S.; Comperat, E. M.; Necchi, A., Risks and Benefits of Adjuvant Radiotherapy After Inguinal Lymphadenectomy in Node-positive Penile Cancer: A Systematic Review by the European Association of Urology Penile Cancer Guidelines Panel. *European urology* **2018,** 74, (1), 76-83.
11. Cheng, L.; Wang, C.; Feng, L.; Yang, K.; Liu, Z., Functional nanomaterials for phototherapies of cancer. *Chemical reviews* **2014,** 114, (21), 10869-939.
12. Zou, L.; Wang, H.; He, B.; Zeng, L.; Tan, T.; Cao, H.; He, X.; Zhang, Z.; Guo, S.; Li, Y., Current Approaches of Photothermal Therapy in Treating Cancer Metastasis with Nanotherapeutics. *Theranostics* **2016,** 6, (6), 762-772.
13. Li, Y.; Lu, W.; Huang, Q.; Huang, M.; Li, C.; Chen, W., Copper sulfide nanoparticles for photothermal ablation of tumor cells. *Nanomedicine (London, England)* **2010,** 5, (8), 1161-71.
14. Chen, Y. W.; Su, Y. L.; Hu, S. H.; Chen, S. Y., Functionalized graphene nanocomposites for enhancing photothermal therapy in tumor treatment. *Advanced drug delivery reviews* **2016,** 105, (Pt B), 190-204.
15. Jaque, D.; Martinez Maestro, L.; del Rosal, B.; Haro-Gonzalez, P.; Benayas, A.; Plaza, J. L.; Martin Rodriguez, E.; Garcia Sole, J., Nanoparticles for photothermal therapies. *Nanoscale* **2014,** 6, (16), 9494-530.
16. Chen, J.; Ning, C.; Zhou, Z.; Yu, P.; Zhu, Y.; Tan, G.; Mao, C., Nanomaterials as photothermal therapeutic agents. *Progress in Materials Science* **2019,** 99, 1-26.
17. Jang, B.; Park, J. Y.; Tung, C. H.; Kim, I. H.; Choi, Y., Gold nanorod-photosensitizer complex for near-infrared fluorescence imaging and photodynamic/photothermal therapy in vivo. *ACS Nano* **2011,** 5, (2), 1086-94.
18. Norouzi, H.; Khoshgard, K.; Akbarzadeh, F., In vitro outlook of gold nanoparticles in photo-thermal therapy: a literature review. *Lasers in medical science* **2018,** 33, (4), 917-926.
19. Gharatape, A.; Davaran, S.; Salehi, R.; Hamishehkar, H., Engineered gold nanoparticles for photothermal cancer therapy and bacteria killing. *RSC Advances* **2016,** 6, (112), 111482-111516.
20. Hsiao, C. W.; Chuang, E. Y.; Chen, H. L.; Wan, D.; Korupalli, C.; Liao, Z. X.; Chiu, Y. L.; Chia, W. T.; Lin, K. J.; Sung, H. W., Photothermal tumor ablation in mice with repeated therapy sessions using NIR-absorbing micellar hydrogels formed in situ. *Biomaterials* **2015,** 56, 26-35.

21. Leroux, J.-C.; Allémann, E.; De Jaeghere, F.; Doelker, E.; Gurny, R., Biodegradable nanoparticles — From sustained release formulations to improved site specific drug delivery. *Journal of Controlled Release* **1996,** 39, (2), 339-350.
22. Chen, F.; Cai, W., Nanomedicine for targeted photothermal cancer therapy: where are we now? *Nanomedicine (London, England)* **2015,** 10, (1), 1-3.
23. Blanco, E.; Shen, H.; Ferrari, M., Principles of nanoparticle design for overcoming biological barriers to drug delivery. *Nature biotechnology* **2015,** 33, (9), 941-51.
24. Jaque, D.; Martínez Maestro, L.; del Rosal, B.; Haro-Gonzalez, P.; Benayas, A.; Plaza, J. L.; Martín Rodríguez, E.; García Solé, J., Nanoparticles for photothermal therapies. *Nanoscale* **2014,** 6, (16), 9494-9530.
25. Singh, R.; Lillard, J. W., Jr., Nanoparticle-based targeted drug delivery. *Experimental and molecular pathology* **2009,** 86, (3), 215-223.
26. Ma, H.; Jiang, C.; Zhai, D.; Luo, Y.; Chen, Y.; Lv, F.; Yi, Z.; Deng, Y.; Wang, J.; Chang, J.; Wu, C., A Bifunctional Biomaterial with Photothermal Effect for Tumor Therapy and Bone Regeneration. *Advanced Functional Materials* **2016,** 26, (8), 1197-1208.
27. Zhang, J.; Li, J.; Chen, S.; Kawazoe, N.; Chen, G., Preparation of gelatin/Fe3O4 composite scaffolds for enhanced and repeatable cancer cell ablation. *Journal of Materials Chemistry B* **2016,** 4, (34), 5664-5672.
28. Zhang, Y.; Zhai, D.; Xu, M.; Yao, Q.; Chang, J.; Wu, C., 3D-printed bioceramic scaffolds with a Fe3O4/graphene oxide nanocomposite interface for hyperthermia therapy of bone tumor cells. *Journal of Materials Chemistry B* **2016,** 4, (17), 2874-2886.
29. Zhang, J.; Li, J.; Kawazoe, N.; Chen, G., Composite scaffolds of gelatin and gold nanoparticles with tunable size and shape for photothermal cancer therapy. *Journal of Materials Chemistry B* **2017,** 5, (2), 245-253.
30. Xiang, Y.; Wu, X.; Liu, D.; Feng, L.; Zhang, K.; Chu, W.; Zhou, W.; Xie, S., Tuning the Morphology of Gold Nanocrystals by Switching the Growth of {110} Facets from Restriction to Preference. *The Journal of Physical Chemistry C* **2008,** 112, (9), 3203-3208.
31. Li, J.; Li, J. E. J.; Zhang, J.; Wang, X.; Kawazoe, N.; Chen, G., Gold nanoparticle size and shape influence on osteogenesis of mesenchymal stem cells. *Nanoscale* **2016,** 8, (15), 7992-8007.
32. Zhang, Q.; Lu, H.; Kawazoe, N.; Chen, G., Pore size effect of collagen scaffolds on cartilage regeneration. *Acta biomaterialia* **2014,** 10, (5), 2005-13.
33. Shangwu, C.; Qin, Z.; Tomoko, N.; Naoki, K.; Guoping, C., Gelatin Scaffolds with Controlled Pore Structure and Mechanical Property for Cartilage Tissue Engineering. *Tissue Engineering Part C: Methods* **2016,** 22, (3), 189-198.
34. Dutra, A. K.; Andrade, W. P.; Carvalho, S. M.; Makdissi, F. B.; Yoshimatsu, E. K.; Domingues, M. C.; Maciel, M. S., Immediate breast reconstruction using autologous skin graft associated with breast implant. *Journal of plastic, reconstructive & aesthetic surgery : JPRAS* **2012,** 65, (2), 187-94.
35. Urruticoechea, A.; Alemany, R.; Balart, J.; Villanueva, A.; Vinals, F.; Capella, G., Recent advances in cancer therapy: an overview. *Curr Pharm Des* **2010,** 16, (1), 3-10.
36. Baudino, T. A., Targeted Cancer Therapy: The Next Generation of Cancer Treatment. *Current drug discovery technologies* **2015,** 12, (1), 3-20.
37. Wu, X.; Chen, G.; Shen, J.; Li, Z.; Zhang, Y.; Han, G., Upconversion Nanoparticles: A Versatile Solution to Multiscale Biological Imaging. *Bioconjugate Chemistry* **2015,** 26, (2), 166-175.
38. Huang, Y.; Chen, C.; Li, H.; Xiao, A.; Guo, T.; Guan, B.-O., Insight into the local near-infrared

photothermal dynamics of graphene oxide functionalized polymers through optical microfibers. *Physical Chemistry Chemical Physics* **2018,** 20, (7), 5256-5263.

39. Mackey, M. A.; Ali, M. R.; Austin, L. A.; Near, R. D.; El-Sayed, M. A., The most effective gold nanorod size for plasmonic photothermal therapy: theory and in vitro experiments. *The journal of physical chemistry. B* **2014,** 118, (5), 1319-26.
40. Wang, X.; Lv, F.; Li, T.; Han, Y.; Yi, Z.; Liu, M.; Chang, J., Electrospun Micropatterned Nanocomposites Incorporated with Cu2S Nanoflowers for Skin Tumor Therapy and Wound Healing. *ACS Nano* **2017,** 11, (11), 11337-11349.

Chapter 4

Adipogenic differentiation of hMSCs in AuNRs-gelatin composite scaffolds

4.1 Summary

Breast cancer is a major public health issue, whose morbidity and mortality are increasing across the world. It is still a challenge to reconstruct tumor-initiated breast defects after surgical resection. Porous scaffolds with hyperthermal and tissue regeneration functions are a desirable option to achieve the effects. In this study, composite porous scaffolds of gold nanorods (AuNRs) and gelatin with well controlled pore structures were prepared by introducing AuNRs into the porous matrices of gelatin and mixing with ice particles as a template. The AuNRs-gelatin porous scaffolds supported cell adhesion and promoted proliferation and adipogenic differentiation of human bone-marrow derived mesenchymal stem cells (hMSCs). Consequently, the AuNRs-gelatin scaffold has a potential of breast reconstruction by promoting adipogenic differentiation of stem cells for adipose tissue regeneration.

4.2 Introduction

Breast cancer becomes one of the major threats to human life due to its increasing morbidity and mortality [1, 2]. Until now, surgery, chemo- or radio-therapy and their combination have been widely applied to treat breast tumor in clinic [3-5]. However, large breast defect is always accompanied with cancer removal, which is difficult to self-heal [6]. Until now, it still remains a big challenge to realize breast reconstruction after tumor therapy [7, 8]. Therefore, it is expected to design highly functional biomaterials that can be used to promote breast reconstruction as bioactive scaffolds [9-13].

It has been reported that adipose tissue can be regenerated by combining a 3D biodegradable porous scaffold with adipose-derived stromal cells or bone-marrow derived mesenchymal stem cells [12, 14]. 3D scaffold for adipose tissue engineering should bear soft tissue-like mechanical property, biocompatibility and biodegradability [14-18]. Gelatin has been used for preparation of tissue regeneration scaffolds because of its high bioactivity, low antigenicity and low immunogenicity [19, 20]. Gelatin scaffold has been reported favorable for adipose tissue engineering because of its soft tissue-like mechanical property, as compared to stiff scaffold such as poly lactic-co-glycolic acid

scaffold [14, 21-23]. In addition, 3D scaffolds should have an appropriate pore structure with open and interconnected pores to promote cell penetration and nutrition and metabolite exchange [24]. Although a variety of methods have been explored to fabricate porous scaffolds such as electrospinning, 3D printing and porogen leaching method [25-27], freeze-drying method has become a common used method for preparing polymers-scaffolds especially for collagen and gelatin scaffolds [28]. Pre-prepared ice particulates can be mixed with naturally derived polymers before freeze-drying to precisely control pore structures of scaffolds [29, 30].

Based on the above considerations, functional composite porous scaffold of AuNRs and gelatin were fabricated by incorporating AuNRs in gelatin matrices through a freeze-drying method in this study. Ice particulates with optimized size were used as a template and mixed with AuNRs/gelatin mixture solution to construct the pore structures of scaffolds. The composite porous scaffolds of AuNRs and gelatin with well controlled pore structures were applied for 3D culture of human bone-marrow derived mesenchymal stem cells (hMSCs) to explore their capacity to promote adipogenic differentiation of hMSCs.

4.3 Materials and methods

4.3.1 Preparation and characterization of AuNRs-gelatin composite porous scaffolds

AuNRs-gelatin composite porous scaffolds were prepared by freeze-drying the mixture solution of gelatin-coated AuNRs, gelatin and pre-prepared ice particulates as previously reported [29, 31]. Briefly, the ultrapure water were sprayed into liquid nitrogen to prepare the ice particles. Then the proper size (between 425 μm and 500 μm) of pre-prepared ice particles was optimized by sieving the ice particles with two meshes. Subsequently, A 70% acetic acid solution of 8 (w/v) % gelatin was mixed with 4.0 or 8.0 mM AuNRs solution at a ratio of 1:1 (v/v) under sonication to prepare AuNRs/gelatin mixture solutions. The final concentration of gelatin in the mixture solutions was 4 (w/v) % while AuNRs concentration was 2.0 and 4.0 mM because our previous study showed that these two concentrations had good heating effect. The ice particulates, gelatin aqueous solution and AuNRs/gelatin mixture solution were kept in the chamber setting the temperature of -4 ℃ for 6 hours to balance. Subsequently, 7.0 g ice particles were homogenously mixed with 3 mL AuNRs-gelatin mixture solution. The mixture of ice particulates and AuNRs-gelatin solution was poured into a silicone mold. Finally, the whole constructs were transferred into -20 ℃ freezer for 12 hours and then moved to a -80 ℃ freezer for 4 hours. After that, the constructs were transferred into the freeze-dryer (FDU-2200, Japan) for freeze-drying to obtain the porous scaffolds. Then the AuNRs-gelatin porous composite scaffolds were chemically cross-linked using 1-ethyl-3-(3-dimethylaminopropyl) carbodiimide and N-hydroxysuccimide (EDC/NHS) to obtain the AuNRs-gelatin composite porous scaffolds. The morphology of AuNRs-gelatin composite scaffolds was characterized with a field emission scanning electron microscope (FESEM: SU8220, Hitachi, Japan). The AuNRs-gelatin composite scaffold prepared with an AuNRs concentration of 2.0 and 4.0 mM was defined as 2.0 mM AuNRs-gelatin scaffold and 4.0 mM AuNRs-gelatin scaffold, respectively. Gelatin scaffold without incorporation of AuNRs was also prepared as a control with the above-mentioned procedures without addition of AuNRs.

Pore size of gelatin scaffold and AuNRs-gelatin composite scaffolds was analyzed by measuring the diameters of pores from four SEM images of each type of scaffold with a ImageJ software.

4.3.2 *In vitro* culture of hMSCs

The hMSCs at passage 2 (P2) were obtained from Lonza (Walkersville MD, USA) and subcultured in basal medium (Lonza, Swiss). When the cells proliferated to 80% in the flask, the medium was removed and washed with PBS. Then 0.25% trypsin solution was added into flask and incubated for 5 min to detach the cells from the surface of flask and stocked in liquid nitrogen. The harvested hMSCs (P4, 4.0×10^6 cells/mL) suspension was seeded into both sides of gelatin scaffold, 2.0 mM AuNRs-gelatin scaffold and 4.0 mM AuNRs-gelatin scaffold and cultured in DMEM medium. Then the medium was refreshed every 3 days by adding the 1 μM dexamethasone, 0.5 mM Methyl-isobutylxanthine, 100 μM Indomethacin and 10 μg/mL insulin.

4.3.3 Adhesion of hMSCs in AuNRs-gelatin composite scaffolds

Cell attachment was analyzed by SEM observation. Briefly, after being cultured for 1 day, the hMSCs were fixed in the gelatin porous scaffold, 2.0 mM AuNRs-gelatin porous composite scaffold and 4.0 mM AuNRs-gelatin porous composite scaffold using 2.5% glutaraldehyde solution. Subsequently, the fixed samples were dehydrated by an gradient alcohol series including 50%, 70%, 80%, 90%, 100%, 100% ethanol: H_2O (w/w%). Then these samples were treated an gradient an t-Butyl alcohol series including 50%, 70%, 80%, 90%, 100%, 100% t-Butyl alcohol: ethanol (w/w%). Finally, these samples were immersed into 100% t-Butyl alcohol solution and kept at 4 ^oC for freezing. After that, these samples were lyophilized to observe cell adhesion and morphology in these three types of AuNRs-gelatin porous composite scaffolds by FE-SEM..

4.3.4 DNA quantification assay of hMSCs in AuNRs-gelatin composite scaffolds

Cell proliferation was investigated by measuring DNA amount of hMSCs cultured in gelatin porous scaffold, 2.0 mM AuNRs-gelatin porous composite scaffold and 4.0 mM AuNRs-gelatin porous composite scaffold. Briefly, after culture of hMSCs in AuNRs-gelatin porous composite scaffold for 1, 7 and 14 days, the hMSCs were fixed in AuNRs-gelatin porous composite scaffold using 4% paraformaldehyde solution. Then the samples were washed with ultrapure water, frozen in a -80 ^oC freezer and freeze-dried for 2 days. Subsequently, the freeze-dried samples were digested using the papain solution (400 μg/mL, pH: 6.0, phosphate buffer solvent). After that, the DNA dissolved in papain solution was mixed with Hoechst 33250 dye and detected using the fluorescence spectrometer. The mean and standard deviation were calculated through three parallel samples of each group.

4.3.5 Oil Red O staining and quantitative analysis in AuNRs-gelatin composite scaffolds

Oil Red O staining was carried out to observe lipid vacuoles formation. Briefly, after culture of hMSCs in gelatin porous scaffold, 2.0 mM AuNRs-gelatin porous composite scaffold and 4.0 mM AuNRs-gelatin porous composite scaffold for 14 days, the hMSCs were fixed in these three types of scaffolds using 4% paraformaldehyde solution. After that, the samples were washed with ultrapure water and immersed into isopropanol solution (60%) and then immersed into Oil Red O solution to stain the lipid vacuoles. Subsequently, the stained samples were imaged under the microscope. In addition, the Oil Red O dye stained in these three types of scaffolds was extracted by treatment with isopropanol for 2 hours at room temperature.

Finally, the absorbance value was measured with a microplate reader at a wavelength of 540 nm [32].

4.3.6 Real-time PCR assay for adipogenesis-related genes expression

After culture of hMSCs in gelatin porous scaffold, 2.0 mM AuNRs-gelatin porous composite scaffold and 4.0 mM AuNRs-gelatin porous composite scaffold for 14 days, the expression level of adipogenesis-related genes containing fatty acid binding protein 4 (FABP4), peroxisome proliferator-activated receptor gamma (PPARG), CCAAT/enhancer binding protein (CEBPA) ipoprotein lipase (LPL) and fatty acid synthase (FASN) was detected using real-time polymerase chain reaction (RT-PCR). Briefly, the hMSCs/AuNRs-gelatin composite scaffolds were transferred into a niche containing liquid nitrogen to be frozen, then the samples were crushed into powders with a special crushing machine. Subsequently, the powders were transferred into Sepasol solution for isolating total RNA from samples. After that, the first stand cDNA synthesis kit was used to convert the extracted RNA into cDNA according to the protocol offered by applied biosystems. Finally, the RT-PCR was carried out to detected the expression level of the adipogensis-related genes using RT-PCR system (7500, applied biosystems, USA) [33]. The serial number of primer and prober for different adipogensis-related genes were listed in Table 4.1. Moreover, the endogenous control was the expression of GAPDH and the $2^{-\Delta\Delta Ct}$ method was used to calculate the relative gene expression value. The hMSCs at P4 used for cell seeding was used as a control for comparison. Every three samples were used for the measurement to calculate the average and standard deviation. The mean and standard deviation were calculated through three parallel samples of each group.

Table 4.1 The serial number of primer and probe for real-time PCR

mRNA	Oligonucleotide
GAPDH	Hs99999905_m1
PPARG	Hs01115510_m1
LPL	Hs00173425_m1
FABP4	Hs00609791_m1
FASN	Hs00188012_m1
CEBPA	Hs00269972_s1

4.3.7 Statistical analysis

The quantitative experiment in this study was repeated using three parallel samples and the results were expressed with average ± standard deviation (SD). The statistical analysis including significant difference was carried out by one-way ANOVA analysis software. The p value of 0.05 was considered statistically significant difference. The data were classified according to their p values and denoted by (*) for p less than 0.05, (**) for p less than 0.01 and (***) for p less than 0.001

4.4 Results

4.4.1 Morphology and pore structure of AuNRs-gelatin composite scaffolds

SEM observation showed that the AuNRs-gelatin composite scaffolds had spherical large micropores with good interconnectivity, which were the same as those of the gelatin porous scaffold (Fig. 4.1). The size of the spherical large micropores (Table 4.2) in gelatin scaffold, 2.0 mM AuNRs-gelatin scaffold and 4.0 mM AuNRs-gelatin scaffold was 439 ± 38 μm, 442 ± 21 μm and 435 ± 44 μm, respectively. The large micropore size was at the same range because the same ice particulates with a diameter range between 425 μm and 500 μm were optimized for preparation of the gelatin scaffold and 2.0 mM and 4.0 mM AuNRs-gelatin composite scaffolds. Small micropores connecting the large micropores were observed on the wall of the spherical large micropores. The size of interconnected small micropores (Table 4.2) in gelatin scaffold, 2.0 mM AuNRs-gelatin scaffold and 4.0 mM AuNRs-gelatin scaffold was 66 ± 25 μm, 76 ± 18 μm and 69 ± 23 μm, respectively. The three types of scaffolds had the same range of small micropores.

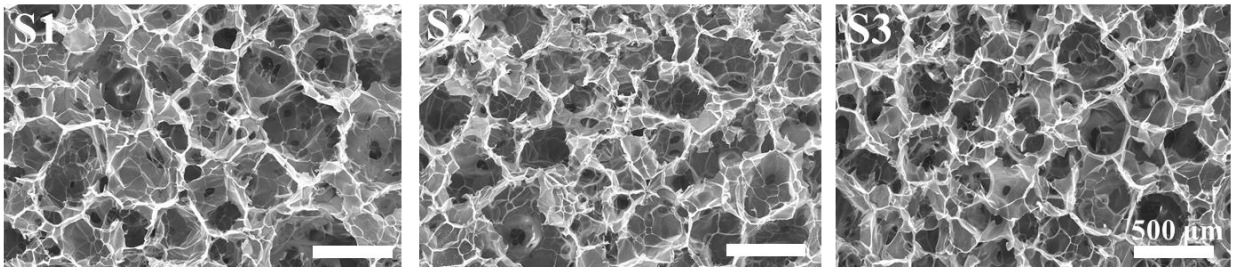

Fig. 4.1 SEM images of gelatin scaffold (S1), 2.0 mM AuNRs-gelatin scaffold (S2) and 4.0 mM AuNRs-gelatin scaffold (S3).

Table 4.2 Pore size analysis of gelatin scaffold (S1), 2.0 mM AuNRs-gelatin scaffold (S2) and 4.0 mM AuNRs-gelatin scaffold (S3).

Sample / Pore size (μm)	S1	S2	S3
Spherical large micropores	439 ± 38	442 ± 21	435 ± 44
Interconnected Small micropores	66 ± 25	76 ± 18	69 ± 23

4.4.2 Adhesion and distribution of hMSCs in AuNRs-gelatin composite scaffolds

To investigate the capacity of AuNRs-gelatin composite scaffolds for adipose tissue regeneration, the composite scaffolds were used for 3D culture of hMSCs. After 1 day culture, attachment and distribution of hMSCs within the scaffolds were observed using SEM (Fig. 4.2). SEM images showed that hMSCs adhered well with typical filopodia on the wall of micropores in all the gelatin scaffold and AuNRs-gelatin composite

scaffolds. The cells distributed throughout the scaffolds.

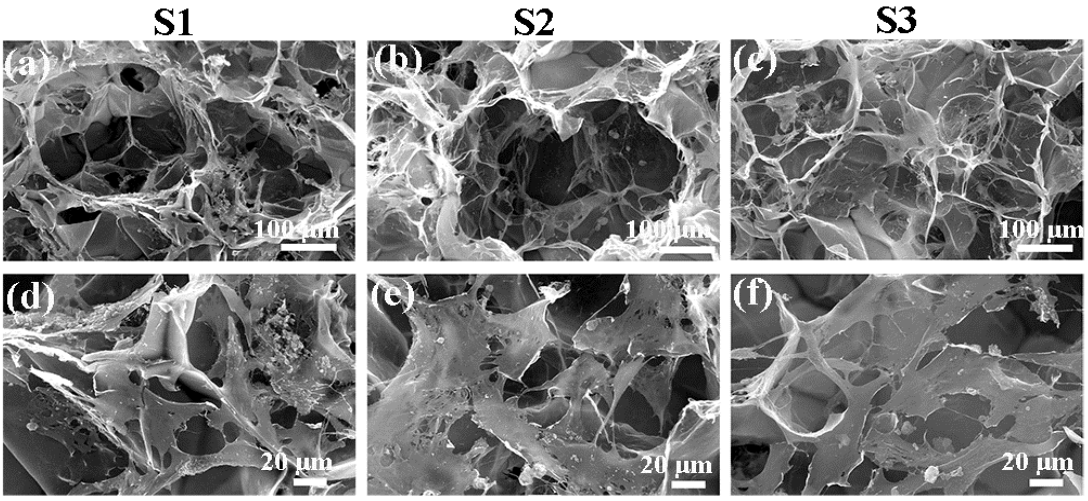

Fig. 4.2 SEM images of hMSCs/scaffold constructs at a low magnification (a-c) and a high magnification (d-f) after hMSCs were cultured in gelatin scaffold (S1, a, d), 2.0 mM AuNRs-gelatin scaffold (S2, b, e) and 4.0 mM AuNRs-gelatin scaffold (S3, c, f) for 1 day.

4.4.3 Proliferation of hMSCs in AuNRs-gelatin composite scaffolds

DNA quantification (Fig. 4.3) showed that DNA content increased significantly after being cultured for 1, 7 and 14 days in all the scaffolds. DNA content had no significant difference among all these three kinds of scaffolds. The results suggested that both gelatin scaffold and 2.0 mM, 4.0 mM AuNRs-gelatin composite scaffolds supported cell adhesion and promoted proliferation of hMSCs. Incorporation of AuNRs into gelatin scaffold had no significant influence on adhesion and proliferation of hMSCs.

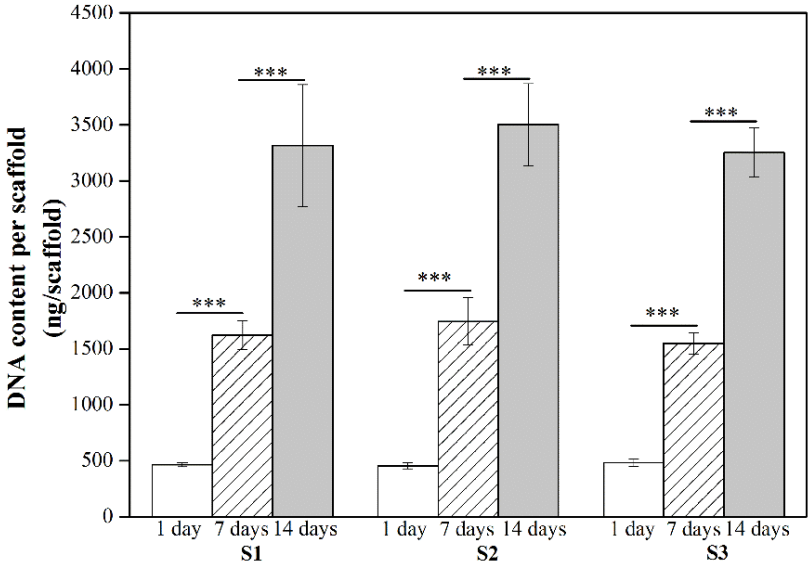

Fig. 4.3 Quantification of DNA content of hMSCs/scaffold constructs after hMSCs were cultured in gelatin scaffold (S1), 2.0 mM AuNRs-gelatin scaffold (S2) and 4.0 mM AuNRs-gelatin scaffold (S3) for 1, 7 and 14 days. The data are presented as mean ± standard deviation, n = 3. Significant difference: *** $p < 0.001$.

4.4.4 Lipid vacuoles formation in AuNRs-gelatin composite scaffolds

Adipogenic differentiation of hMSCs in AuNRs-gelatin composite scaffolds was analyzed by Oil Red O staining and expression of adipogenesis genes after being cultured in adipogenesis-induction medium for 14 days. Oil Red O staining images showed that lipid vacuoles were detected when hMSCs were cultured in gelatin scaffold, 2.0 mM AuNRs-gelatin scaffold and 4.0 mM AuNRs-gelatin scaffold (Fig. 4.4a-c). Quantification of the extracted Oil Red O dye showed that lipid vacuoles amount had no significant difference among the three types of scaffolds (Fig. 4.4d).

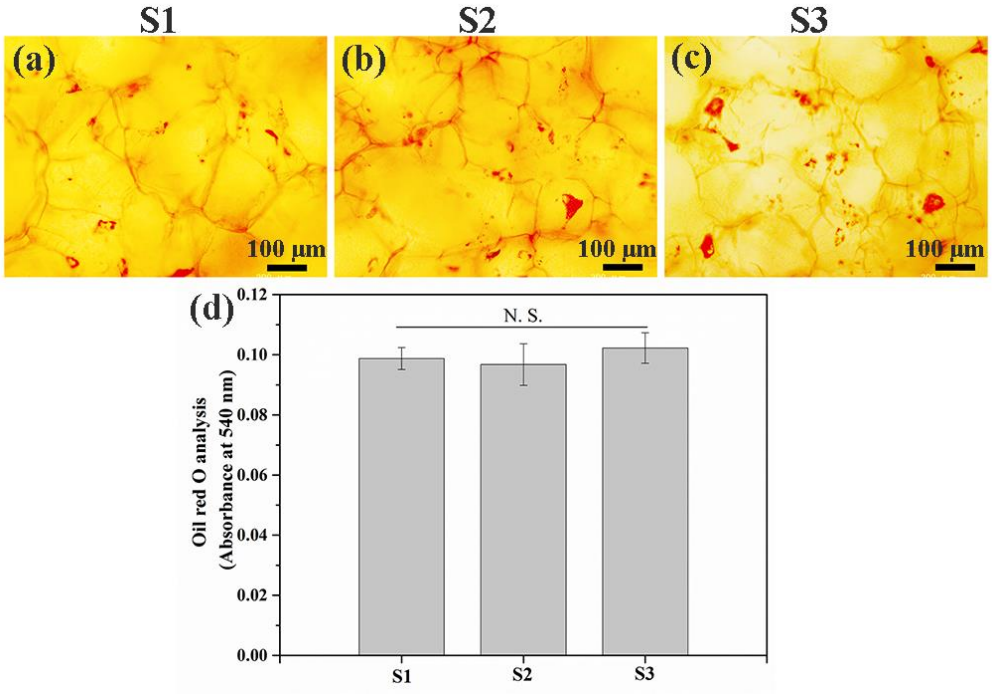

Fig. 4.4 Oil Red O staining images (a-c) and quantification of extracted Oil Red O dye (d) of cell/scaffold constructs after hMSCs were cultured in gelation scaffold (S1, a), 2.0 mM AuNRs-gelatin scaffold (S2, b) and 4.0 mM AuNRs-gelatin scaffold (S3, c) for 14 days. The data are presented as average ± standard deviation, n = 3. No significant difference: N.S.

4.4.5 Expression of adipogenesis-related genes in AuNRs-gelatin composite scaffolds

Expression of genes encoding CEBPA, PPARG, LPL, FABP4 and FASN showed that all these genes were upregulated when hMSCs were cultured in gelatin scaffold and AuNRs-gelatin composite scaffolds in comparison with the subcultured hMSCs (control) (Fig. 4.5). Expression level of these genes had no significant difference among gelatin scaffold, 2.0 mM AuNRs-gelatin scaffold and 4.0 mM AuNRs-gelatin scaffold. Oil Red O staining and gene expression results indicated that gelatin scaffold and AuNRs-gelatin composite scaffolds had the same promotive effects on adipogenic differentiation of hMSCs. Incorporation of AuNRs in gelatin scaffold had no influence on the promotive effect of gelatin scaffold for adipogenic differentiation of hMSCs.

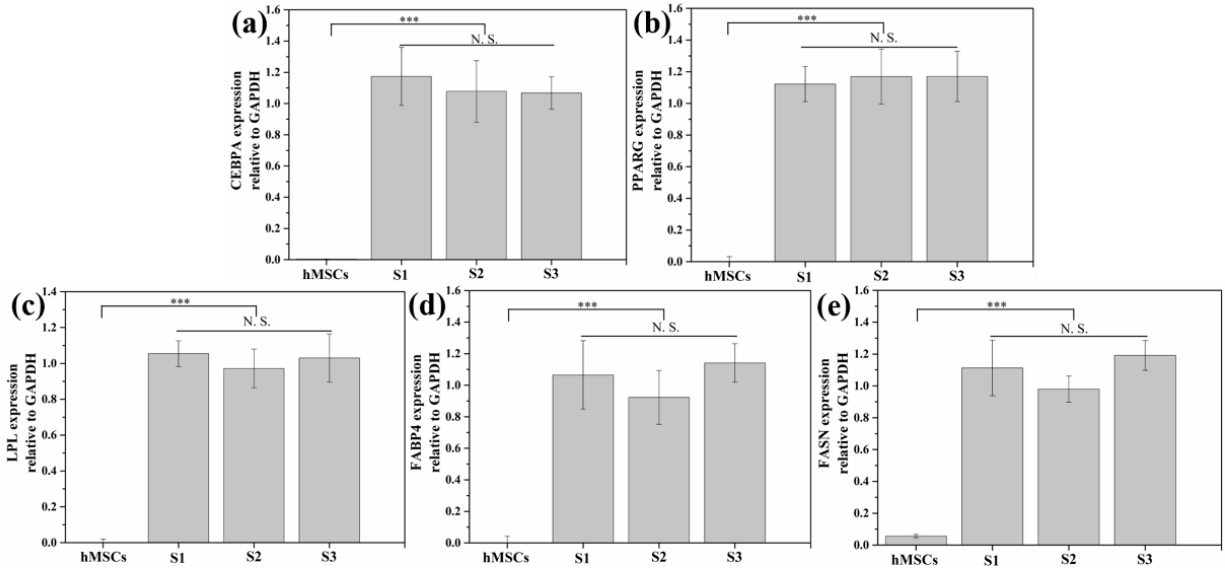

Fig. 4.5 Expression of genes encoding CEBPA (a), PPARG (b), LPL (c), FABP4 (d) and FASN (e) by hMSCs cultured in gelatin scaffold (S1), 2.0 mM AuNRs-gelatin scaffold (S2) and 4.0 mM AuNRs-gelatin scaffold (S3) for 14 days. The subcultured hMSCs used for cell seeding was used as a control. Data represent means ± SD, n = 3. No significant difference: N.S.; significant difference: *** $p < 0.001$.

4.5 Discussion

Successful reconstruction of tumor-initiated breast defects after surgical resection remain a critical challenge in breast cancer therapy [6, 34-36]. To address this issue, bifunctional AuNRs-gelatin composite porous scaffolds were designed and prepared by incorporating photothermal conversion nanoparticles, AuNRs, in gelatin porous scaffold. AuNRs aqueous solutions at a different concentration of AuNRs (2.0, 4.0 mM) were used to introduce different amount of AuNRs in the composite scaffolds. Optimized ice particulates were used as a template to construct the pore structure of composite scaffolds. The composite scaffolds had the same size of spherical large micropores and small micropores as those of gelatin scaffold (Fig. 4.1 and Table 4.2). The spherical large micropores were well interconnected by the small micropores on the walls of spherical large micropores. All the gelatin scaffold and composite scaffolds had the same pore structures because the same ice particulates were used and the freezing temperature was the same during the preparation process. The size and shape of spherical large micropores were controlled by the incorporated ice particulates based on the ground that they should be the negative replicas of pre-prepared ice particulates. While the small micropores on the wall of large micropores should be the replica of new ice crystals that were formed around the pre-prepared ice particulates during freezing process of the ice particulates-AuNRs-gelatin mixture solution. Porous structure and good interconnectivity of the composite scaffolds were beneficial to the cell adhesion and distribution throughout the scaffolds as shown in Fig. 4.2.

Adipose tissue regeneration is required to realize breast reconstruction to improve quality of life of the patients. The potential of AuNRs-gelatin composite scaffolds for adipose tissue engineering was confirmed by examining their promotive effect on adipogenic differentiation of hMSCs. The composite scaffolds not only supported adhesion and proliferation of hMSCs as shown in Fig. 4.2

and Fig. 4.3, but also enhanced formation of lipid vacuoles (Fig. 4.4) and expression of adipogenic genes (CEBPA, PPARG, LPL, FABP4 and FASN) (Fig. 4.5). In addition, the composite scaffolds showed the same level of lipid vacuole formation and the same adipogensis-related gene expression level as did the gelatin scaffold, which suggested incorporation of AuNRs had no influence on adipogenic differentiation of hMSCs. Although *in vivo* adipogenesis promotion effect of the composite scaffolds will be further confirmed in future, the results in present study indicated the AuNRs-gelatin composite scaffolds had a bifunctional property for simultaneous photothermal ablation of breast tumor and adipogenic differentiation of hMSCs.

4.6 Conclusions

In summary, functional AuNRs-gelatin porous scaffolds were prepared by introducing AuNRs in the porous structure of gelatin matrices via a freeze-drying method. Pre-prepared ice particulates were used as templates to construct the pore structure of scaffolds. The AuNRs-gelatin composite scaffolds showed well controlled pore structure with interconnectivity. The AuNRs-gelatin composite scaffolds supported adhesion, promoted proliferation and enhanced adipogenic differentiation of hMSCs. The results demonstrated that the AuNRs-gelatin scaffolds had the potential of adipose tissue regeneration for breast reconstruction after breast cancer therapy.

4.7 References

1. Li, H.; Wang, K.; Yang, X.; Zhou, Y.; Ping, Q.; Oupicky, D.; Sun, M., Dual-function nanostructured lipid carriers to deliver IR780 for breast cancer treatment: Anti-metastatic and photothermal anti-tumor therapy. *Acta biomaterialia* **2017,** 53, 399-413.
2. Micalizzi, D. S.; Maheswaran, S., On the trail of invasive cells in breast cancer. *Nature* **2018,** 554, (7692), 308-309.
3. Ruda, R.; Bruno, F.; Soffietti, R., What Have We Learned from Recent Clinical Studies in Low-Grade Gliomas? *Current treatment options in neurology* **2018,** 20, (8), 33.
4. Baskar, R.; Lee, K. A.; Yeo, R.; Yeoh, K. W., Cancer and radiation therapy: current advances and future directions. *International journal of medical sciences* **2012,** 9, (3), 193-9.
5. Yang, Y.-S.; Carney, R. P.; Stellacci, F.; Irvine, D. J., Enhancing Radiotherapy by Lipid Nanocapsule-Mediated Delivery of Amphiphilic Gold Nanoparticles to Intracellular Membranes. *ACS Nano* **2014,** 8, (9), 8992-9002.
6. Quirke, P.; Durdey, P.; Dixon, M. F.; Williams, N. S., Local recurrence of rectal adenocarcinoma due to inadequate surgical resection. Histopathological study of lateral tumour spread and surgical excision. *Lancet (London, England)* **1986,** 2, (8514), 996-9.
7. Tachi, M.; Yamada, A., Choice of flaps for breast reconstruction. *International journal of clinical oncology* **2005,** 10, (5), 289-97.
8. Becker, S., A historic and scientific review of breast cancer: The next global healthcare challenge. *International Journal of Gynecology & Obstetrics* **2015,** 131, S36-S39.
9. Sasikala, A. R. K.; Unnithan, A. R.; Thomas, R. G.; Ko, S. W.; Jeong, Y. Y.; Park, C. H.; Kim, C. S., Multifaceted Implantable Anticancer Device for Potential Postsurgical Breast Cancer Treatment: A Single Platform for Synergistic Inhibition of Local Regional Breast Cancer Recurrence, Surveillance, and Healthy Breast Reconstruction. *Advanced Functional Materials* **2018,** 28, (8), 1704793.

10. Wang, X.; Li, T.; Ma, H.; Zhai, D.; Jiang, C.; Chang, J.; Wang, J.; Wu, C., A 3D-printed scaffold with MoS2 nanosheets for tumor therapy and tissue regeneration. *Npg Asia Materials* **2017,** 9, e376.
11. Van Nieuwenhove, I.; Tytgat, L.; Ryx, M.; Blondeel, P.; Stillaert, F.; Thienpont, H.; Ottevaere, H.; Dubruel, P.; Van Vlierberghe, S., Soft tissue fillers for adipose tissue regeneration: From hydrogel development toward clinical applications. *Acta biomaterialia* **2017,** 63, 37-49.
12. Ogino, S.; Morimoto, N., Development of a novel bioabsorbable implant that is substituted by adipose tissue in vivo. **2018,** 12, (3), 633-641.
13. Unnithan, A. R.; Sasikala, A. R. K.; Thomas, S. S.; Nejad, A. G.; Cha, Y. S.; Park, C. H.; Kim, C. S., Strategic Design and Fabrication of Biomimetic 3D Scaffolds: Unique Architectures of Extracellular Matrices for Enhanced Adipogenesis and Soft Tissue Reconstruction. *Scientific Reports* **2018,** 8, (1), 5696.
14. Hong, L.; Peptan, I.; Clark, P.; Mao, J. J., Ex Vivo Adipose Tissue Engineering by Human Marrow Stromal Cell Seeded Gelatin Sponge. *Annals of Biomedical Engineering* **2005,** 33, (4), 511-517.
15. Sung, H. J.; Meredith, C.; Johnson, C.; Galis, Z. S., The effect of scaffold degradation rate on three-dimensional cell growth and angiogenesis. *Biomaterials* **2004,** 25, (26), 5735-42.
16. Akhtar, R.; Sherratt, M. J.; Cruickshank, J. K.; Derby, B., Characterizing the elastic properties of tissues. *Materials today (Kidlington, England)* **2011,** 14, (3), 96-105.
17. Zhang, H.; Zhou, L.; Zhang, W., Control of scaffold degradation in tissue engineering: a review. *Tissue engineering. Part B, Reviews* **2014,** 20, (5), 492-502.
18. Naahidi, S.; Jafari, M.; Logan, M.; Wang, Y.; Yuan, Y.; Bae, H.; Dixon, B.; Chen, P., Biocompatibility of hydrogel-based scaffolds for tissue engineering applications. *Biotechnology Advances* **2017,** 35, (5), 530-544.
19. PAUL H. MAURER, The effect of physical and enzymatic treatment of gelatin on the subsequent precipitin reaction. **1957**.
20. Maurer, P. H., II. Antigenicity of gelatin in rabbits and other species. *The Journal of experimental medicine* **1954,** 100, (5), 515-23.
21. Kimura, Y.; Inamoto, T.; Tabata, Y., Adipose tissue formation in collagen scaffolds with different biodegradabilities. *Journal of biomaterials science. Polymer edition* **2010,** 21, (4), 463-76.
22. Kimura, Y.; Tsuji, W.; Yamashiro, H.; Toi, M.; Inamoto, T.; Tabata, Y., In situ adipogenesis in fat tissue augmented by collagen scaffold with gelatin microspheres containing basic fibroblast growth factor. *Journal of tissue engineering and regenerative medicine* **2010,** 4, (1), 55-61.
23. Kimura, Y.; Ozeki, M.; Inamoto, T.; Tabata, Y., Adipose tissue engineering based on human preadipocytes combined with gelatin microspheres containing basic fibroblast growth factor. *Biomaterials* **2003,** 24, (14), 2513-21.
24. Hutmacher, D. W., Scaffolds in tissue engineering bone and cartilage. *Biomaterials* **2000,** 21, (24), 2529-43.
25. Mele, E., Electrospinning of natural polymers for advanced wound care: towards responsive and adaptive dressings. *Journal of Materials Chemistry B* **2016,** 4, (28), 4801-4812.
26. Zhu, H.; Zhai, D.; Lin, C.; Zhang, Y.; Huan, Z.; Chang, J.; Wu, C., 3D plotting of highly uniform Sr5(PO4)2SiO4 bioceramic scaffolds for bone tissue engineering. *Journal of Materials Chemistry B* **2016,** 4, (37), 6200-6212.
27. Yoon, J. J.; Park, T. G., Degradation behaviors of biodegradable macroporous scaffolds prepared by gas foaming of effervescent salts. *Journal of biomedical materials research* **2001,** 55, (3), 401-8.
28. Wu, X.; Liu, Y.; Li, X.; Wen, P.; Zhang, Y.; Long, Y.; Wang, X.; Guo, Y.; Xing, F.; Gao, J.,

Preparation of aligned porous gelatin scaffolds by unidirectional freeze-drying method. *Acta biomaterialia* **2010,** 6, (3), 1167-77.

29. Zhang, Q.; Lu, H.; Kawazoe, N.; Chen, G., Pore size effect of collagen scaffolds on cartilage regeneration. *Acta biomaterialia* **2014,** 10, (5), 2005-13.
30. Oh, H. H.; Ko, Y. G.; Lu, H.; Kawazoe, N.; Chen, G., Preparation of porous collagen scaffolds with micropatterned structures. *Advanced materials* **2012,** 24, (31), 4311-6.
31. Shangwu, C.; Qin, Z.; Tomoko, N.; Naoki, K.; Guoping, C., Gelatin Scaffolds with Controlled Pore Structure and Mechanical Property for Cartilage Tissue Engineering. *Tissue Engineering Part C: Methods* **2016,** 22, (3), 189-198.
32. Li, J.; Chen, Y.; Kawazoe, N.; Chen, G., Ligand density-dependent influence of arginine–glycine–aspartate functionalized gold nanoparticles on osteogenic and adipogenic differentiation of mesenchymal stem cells. *Nano Research* **2018,** 11, (3), 1247-1261.
33. Chen, Y.; Li, J.; Kawazoe, N.; Chen, G., Preparation of dexamethasone-loaded calcium phosphate nanoparticles for the osteogenic differentiation of human mesenchymal stem cells. *Journal of Materials Chemistry B* **2017,** 5, (33), 6801-6810.
34. Dutra, A. K.; Andrade, W. P.; Carvalho, S. M.; Makdissi, F. B.; Yoshimatsu, E. K.; Domingues, M. C.; Maciel, M. S., Immediate breast reconstruction using autologous skin graft associated with breast implant. *Journal of plastic, reconstructive & aesthetic surgery : JPRAS* **2012,** 65, (2), 187-94.
35. Rossi, E.; Guerrero, J.; Aprile, P.; Tocchio, A.; Kappos, E. A.; Gerges, I.; Lenardi, C.; Martin, I.; Scherberich, A., Decoration of RGD-mimetic porous scaffolds with engineered and devitalized extracellular matrix for adipose tissue regeneration. *Acta biomaterialia* **2018,** 73, 154-166.
36. Gerber, B.; Marx, M.; Untch, M.; Faridi, A., Breast Reconstruction Following Cancer Treatment. *Deutsches Arzteblatt international* **2015,** 112, (35-36), 593-600.

Chapter 5

Concluding remarks and future prospects

5.1 Concluding remarks

This dissertation describes the design and preparation of bifunctional AuNRs-gelatin composite scaffolds for both photothermal therapy of breast tumor and adipose tissue regeneration.

In chapter 1, general backgrounds are introduced to describe the current challenges and problems for breast cancer therapy, especially for the new strategy: photothermal therapy. In order to achieve the high repeated photothermal efficiency and realize the new adipose tissue regeneration for breast reconstruction, bifunctional scaffolds are designed by incorporating photothermal conversion nanoparticles into a porous scaffold, which provide photothermal ablation of breast tumor and induce adipogenic differentiation of MSCs for adipose tissue regeneration.

In chapter 2, gold nanorods (AuNRs) were synthesized by a seed-mediated growth method, and BSA were coated on the surface of AuNRs. The BSA-coated AuNRs showed good monodispersity and low cytotoxicity as well as high cellular uptake by tumor cells in the studied concentration. The BSA-coated AuNRs also showed excellent photothermal performance based on the strong SPR in the NIR region and showed high photothermal ablating efficiency towards breast tumor cells. Moreover, the photothermally ablated tumor cells triggered immune-stimulatory responses of immature DCs through both cell–cell interaction and soluble factors released from the ablated tumor cells.

In chapter 3, AuNRs-gelatin porous scaffolds were prepared by introducing AuNRs in porous gelatin matrices via a freeze-drying method. Pre-prepared ice particulates were used as a template to control the pore structure. The AuNRs-gelatin composite scaffolds showed high photothermal conversion efficiency. The AuNRs-gelatin composite scaffolds also showed excellent photothermal ablation capacity of breast tumor cells *in vitro* and *in vivo*. Moreover, DCs were activated by ablated tumor cells in AuNRs-gelatin composite scaffold.

In chapter 4, functional AuNRs-gelatin porous scaffolds were also used for adipose tissue regeneration. The AuNRs-gelatin composite scaffolds supported adhesion, promoted proliferation, and enhanced the adipogenic differentiation of hMSCs. The results demonstrated that the AuNRs-gelatin scaffolds had

simultaneous effects on photothermal ablation of breast tumor and regeneration of adipose tissue. The composite scaffolds should be useful for the treatment of breast tumors.

In conclusions, a bifunctional scaffold of gelatin and AuNRs with well-controlled pore structures were designed and used for both photothermal ablation of tumor cells and adipogenic differentiation of hMSCs, indicating that the AuNRs-gelatin composite scaffolds had a potential for adipose tissue regeneration for breast reconstruction after breast tumor therapy.

5.2 Future prospects

The achievements and conclusions of this study provide useful information for the design and application of multifunctional biomaterials for both photothermal-immunotherapy of primary and metastatic cancer and tissue regeneration of tumor-initiated detects. In order to further demonstrate the multifunctions of AuNRs-gelatin composite scaffolds and their future applications in the clinic, the following studies should be considered in the future.

(1) Based on the current problems of nanoparticles-mediated photothermal therapy, the immune responses of DCs triggered by photothotermally ablated tumor cells using BSA-coated AuNRs were demonstrated *in vitro*. Immunotherapy of metastatic cancer induced by ablated tumor cells using photothermal effects of BSA-coated AuNRs *in vivo* is required.

(2) AuNRs-gelatin composite scaffolds showed excellent photothermal ablation effects towards breast tumor cells *in vitro* and *in vivo*. The photothermal-immunotherapy of AuNRs-gelatin composite scaffolds for primary and metastatic cancer should be investigated by animal experiments.

(3) Besides breast tumor therapy, the adipogenic differentiation of hMSCs in AuNRs-gelatin composite porous scaffolds was successfully induced *in vitro*. For clinic application of the porous scaffolds for effective breast reconstruction, *in vivo* adipogenesis promotion effect of the composite scaffolds after photothermal therapy of breast tumor should be considered.

List of publications and awards

Publications

1. Xiuhui Wang, Jing Zhang, Jingchao Li, Ying Chen, Yazhou Chen, Naoki Kawaz oe and Guoping Chen. Bifunctional scaffolds for photothermal therapy of breast tumor and adipose tissue regeneration. Journal of Material Chemistry B, 2018, 6, 7728-7736.

2. Xiuhui Wang, Jingchao Li, Naoki Kawazoe and Guoping Chen. Photothermal ablation of cancer cells by albumin-modified gold nanorods and activation of dendritic cells. Materials, 2019, 12, 31, DOI:10.3390/ma12010031.

3. Xiuhui Wang, Rong Cai, Naoki Kawazoe and Guoping Chen. Interaction of immune cells and tumor cells in gold nanorods-gelatin composite scaffolds. Submitted.

4. Jing Zhang, Jingchao Li, Xiuhui Wang, Naoki Kawazoe and Guoping Chen. Targeting ligand-functionalized photothermal scaffolds for cancer cell capture and *in situ* ablation. Biomaterials Science, 2017, 5, 2276-2284.

Awards

1. **Excellent poster presentation award**, Xiuhui Wang, Naoki Kawazoe and Guoping Chen. Biomedical engineering collaboration Forum, Tsukuba, Japan, January 26, 2018.

2. **Best oral presentation award**, Xiuhui Wang, Naoki Kawazoe and Guoping Chen. 3rd Asian university symposium on biomedical engineering, Seoul, Korea, July 5-7, 2018.

Acknowledgements

First and foremost, I want to express my sincere gratitude to my supervisor, Prof. Guoping Chen. Without his patient guidance, this dissertation cannot be accomplished smoothly. During my PhD period, Prof. Chen always devoted himself to supervising my research, including how to design the research topic and carry out the experiments, how to solve the problems encountered in my research, how to revise the manuscripts and dissertation. His profound knowledge, unique insight and creative spirit on scientific research deeply impressed me. His patient supervision, constructive comments and enthusiastic help greatly encouraged me to become better and better within the past three years. Besides my research, Prof. Chen also give me generous advices and selfless helps in my daily life in Japan. It is the great honor for me to have this precious opportunity to join and study in Prof. Chen' group for these three years.

Special thanks are also expressed to Dr. Naoki Kawazoe. Without his kind and selfless help, I cannot carry out my experiments smoothly. His diligence, thoughtful consideration and warm encouragement deeply impressed me. I am very pleased to work with him and also grateful to learn many knowledge from him.

I also want to give my sincere appreciates for their valuable suggestions and warm accompanies from the members of Prof. Chen' group: Prof. Gang Wu, Prof. Shujun Dong, Dr. Jianmin Yang, Dr. Xiaohong Hu, Dr. Xinlong Wang, Dr. Xiaohong Hu, Dr. Jing Zhang, Dr. Jingchao Li, Dr. Xiaomeng Li, Dr. Ying Chen, Ma. Nur Rofiqoh, Mr. Yingjun Yang, Mr. Yazhou Chen, Mr. Kyubae Lee, Mr. Yongtao Wang, Mr. Tsung-Chun Huang, Mrs. Fusako Hidaka, Mrs. Akiko Ito and Mrs. Haruyo Akiyama. Our philosophical debates, exchanges of knowledge, skills and advices enrich my experiences in my life.

I would also like to give my sincere thanks to the professors of my defense committee: Prof. Yukio Nagasaki, Prof. Kohsaku Kawakami and Prof. Tetsushi Taguchi. I am very grateful for their insightful comments, constructive suggestions and encouragement during my PhD defense.

I also want to express my sincere appreciates to my family and friends for their love, support and encouragement within the past three years.

This work was performed at Tissue Regeneration Materials group, Research Center for Functional Materials, National Institute for Materials Science (NIMS) and Graduate School of Pure and Applied Science of University of Tsukuba. I also acknowledge the financial support from the Doctoral Program in Materials Science and Engineering of University of Tsukuba and Junior Research Assistantship of NIMS.